Distribution Agreement

In presenting this thesis or dissertation as a partial fulfillment of the requirements for an advanced degree from Emory University, I hereby grant to Emory University and its agents the non-exclusive license to archive, make accessible, and display my thesis or dissertation in whole or in part in all forms of media, now or hereafter known, including display on the world wide web. I understand that I may select some access restrictions as part of the online submission of this thesis or dissertation. I retain all ownership rights to the copyright of the thesis or dissertation. I also retain the right to use in future works (such as articles or books) all or part of this thesis or dissertation.

Signature:

_____ _____

Li Li Date

Regulation of Endothelial Tetrahydrobiopterin in Normal and Pathophysiological States

By

Li Li

Doctor of Philosophy

Graduate Division of Biological and Biomedical Sciences
Molecular and Systems Pharmacology

_____
David G. Harrison, M.D.
Advisor

_____
Haian Fu, Ph.D.
Committee Member

_____
Kathy Griendling, Ph.D.
Committee Member

_____
Roy Sutliff, Ph.D.
Committee Member

Accepted:

_____
Lisa A. Tedesco, Ph.D.
Dean of the James T. Laney School of Graduate Studies

_____
Date

Regulation of Endothelial Tetrahydrobiopterin in Normal and Pathophysiological States

By

Li Li
B.S., Tsinghua University, 2006

Advisor: David G. Harrison, M.D.

An abstract of
A dissertation submitted to the Faculty of the
James T. Laney School of Graduate Studies of Emory University
in partial fulfillment of the requirements for the degree of
Doctor of Philosophy
in
Graduate Division of Biological and Biomedical Sciences
Molecular and Systems Pharmacology

2011

ABSTRACT

Regulation of Endothelial Tetrahydrobiopterin in Normal and Pathophysiological States

By Li Li

Tetrahydrobiopterin (BH_4) is an essential cofactor for NO synthases (NOS). In the absence of BH_4, NOS produces superoxide rather than NO, a situation referred to as NOS uncoupling. The rate-limiting enzyme for de novo biosynthesis of BH_4 is GTP Cyclohydrolase I (GTPCH-1). GTPCH-1 activity is regulated via interaction with the GTP cyclohydrolase feedback regulatory protein (GFRP). We have shown that laminar shear stress stimulates GTPCH-1 phosphorylation by Casein Kinase 2. The role of GFRP in modulating GTPCH-1 phosphorylation and activity in the endothelium and how phosphorylation affects GTPCH-1 activity remained undefined. My dissertation demonstrates that GFRP inhibits endothelial GTPCH-1 phosphorylation, BH_4 levels, and NO production. Phosphorylation of GTPCH-1 increases its activity, reduces its binding to GFRP and confers resistance to inhibition by GFRP. Moreover, laminar, but not oscillatory shear stress, causes dissociation of GTPCH-1 and GFRP, which promotes GTPCH-1 phosphorylation and activation of the enzyme.

I found that disturbed flow produced by partial carotid ligation in mice reduces GTPCH-1 phosphorylation and BH_4 levels in vivo. BH_4 deficiency caused by disturbed flow leads to NOS uncoupling and induces accelerated atherosclerosis at these sites. BH_4 deficiency and NOS uncoupling contribute to vascular superoxide production, endothelial dysfunction, vascular inflammation and abnormal cytokine milieu at sites of disturbed flow.

Since interaction of GFRP with GTPCH-1 inhibits its phosphorylation and enzyme activity, we propose that agents that disrupt GTPCH-1/GFRP binding would increase cellular BH_4 levels. I thus developed a time-resolved fluorescence resonance energy transfer (TR-FRET) assay to monitor GTPCH-1/GFRP interaction. This assay has achieved a signal-to-background ratio of 12 and a Z' factor of 0.8. By adapting this assay for high throughput screening (HTS) and subsequent testing in confirmatory assays, I discovered compounds that inhibit GTPCH-1/GFRP interaction and increase cellular BH_4 levels.

In summary, these data revealed a novel mechanism of GTPCH-1 regulation involving GTPCH-1 phosphorylation and its interaction with GFRP. This mechanism modulates in vivo BH_4 levels and ultimately atherosclerosis. Our newly developed TR-FRET assay could be applied in future HTS to search for molecules that increase cellular BH_4 levels.

Regulation of Endothelial Tetrahydrobiopterin in Normal and Pathophysiological States

By

Li Li
B.S., Tsinghua University, 2006

Advisor: David G. Harrison, M.D.

A dissertation submitted to the Faculty of the
James T. Laney School of Graduate Studies of Emory University
in partial fulfillment of the requirements for the degree of
Doctor of Philosophy
in
Graduate Division of Biological and Biomedical Sciences
Molecular and Systems Pharmacology

2011

ACKNOWLEDGEMENTS

I would like to express my sincere thanks to all of the people who have helped, supported, and encouraged me throughout my graduate career at Emory. They have made it possible for me to be where I am now.

First and foremost, I am heartily thankful to my advisor, Dr. David Harrison, whose encouragement, guidance and support throughout my graduate career made my Ph.D. experience productive and stimulating. I am also thankful for the enormous example he has provided as a dedicated and respected scientist and mentor. I not only appreciate the support he gave me on research, but also sincerely acknowledge his thoughtfulness and kindness in supporting my pursuit of interests in other areas. I could not have imagined having a better advisor and mentor for my Ph.D. study.

I would like to thank my dissertation committee members, Drs. Haian Fu, Kathy Griendling, and Roy Sutliff, who have provided me with excellent counsel and recommendations.

I would also like to extend my appreciation to the many members of the Harrison laboratory, with whom I had the fortune of learning from and interacting with. I would especially like to recognize Dr. Wei Chen for her continuous advice and help since the first day I joined the lab.

I am grateful to Drs. Hanjoong Jo and Amir Rezvan, who kindly provided me the partial carotid ligation model, which enabled my study of disturbed flow in vivo. I am also grateful to Drs. Yuhong Du and Haian Fu at the Emory Chemical Biology Discovery Center, without whom I could not have started the exciting high throughput

screening project. Besides, I would like to thank the Free Radicals in Medicine Core and the Internal Medicine Imaging Core at Emory, which trained me in using their instruments and assisted me in generating accurate data.

I gratefully acknowledge my funding source, American Heart Association, which awarded me the Predoctoral Fellowship for the last two years of my Ph.D. study.

I wish to thank all my friends for helping me get through the difficult times, and for all the emotional support, entertainment, and caring they provided in the past five years.

Finally, I would like to thank my family for all their love and encouragement. I am especially grateful to my parents who raised me with love and supported me in all my pursuits. And I dedicate this dissertation to my best friend, my beloved one, my husband, Xiaojun Yan, for his forever and faithful support, encouragement, patience, and love.

TABLE OF CONTENTS

Page

Chapter 1: Introduction 1

1.1 Overview 2

1.2 Shear stress 3

1.2.1 Laminar shear stress 3

1.2.2 Oscillatory shear stress 4

1.2.3 Experimental models of shear stress 5

1.3 Tetrahydrobiopterin (BH_4) 9

1.3.1 Biosynthesis of BH_4 9

1.3.1.1 *De novo* synthesis pathway 9

1.3.1.2 Salvage pathway 11

1.3.2 Metabolism of BH_4 14

1.3.3 Biological functions of BH_4 15

1.3.3.1 Cofactor functions 15

1.3.3.2 Cellular functions 18

1.4 Nitric Oxide Synthase (NOS) 18

1.4.1 Role of BH_4 in NOS function 19

1.4.2 NOS uncoupling and production of superoxide 21

1.4.3 Role of NOS uncoupling in vascular diseases 22

1.5 GTP Cyclohydrolase I (GTPCH-1) and regulation of BH_4 synthesis 25

1.5.1 GTPCH-1 structure 26

1.5.2 Regulation of GTPCH-1 gene expression 26

1.5.3 Post-translational modification of GTPCH-1 26

1.5.4 GTPCH-1 protein interactions 28

1.6 Summary 28

1.7 Objectives of this dissertation 29

Chapter 2: The interplay between GTPCH-1 phosphorylation and GFRP and their roles in regulating endothelial cell BH_4 levels and NO production 31

2.1 Introduction 32

2.2 Materials and methods 33

2.3 Results 41

2.4 Discussion 69

Chapter 3: Regulation of GTPCH-1 phosphorylation and BH_4 levels by disturbed flow in vivo and their roles in augmented atherosclerosis at sites of disturbed flow 78

3.1 Introduction 79

3.2 Materials and methods 81

3.3 Results 86

3.4 Discussion 102

Chapter 4: Identification of inhibitors of GTPCH-1 and GFRP interaction and development of a homogenous time-resolved fluorescence resonance energy transfer assay to monitor GTPCH-1 and GFRP interaction 109

4.1 Introduction 110

4.2 Materials and methods 115

4.3 Results 121

4.4 Discussion 135

Chapter 5: Discussion and future directions 145

5.1 What are other mechanisms of GTPCH-1 regulation? 146

5.2 What is the role of BH_4 deficiency and NOS uncoupling in atherosclerosis? 149

5.3 Is BH_4 supplementation effective in long-term treatment of human diseases? 151

5.4 Development of new therapeutic agents that disrupt GTPCH-1/GFRP interaction and increase intracellular BH_4 157

5.5 Future directions 159

Chapter 6: References 162

INDEX OF FIGURES

		Page
Figure 1.1	Schematic demonstrating the flow reversal that occurs on the outer wall of the internal carotid during systole	6
Figure 1.2	Cone-in-plate shear apparatus	7
Figure 1.3	Partial ligation of left common carotid artery (LCA) causes low and oscillatory flow	10
Figure 1.4	*De Novo* pathway of BH_4 synthesis from GTP	12
Figure 1.5	Salvage Pathways for recovery of BH_4 from Sepiapterin, BH_2 and q-BH_2	13
Figure 1.6	Oxidation of BH_4 to the BH3• radical and ultimately to BH_2	16
Figure 1.7	Function of BH_4 in Aromatic Amino Acid Hydroxylases and NOS catalysis	17
Figure 1.8	The general structure of the NOS enzymes	20
Figure 1.9	Effect of ROS and diseases on NOS uncoupling	24
Figure 1.10	Crystal structures of GTPCH-1 and GFRP	27
Figure 2.1	BRET saturation curve for constitutive interaction between GTPCH-1 and GFRP	40
Figure 2.2	Interaction of GTPCH-1 and Aha1 and the effect of Aha1 in modulating BH_4 levels in HAECs	43
Figure 2.3	Effect of GFRP down-regulation by siRNA in modulating endothelial GTPCH-1 S81 phosphorylation and activity, BH_4	44

levels and NO production

Figure 2.4 Effect of GFRP overexpression on endothelial GTPCH-1 S81 phosphorylation and BH_4 levels 47

Figure 2.5 Interaction of GTPCH-1 and GFRP in HAECs by co-IP 50

Figure 2.6 Colocalization and FRET imaging of GFP-tagged GTPCH-1 and DsRed-tagged GFRP 51

Figure 2.7 Effect of GTPCH-1 S81 phosphorylation on endothelial BH_4 levels, GTPCH-1 activity and NO production in HAECs 55

Figure 2.8 Effect of GTPCH-1 S81 phosphorylation on its interaction with GFRP 60

Figure 2.9 Effects of GTPCH-1 phosphorylation and GFRP down-regulation on eNOS coupling in HAECs exposed to oscillatory shear stress 61

Figure 2.10 Comparison of laminar vs. oscillatory shear stress on the association of GTPCH-1 and GFRP and the role of GTPCH-1 phosphorylation in its dissociation from GFRP 63

Figure 2.11 Roles of p38, ROCK and PI3K in laminar shear induced increase in BH_4 levels in HAECs 67

Figure 2.12 Proposed mechanism for shear regulation of GTPCH-1 71

Figure 3.1 Effect of disturbed flow on GTPCH-1 phosphorylation and BH_4 levels in vivo 87

Figure 3.2 Pterin levels in the carotids that underwent partial ligation for 89

one week

Figure 3.3 Identification of NOS uncoupling at areas of disturbed flow 90

Figure 3.4 Role of NOS uncoupling in atherosclerosis induced by partial carotid ligation 92

Figure 3.5 Effect of BH_4 treatment on atherosclerosis in the brachiocephalic and intercostal arteries of $ApoE^{-/-}$ mice fed a high fat diet 94

Figure 3.6 Role of NOS uncoupling in endothelial dysfunction induced by partial carotid ligation 97

Figure 3.7 Role of NOS uncoupling in infiltration of T cells and T cell activation induced by partial carotid ligation 99

Figure 3.8 Effect of BH_4 treatment on T cell numbers and activation in the peripheral blood and spleen after partial carotid ligation 100

Figure 3.9 Role of NOS uncoupling in infiltration and activation of monocytes and macrophages induced by partial carotid ligation 101

Figure 3.10 Role of NOS uncoupling in ex vivo cytokine production of the carotid induced by partial ligation 103

Figure 4.1 Amino acid sequence of Human GTPCH-1 112

Figure 4.2 Interaction of GFRP with GTPCH-1 truncations in HAECs by co-IP 123

Figure 4.3 GST Pull-down assay using GST-tagged GFRP to immunoprecipitate His-tagged GTPCH-1 in the presence of 125

various synthetic peptides

Figure 4.4 Design of a TR-FRET assay for monitoring the binding of GTPCH-1 and GFRP protein 127

Figure 4.5 Optimization of GTPCH-1/GFRP TR-FRET binding assay 128

Figure 4.6 TR-FRET assay stability with time and in the presence of DMSO 130

Figure 4.7 Ultra-high-throughput Screening (uHTS) format assay validation 133

Figure 4.8 Confirmation of the compounds in the GST pull-down assay 134

Figure 4.9 Effect of the disruption of GTPCH-1/GFRP binding on endothelial cell biopterin levels 136

Figure 5.1 Proposed mechanism for the role of NOS coupling in atherosclerosis induced by disturbed flow 152

Figure 5.2 NO-based therapeutic approaches for atherosclerosis 154

INDEX OF TABLES

Page

Table 2.1 Kinetic properties of WT and S81D GTPCH-1 in the presence and absence of GFRP 58

Table 3.1 EC_{50} and peak relaxation values of LCA and RCA of $ApoE^{-/-}$ mice treated with vehicle or BH_4 in response to acetylcholine 96

Table 4.1 List of primers used to generate GTPCH-1 truncation constructs 116

LIST OF ABBREVIATIONS

Abbreviation	Definition
CVD	Cardiovascular disease
NO	Nitric Oxide
NOS	Nitric Oxide Synthase
eNOS	endothelial Nitric Oxide Synthase
iNOS	inducible Nitric Oxide Synthase
nNOS	neuronal Nitric Oxide Synthase
MAPK	MAP kinase
VCAM-1	vascular cell adhesion molecule-1
ICAM-1	inter-cellular adhesion molecule-1
ApoE	Apolipoprotein E
GTPCH-1	GTP Cyclohydrolase I
PTPS	6-pyruvoyl-tetrahydrobiopterin synthase
SR	sepiapterin reductase
H_2NTP	7,8-dihydroneopterin triphosphate
BH_4	tetrahydrobiopterin
BH_2	7,8-dihydrobiopterin
q-BH_2	quinoid dihydrobiopterin
DHFR	dihydrofolate reductase
DHPR	dihydropteridine reductase

siRNA	small interfering RNA
$O_2^{\bullet-}$	superoxide
$OONO^{\bullet-}$	peroxynitrite
PAH	phenylalanine hydroxylase
TH	tyrosine hydroxylase
TPH	tryptophan hydroxylase
ROS	reactive oxygen species
H_2O_2	hydrogen peroxide
NOHA	N-hydroxy L-arginine
L-NAME	L-N^G-Nitroarginine methyl ester
LPS	lipopolysaccharide
PI3K	phosphatidylinositol-3-kinase
HAEC	human aortic endothelial cells
GFRP	GTP Cyclohydrolase I Feedback Regulatory Protein
LCA	left common carotid artery
RCA	right common carotid artery
S81	Serine 81
CK2α’	Casein Kinase II alpha prime
Aha1	Activator of Hsp90 ATPase
HPLC	high-performance liquid chromatography
ESR	electron spin resonance
$Fe[DETC]_2$	Fe^{2+} diethyldithiocarbamate

IPTG	isopropyl-β-d-thiogalactopyranoside
Co-IP	co-immunoprecipitation
FRET	fluorescence resonance energy transfer
BRET	bioluminescence resonance energy transfer
AcGFP	Aequorea coerulescens green fluorescent protein
Rluc	Renilla luciferase
S81A	serine 81/alanine mutant of GTPCH-1
S81D	serine 81/aspartate mutant of GTPCH-1
GST	glutathione S-transferase
TBB	4,5,6,7-tetrabromobenzotriazole
VEGF	vascular endothelial growth factor
NH_4	5,6,7,8-tetrahydro-D-neopterin
DHE	dihydroethidium
SNP	sodium nitroprusside
PMA	phorbol myristate acetate
VSMC	vascular smooth muscle cell
LDL	low-density lipoprotein cholesterol
Ach	Acetylcholine
TR-FRET	time-resolved fluorescence resonance energy transfer
HTS	high throughput screening
uHTS	ultra high throughput screening
APC	Allophycocyanin

LOPAC	Library of Pharmacologically Active Compounds
S/B	signal-to-background ratio
FI	fluorescent intensity
KI	knock-in
SAR	structure-activity relationship
ACE	angiotensin-converting enzyme
ARB	angiotensin II receptor blocker
MHC	Major histocompatibility complex

Chapter 1

Introduction

1.1 Overview

Cardiovascular disease (CVD) accounts for considerable mortality and morbidity in Western countries. Most of the common forms of CVD, such as atherosclerosis and hypertension, are caused by functional and structural changes in the blood vessel wall. These changes include abnormal vasoconstriction, enhanced interaction of blood cells with the vessel wall, and migration and proliferation of vascular smooth muscle cells.

In the past several decades, researchers discovered that the endothelium, a one cell layer lining of the walls of the body's blood vessels, plays a crucial role in regulating the development and progression of CVD. The endothelium is a source of a variety of mediators regulating vascular tone and growth as well as platelet function and aggregation. One important endothelium-derived mediator is nitric oxide (NO), which is formed from L-arginine synthesized by the enzyme nitric oxide synthase (NOS) (Palmer et al., 1988). NO is released away from the lumen to relax the vascular smooth muscle, thus it protects against thrombosis, vasoconstriction and other abnormalities associated with different forms of CVD.

As a result of its prime location, the endothelium experiences two major types of mechanical forces: circumferential stretch and shear stress, the dragging frictional force created by blood flow. Of these, shear stress seems to be the most important due to its modulation of gene expression and release of biologically active substances (Davies, 2002). Shear forces vary throughout the circulation and affect vascular development, function and the development of vascular diseases (Harrison,

2005; Nerem et al., 1993). At certain sites in the circulation, such as the branch points of the arterial tree, flow reverses during the cardiac cycle. Human and experimental atherosclerosis preferentially develops at these nonlinear vascular segments (De Keulenaer et al., 1998). The nonrandom distribution of atherosclerotic plaques is therefore due to the different shear force patterns exerting different biological effects on the endothelium.

1.2 Shear stress

During the past two decades it has become clear that mechanical forces have major effects on endothelial cell biology. Shear stress is the force exerted tangentially on the blood vessel wall as blood flows over the endothelial cell layer. Shear stress is determined by the following equation describing fluid flow through a tube:

$$\tau w = 4\mu Q/\pi r^3$$

Where τw = wall shear stress, μ = blood viscosity, Q = flow rate, and r = radius. The main factors that affect shear stress are blood viscosity, flow rate and vessel radius. Small changes in vessel diameter result in large changes in shear stress since the radius is cubed in the denominator (Glagov et al., 1988).

1.2.1 Laminar shear stress

At linear areas of the vasculature, such as the length of the common carotid artery, blood flows in a laminar pattern and pulses unidirectionally with each contraction of the heart's ventricles. Endothelial cells experience a pulsatile shear stress with a mean positive value on the order of 10 to 30 dynes/cm^2 (Davies, 2002).

The most important effect of laminar shear is an increase in NO released by the endothelium. In fact, shear stress is one of the most potent physiological stimuli for NO production in endothelial cells (Corson et al., 1996). In the short term, laminar shear stimulates an increase in endothelial intracellular calcium and promotes a variety of signaling events including MAP kinase (MAPK) activation, ion channel opening and modulation of reactive oxygen species production. Exposure of endothelial cells to unidirectional laminar shear stimulates the enzyme endothelial nitric oxide synthase (eNOS) to produce NO within seconds, in part by causing eNOS phosphorylation (Corson et al., 1996). Over the long term, laminar shear stimulates an increase in eNOS mRNA and protein expression. In vivo, exercise training increases eNOS expression, most likely by increasing cardiac output and endothelial shear (Davis et al., 2003). The effects of laminar shear are thought to protect against atherosclerosis, because in addition to its role as a vasodilator, NO prevents smooth muscle growth, platelet aggregation, leukocyte adhesion and inhibits lipid oxidation and apoptosis in the vessel wall (Fleming and Busse, 1999; Traub and Berk, 1998).

1.2.2 Oscillatory shear stress

In contrast to linear vessels, flow patterns at branch points are more complex. At vessel bifurcations and curvatures, flow reverses or oscillates during the cardiac cycle. Unlike unidirectional laminar shear, oscillatory shear seems to predispose to atherosclerotic lesion formation (Ku et al., 1985b). Oscillations of flow have been consistently documented with each cardiac cycle in atherosclerosis prone areas of the

circulation, including the carotid bulb, the proximal coronary arteries, the infrarenal aorta and the aortoiliac junction (Ku et al., 1985a; Taylor et al., 1998; Tsuji et al., 2002). The lateral wall of the carotid bulb near the carotid bifurcation exposed to a shear stress oscillating between -7 and +4 dynes/cm^2 during systole (mean shear stress was -0.5 dynes/cm^2) exhibited increased intima-media thickness, a marker for atherosclerosis (Figure 1.1) (Ku et al., 1985b). Disturbed flow stimulates proatherogenic responses, including cell turnover, oxidative stress, inflammation, and thrombosis (Jo et al., 2006). Oscillatory shear increases NADPH oxidase activity and stimulates production of reactive oxygen species (Guzik et al., 2000). Oscillatory shear also induces upregulation of inflammatory adhesion molecules such as E-selectin, vascular cell adhesion molecule-1 (VCAM-1) and Inter-Cellular Adhesion Molecule 1 (ICAM-1) (Libby et al., 2002; Ross, 1999). These endothelial adhesion molecules play essential roles in adhesion and recruitment of monocytes to the endothelial layer and initiation of atherosclerosis.

1.2.3 Experimental models of shear stress

Two in vitro models of shear stress on endothelial cells are commonly used. One is the parallel flow chamber, which involves two plates separated by a small distance with liquid media between them. Cells subject to shear stress are attached to one of the plates and flow of the media is produced in parallel to the two plates. Another more practical method of creating shear stress on cultured cells is by using a cone-in-plate viscometer on cells cultured in 100 mm^2 dishes (Figure 1.2). This is the type of in vitro shear stress model we currently use in our own laboratory. As

Figure 1.1 Schematic demonstrating the flow reversal that occurs on the outer wall of the internal carotid during systole. The insert on the left shows the profile of the wall shear stress at the outer wall of the carotid sinus. The shear stress oscillation from positive to negative values during systole is characteristic of locations along the outer wall of the sinus. (Adapted from (Ku et al., 1985b))

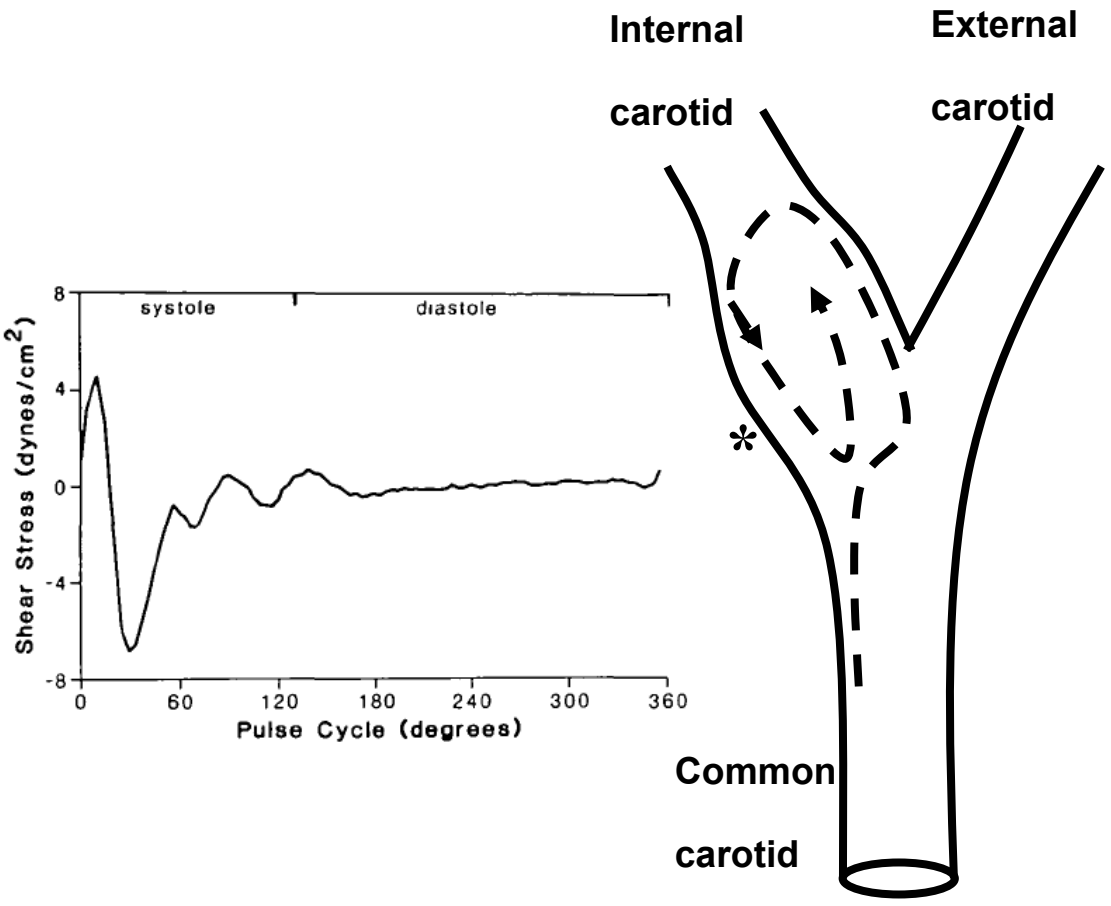

Figure 1.2 Cone-in-plate shear apparatus. Shown is a schematic of the modified cone-in-plate shear apparatus. The entire shear system except for the computer controller unit is housed in a humidified tissue culture incubator (5% CO_2, 37°C). The cone is rotated back and forth or unidirectionally through a computer program and a motor to generate oscillatory shear and laminar shear, respectively.

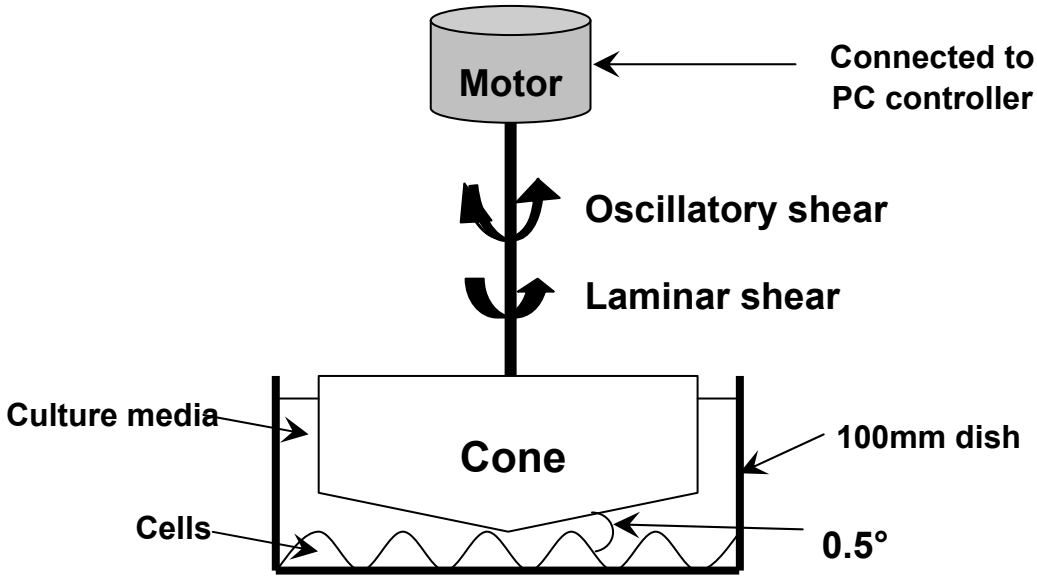

the cone rotates, flow is induced in the media and shear stress is exerted on the endothelial monolayer below. This shear stress can be calculated with the following equation:

$$\tau = \mu\omega r/d$$

Where τ = shear stress, ω = angular velocity of the cone ($\omega = 2\pi f$ where f = frequency of rotation), μ = viscosity of media, r = radius of the cone, and d = distance between the cone and the bottom of the plate. By varying the angular velocity of the cone, it is possible to create many variations of physiological shear stresses (Bussolari et al., 1982).

Although many studies have focused on the areas in the vasculature with naturally occurring different shear patterns, animal models in which acute changes in shear stress have been induced can reveal a causative relationship between disturbed shear stress and atherosclerosis. A constrictive perivascular cuff model has been used to produce distinct flow patterns in neighboring vascular regions (Cheng et al., 2005). In this model, the vessel region constricted by the cuff is exposed to higher shear stress, while a proximal section of the post-constriction area is exposed to disturbed flow. A drawback of this model is the direct manipulation of vessel adventitia that may lead to injury of the vessel.

Nam and coworkers have recently developed an in vivo model of acutely induced oscillatory shear (Nam et al., 2009). This model greatly aids flow-dependent studies in small animals. In this model, the internal carotid, the occipital, and the external carotid are ligated, allowing common carotid blood flow

only through the superior thyroid artery (Figure 1.3). This not only significantly reduces the flow rate, but also results in a flow reversal pattern during diastole, giving rise to a combined low and oscillatory shear pattern that is characteristic of areas of disturbed flow in the arterial tree (Figure 1.3). With this model and a high-fat diet feeding, Nam et al. (Nam et al., 2009) demonstrated that acutely imposed disturbed flow induces robust atherosclerosis by two weeks and complex lesion formation by four weeks after partial ligation in the common carotid artery of $ApoE^{-/-}$ mice.

1.3 Tetrahydrobiopterin (BH_4)

BH_4 is important in mammalian biology because it serves as a critical cofactor for aromatic amino acid hydroxylases, including tryptophan hydroxylase, phenylalanine hydroxylase, and tyrosine hydroxylase, and nitric oxide synthases. Genetic deficiencies of BH_4 are rare, but can cause BH_4-deficient hyperphenylalaninemia due to reduced conversion of phenylalanine to tyrosine (Tada et al., 1970).

1.3.1 Biosynthesis of BH_4

BH_4 is synthesized through two distinct pathways: *de novo* synthesis pathway that proceeds from the substrate GTP via three step enzymatic reactions, and the salvage pathway that converts oxidized products of BH_4 to BH_4.

1.3.1.1 *De novo* synthesis pathway

BH_4 is synthesized by the sequential actions of three enzymes, GTP Cyclohydrolase I (GTPCH-1), 6-pyruvoyl-tetrahydrobiopterin synthase (PTPS), and

Figure 1.3 Partial ligation of left common carotid artery (LCA) causes low and oscillatory flow. A, three branches of the LCA [external carotid artery (ECA), internal carotid artery (ICA), and occipital artery (OA)] were ligated in the LCA, while leaving the superior thyroid artery (STA) open. B, partial ligation reduces blood flow through the LCA, without significantly raising flow in RCA. The dotted line indicates the preligation flow level. (Adapted from (Nam et al., 2009))

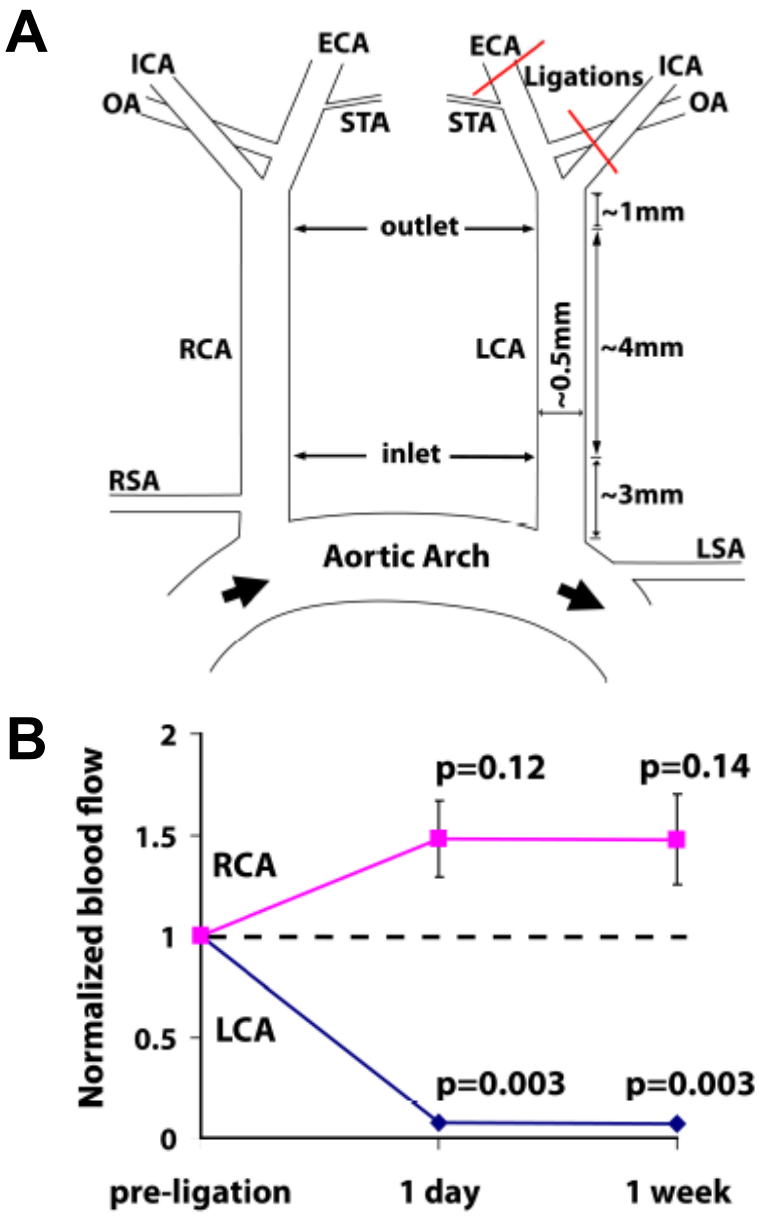

sepiapterin reductase (SR) (Figure 1.4). The first step in this process, which requires the enzyme, GTPCH-1, is generally rate-limiting and is considered a critical regulator of cellular BH_4 levels. This step converts GTP to 7,8-dihydroneopterin triphosphate (H_2NTP), formate and water. Monitoring neopterin formation after dephosphorylation of H_2NTP is used to measure GTPCH-1 activity.

The second reaction in the *de novo* synthesis pathway is the conversion of H_2NTP to 6-pyruvoyl-tetrahydrobiopterin by the enzyme PTPS. The final step, catalyzed by SR, is an NADPH-dependent reaction to produce BH_4. Besides its involvement in the *de novo* biosynthesis of BH_4, SR may also participate in the pterin salvage pathway by catalyzing the conversion of sepiapterin to 7,8-dihydrobiopterin (BH_2), which is then transformed into BH_4 by dihydrofolate reductase (Nichol et al., 1985). In endothelial cells, PTPS activity is about 10-fold higher than GTPCH-1, and SR activity is almost 500-fold greater. Thus, the levels of PTPS and SR activities are sufficient that they are not rate-limiting in endothelial cells at baseline; however, in conditions with a marked increase in GTPCH-1, such as that induced by laminar shear stress, cytokines or other stimuli, it is possible that PTPS becomes rate limiting (Widder et al., 2007).

1.3.1.2 Salvage pathway

Alternative to *de novo* synthesis, intracellular BH_4 can be increased via the salvage pathway using either 7,8-dihydrobiopterin (BH_2) or quinoid dihydrobiopterin (q-BH_2) as substrates (Figure 1.5). q-BH_2 is reconverted to BH_4 by the enzyme dihydropteridine reductase (DHPR). In contrast, the oxidation

Figure 1.4 *De Novo* pathway of BH_4 synthesis from GTP. (Adapted from (Harrison et al., 2010))

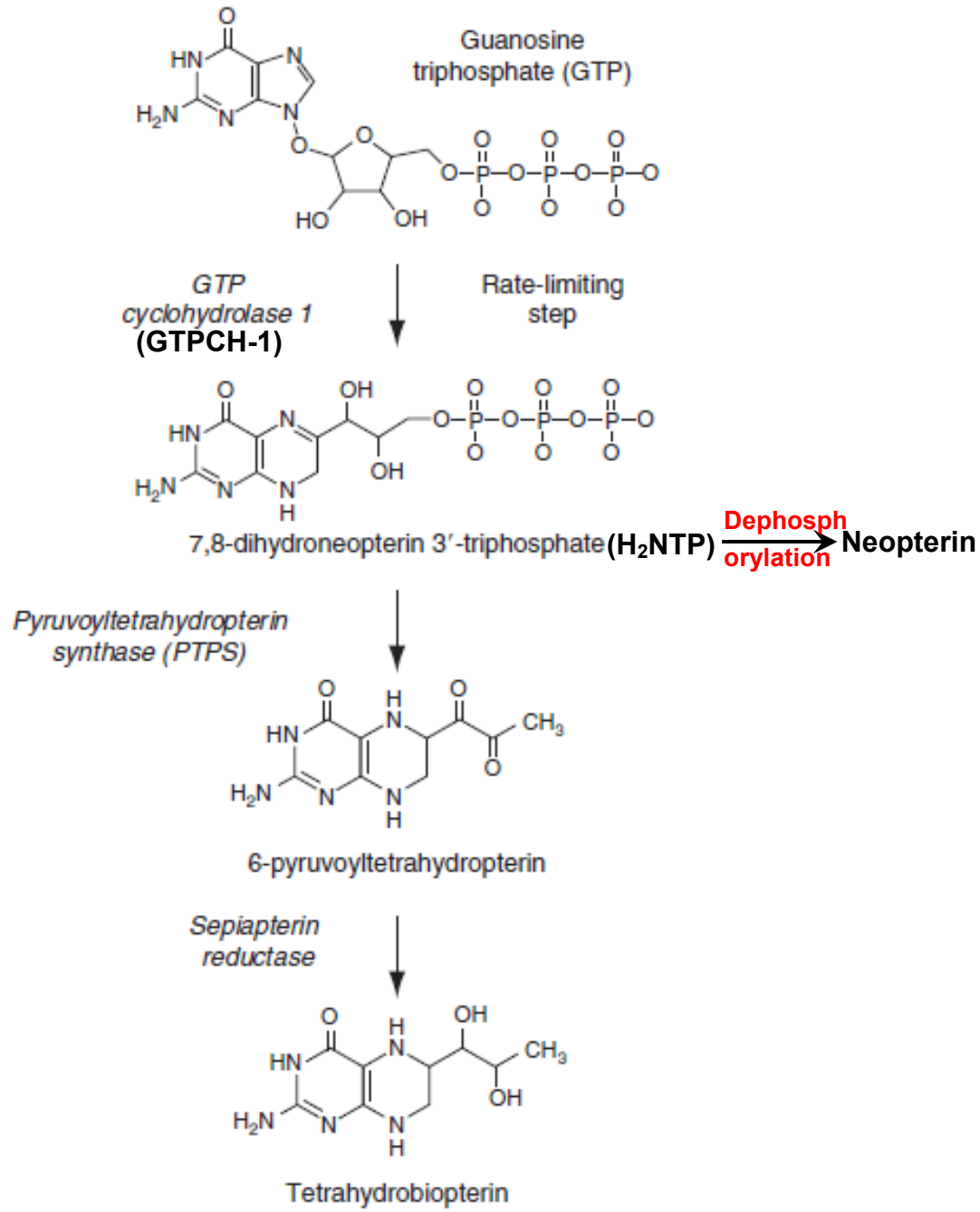

Figure 1.5 Salvage Pathways for recovery of BH_4 from Sepiapterin, BH_2 and q-BH_2. (Adapted from (Harrison et al., 2010))

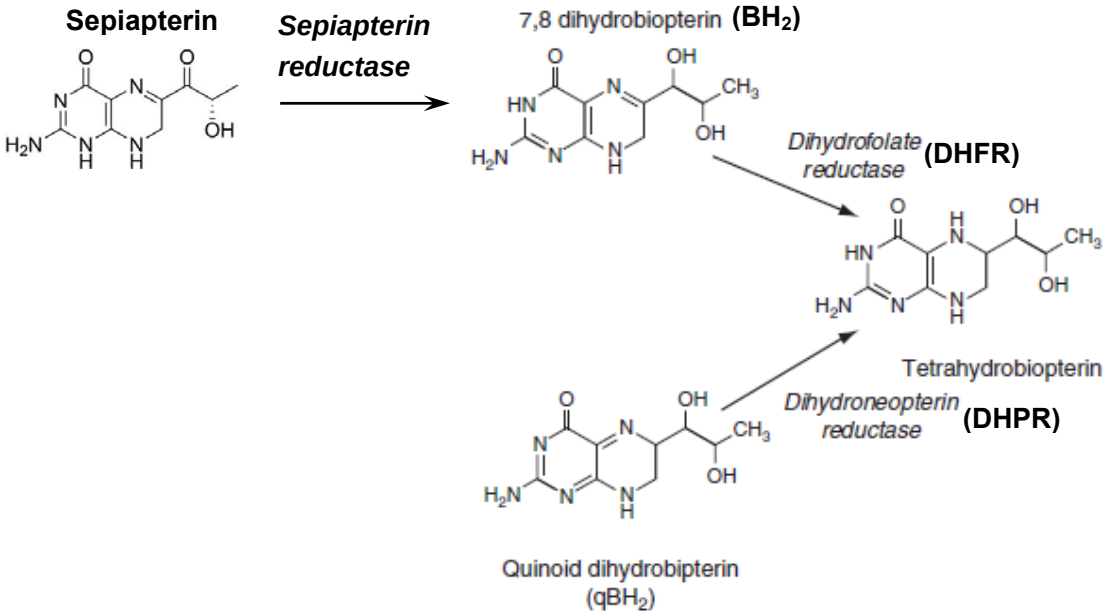

product of BH_4, BH_2, is reconverted to BH_4 by dihydrofolate reductase (DHFR). Pharmacological supplementation of sepiapterin also increases cellular BH_4 levels via the salvage pathway because sepiapterin is converted to BH_2 by SR and then further to BH_4 by DHFR (Figure 1.5).

In endothelial cells, DHFR plays an important role in maintaining BH_4 levels. Chalupsky et al. (Chalupsky and Cai, 2005) showed that siRNA down-regulation of DHFR reduces endothelial BH_4 levels and NO production. In keeping with this, Crabtree et al. and Sugiyama et al. (Crabtree et al., 2009; Sugiyama et al., 2009) have demonstrated the importance of the salvage pathway in modulating BH_4 levels in bovine aortic endothelial cells and transfected murine fibroblasts and endothelial cells, respectively.

1.3.2 Metabolism of BH_4

A significant feature of the biochemical system where BH_4 plays a role is the existence of redox active molecules and oxygen. BH_4 can undergo auto-oxidation involving one electron loss, formation of BH_4 radical ($BH_4\cdot$), and addition of molecular oxygen to form peroxyl radical ($BH_4OO\cdot$), which rearranges to generate q-BH_2 (Vasquez-Vivar, 2009). The $BH_4OO\cdot$ is anticipated to propagate the oxidation reaction with another BH_4 molecule leading to an ongoing oxidation of successive molecules of BH_4. BH_4 is very susceptible to oxidation, particularly by peroxynitrite ($OONO^{\cdot-}$) (Laursen et al., 2001; Milstien and Katusic, 1999). Electron resonance experiments demonstrated that $OONO^{\cdot-}$ oxidizes BH_4 to the BH3· radical (Kuzkaya et al., 2003). In the presence of ascorbic acid, BH3· is

readily converted back to BH_4, while in its absence, BH3· degrades rapidly to BH_2 (Figure 1.6). However, ascorbic acid does not reduce either q-BH_2 or BH_2 to BH_4. Thus, if ascorbic acid is present at the time the BH3· radical is formed; it can prevent loss of BH_4, while addition of ascorbic acid after more extensive oxidation to BH_2 is ineffective. Of note, $OONO^{\cdot-}$ reacts with BH_4 6-10 times faster than with ascorbic acid or thiols, suggesting that even in the presence of common cellular antioxidants such as ascorbic acid and thiols, $OONO^{\cdot-}$ can lead to BH_4 oxidation (Kuzkaya et al., 2003).

The above-mentioned characteristic of BH_4 to undergo oxidation explains its instability in oxygenated solutions. Preparation of BH_4 in oxygen free water, or with the addition of ascorbic acid, DTT or other antioxidants may stabilize BH_4 in solution. These properties need to be taken into consideration when BH_4 is used in biological solutions (Harrison et al., 2010).

1.3.3 Biological functions of BH_4

1.3.3.1 Cofactor functions

One of the best investigated function of BH_4 is its action as a natural cofactor of the aromatic amino acid hydroxylases, including phenylalanine hydroxylase (PAH), tyrosine hydroxylase (TH), and tryptophan hydroxylase (TPH), to produce tyrosine, L-DOPA, and 5-hydroxytryptophan, respectively, as well as all three forms of nitric oxide synthases (NOS) (See discussion in 1.4.2) (Figure 1.7). The reactions of aromatic amino acid hydroxylases have a strict requirement for oxygen, iron and BH_4 and generate biogenic amines and 6a-OH-Tetrahydrobiopterin (Carbinolamine)

Figure 1.6 Oxidation of BH_4 to the BH3· radical and ultimately to BH_2. Ascorbic acid can convert BH3· radical back to BH_4. (Adapted from (Harrison et al., 2010))

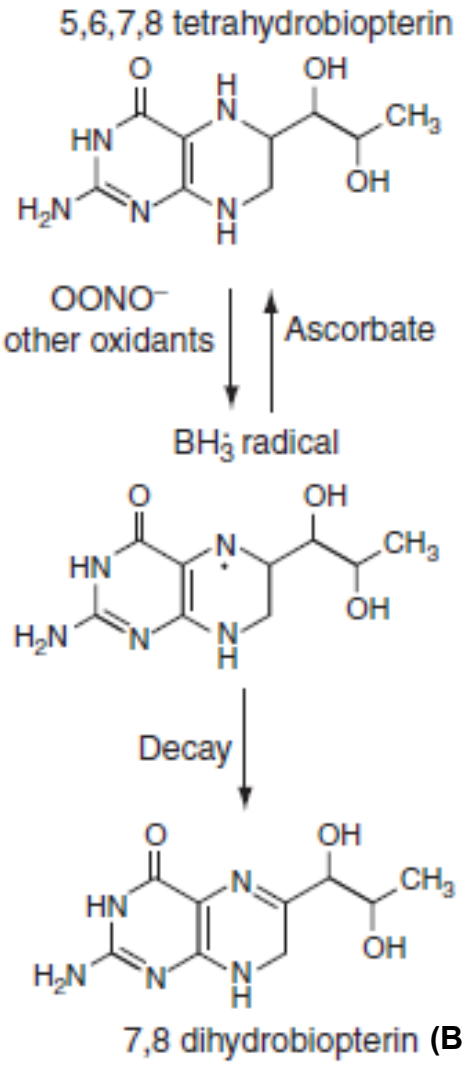

Figure 1.7 Function of BH_4 in Aromatic Amino Acid Hydroxylases and NOS catalysis.

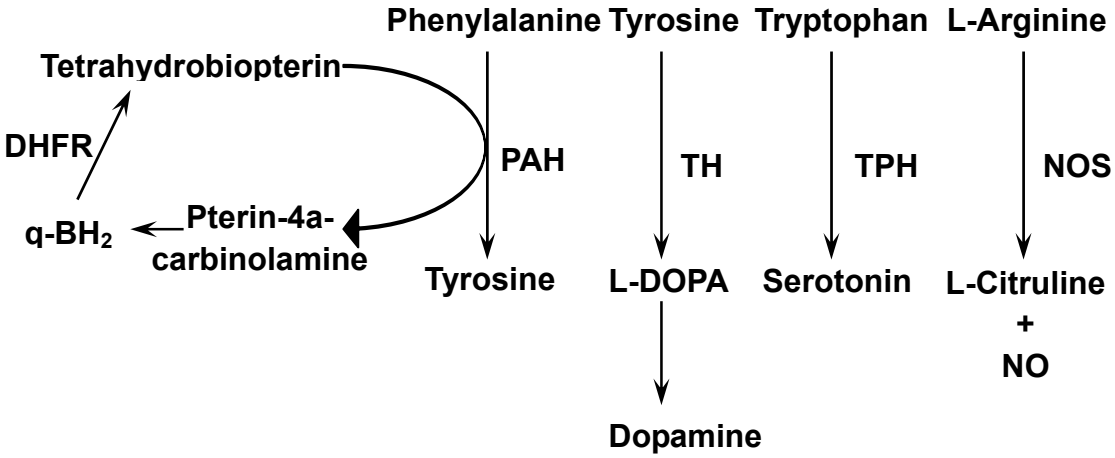

intermediate, which regenerates BH_4 via salvage pathways (Shiman et al., 1990). Perturbations in BH_4 levels can affect the activities of these amino acid hydroxylases and alter levels of dopamine and serotonin, thereby playing a role in Parkinson's disease and other neurological disorders.

The requirement for the BH_4 cofactor is much lower for the NOS enzymes than for PAH. The Km values for BH_4 for PAH and NOS are 2-3 μM and 0.02-0.03 μM, respectively (Pastor et al., 1996). The Km values for BH_4 for the TH and TPH are approximately 30 μM.

1.3.3.2 Cellular functions

It has been theorized that BH_4 react with reactive oxygen species (ROS) in cells; therefore, BH_4 can act as a direct ROS scavenger. $OONO^{\cdot-}$ is much more potent than superoxide ($O_2^{\cdot-}$) in its ability to oxidize BH_4, and there is virtually no reaction between hydrogen peroxide (H_2O_2) and BH_4 (Kuzkaya et al., 2003). The BH_4 oxidized products generated in the reaction with $O_2^{\cdot-}$ and other oxidants are then recycled to regenerate BH_4 via salvage pathways by enzymes, such as DHFR and DHPR.

Some recent observations suggest that BH4 promotes proliferation of haemopoietic cells and other cell types (Tanaka et al., 1989). It has also been shown that BH_4 enhances the release of dopamine directly, independent of its cofactor action on tyrosine hydroxylase, by acting from the outside of neurons (Koshimura et al., 1994).

1.4 Nitric Oxide Synthase (NOS)

BH_4 is a critical cofactor for NOS. Not only is BH_4 critical for the production of optimal amounts of NO but a defect in BH_4 availability promotes $O_2^{\cdot-}$ production from NOS.

1.4.1 Role of BH_4 in NOS catalysis

There are three isoforms of the classical mammalian NOS, namely neuronal NOS (nNOS), inducible NOS (iNOS), and endothelial NOS (eNOS). The three NOS isoforms all contain a reductase and an oxygenase domain (Alderton et al., 2001). The N-terminal reductase domain binds to the flavin cofactors FAD and FMN that transfer electrons from NADPH to the heme group in the C-terminal oxygenase domain forming ferrous iron, which enables oxygen binding and formation of a ferrous-deoxy complex (Fe^{II}-O_2) (Figure 1.8). This electron transfer is dependent upon activation of the enzyme with calcium/calmodulin complex. Another electron is then transferred from BH_4, leading to formation of an iron-oxo (Fe^{II}-O) species that hydroxylates L-arginine to form N-hydroxy L-arginine (NOHA) and the BH3· radical. The second step of NO synthesis (NOHA oxidation to NO) involves a similar transfer of electrons to the BH3· radical, leading to regeneration of BH_4 (Griffith and Stuehr, 1995). In this regard, NOS differs from the amino acid hydroxylases that utilize BH_4 in that BH_2 is not formed and BH_4 is resynthesized during the NOS catalytic cycle.

Importantly, while NOS enzymes have the highest affinity for BH_4, other pterins such as BH_2, sepiapterin can also bind to NOS, but they do not support catalysis of NO. In this regard, oxidized species of BH_4 can act as competitive antagonists to

Figure 1.8 The general structure of the NOS enzymes. The functional NOS is a dimer formed of two identical subunits. There are three distinct domains in each NOS subunit: a reductase domain, a calmodulin-binding domain and an oxygenase domain.

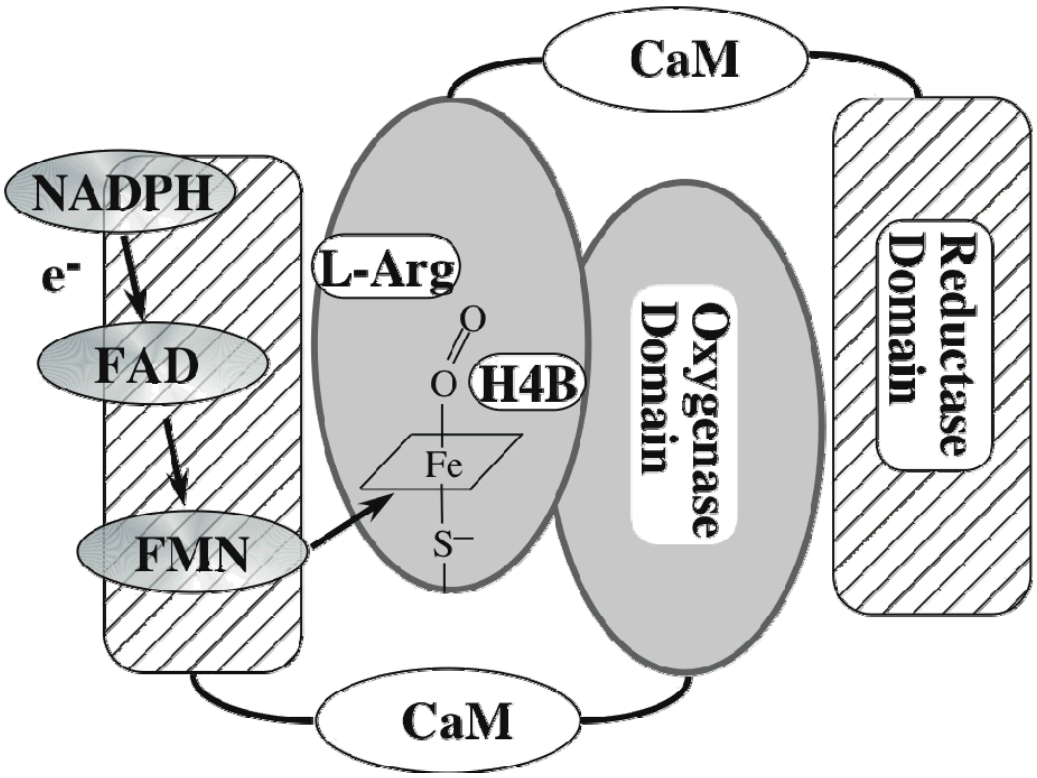

inhibit NO production.

Studies utilizing protein dissociation and limited proteolysis have revealed that dimerization of NOS is essential for its activity, facilitating correct structure of the active site for heme and L-arginine binding (Ghosh and Stuehr, 1995). It has been shown that BH_4 not only participates in catalytic activity but help form and maintain dimeric structure in all three NOS isoforms (Baek et al., 1993). Thus, BH_4 allosterically controls both function and structure of the NOS enzymes.

1.4.2 NOS uncoupling and production of superoxide

In the NO production process, BH_4 plays a critical role by reacting with the intermediate Fe^{II}-O_2 (formed from oxygen and heme), leading to formation of a heme-oxy species that reacts with L-arginine and N-hydroxy-L-arginine, ultimately leading to production of NO and L-citrulline (Wei et al., 2003). When BH_4 is absent, or oxidized, or in insufficient levels, reduction of the intermediate Fe^{II}-O_2 does not occur and it dissociates to release $O_2^{\cdot-}$. Studies using electron spin resonance demonstrated that the BH_4-deficient nNOS could produce $O_2^{\cdot-}$, and that this could be inhibited by the NOS inhibitor, L-N^G-Nitroarginine methyl ester (L-NAME) (Pou et al., 1992). Additional work demonstrated that eNOS similarly could produce $O_2^{\cdot-}$ in the absence of BH_4 (Vasquez-Vivar et al., 1998). This condition of $O_2^{\cdot-}$ production in the absence of appropriate cofactors is referred to as NOS uncoupling. Of note, oxidized forms of BH_4 can bind to NOS and serve as competitive antagonists to uncouple it (Presta et al., 1998). Thus, the ratio of BH_4 to oxidized forms of BH_4 could also influence NOS production of $O_2^{\cdot-}$

(Vasquez-Vivar et al., 2002). Importantly, in the setting of NOS uncoupling, both NO and $O_2^{\cdot-}$ are produced, leading to the formation of $OONO^{\cdot-}$, a potent oxidant that scavenges BH_4 and exacerbates NOS uncoupling.

In addition to BH_4 deficiency or oxidation, there are at least two other mechanisms that can cause NOS uncoupling. Some investigators have found that NOS is uncoupled when L-arginine is absent or present in sub-optimal levels (Vasquez-Vivar et al., 1998). Another mechanism for NOS uncoupling is oxidation of the zinc thiolate bond that forms the binding pocket for BH_4 (Zou et al., 2002).

1.4.3 Role of NOS uncoupling in vascular diseases

The state of NOS uncoupling is particularly relevant to endothelial dysfunction in various common pathological states. NOS uncoupling is associated with low NO levels and increased ROS production. Since NO has numerous important vascular protective functions including regulation of vasomotor tone, vasorelaxation, inhibition of leukocyte adhesion and smooth muscle cell proliferation, a reduction in NO bioavailability is detrimental to vascular homeostasis. Increased ROS production from NOS induces vascular changes by activating redox-sensitive signaling pathways. Under pathological conditions, increased ROS bioactivity leads to endothelial dysfunction, growth of vascular smooth muscle cells, monocyte invasion, lipid oxidation, inflammation, and increased deposition of extracellular matrix proteins. These are all major risk factors for vascular damage in various vascular diseases, such as hypertension, atherosclerosis, hypercholesterolemia, and diabetes.

The essential NOS cofactor BH_4 plays a crucial role in maintaining NOS in the optimal "coupled" state. Early in 1996, Higman et al. (Higman et al., 1996) demonstrated that saphenous veins from smokers produced less NO than veins from non-smokers and this difference was minimized by pretreatment of vessels with BH_4. In keeping with this, Stroes et al. (Stroes et al., 1997) showed that infusion of BH_4 could restore endothelial function in the forearm of humans with hypercholesterolemia. Pieper demonstrated that BH_4 treatment improved endothelium-dependent vasodilation in vessels from diabetic animals (Pieper, 1997). Subsequently, numerous studies have suggested that eNOS is uncoupled in a variety of common diseases including insulin resistance, diabetes (Hink et al., 2001), hypercholesterolemia (Laursen et al., 2001), and hypertension (Landmesser et al., 2003). In many of the cases, it has been found that the ratio of BH_4 to oxidized forms of biopterin is altered. Thus, BH_4 does not need to be depleted to uncouple the NOS enzymes if its oxidized forms accumulate in sufficient concentrations. These findings have led to a paradigm, illustrated in Figure 1.9. NADPH oxidases and other enzymes produce increased amounts of free radicals in response to a variety of pathophysiological stimuli, such as hypercholesterolemia, hypertension, diabetes, smoking, etc. These radicals can oxidize BH_4 to BH_2, which occupies the binding site of NOS, leading to impaired catalysis of NO and production of more ROS that promote the progression of vascular diseases. ROS also inhibits expression of the salvage enzyme DHFR, which further leads to accumulation of BH_2 and uncoupling of NOS. This represents a viscous cycle of increased

Figure 1.9 Effect of ROS and diseases on NOS uncoupling. Various enzymes, including the NADPH oxidases, produce oxidants in response to a variety of pathophysiological stimuli. These radicals can oxidize BH_4 to BH_2, which occupies the binding site of NOS, leading to impaired catalysis of NO and production of more ROS that promote the progression of vascular diseases. ROS can also inhibit expression of the salvage enzyme DHFR, which further leads to accumulation of BH_2 and uncoupling of NOS.

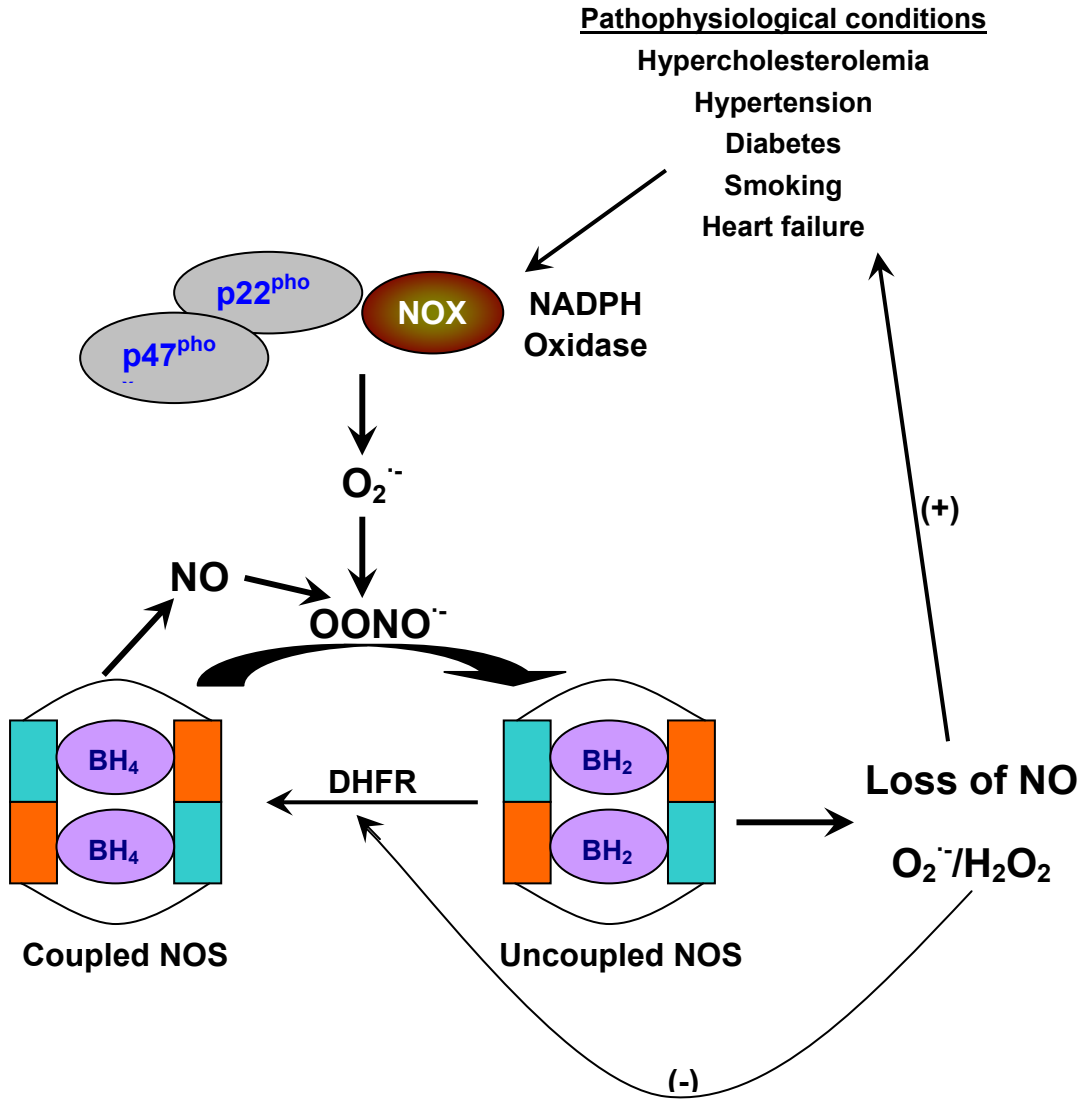

oxidative stress that promotes the progression of these diseases.

Given the crucial role of BH_4 in supporting NOS catalysis and maintaining adequate levels of NO as well as a balanced redox state, one might expect that measures to prevent NOS uncoupling, such as increasing levels of BH_4, would ameliorate vascular diseases. Indeed, there is substantial evidence to support this concept. In the study by Alp et al. (Alp et al., 2004), genetic enhancement of BH_4 in the endothelium reduced atherosclerosis in the aortic root. A recent study showed that oral BH_4 treatment of $ApoE^{-/-}$ mice not only reduced atherosclerotic lesion formation, but also decreased the content of inflammatory cells in the vessels (Schmidt et al., 2010). Several studies, including one from our own laboratory, have shown that BH_4 treatment lowers blood pressure in mice with DOCA-salt hypertension (Hong et al., 2001; Landmesser et al., 2003) and during chronic angiotensin II infusion (Kase et al., 2005). Efforts to increase BH_4 in the vessels might therefore provide an effective therapeutic option that corrects underlying pathophysiology in diseases like atherosclerosis and hypertension.

1.5 GTP Cyclohydrolase I (GTPCH-1) and regulation of BH_4 synthesis

The rate-limiting enzyme for *de novo* synthesis of BH_4 is GTP Cyclohydrolase I (GTPCH-1), which converts GTP to 7,8-dihydroneopterin triphosphate. This enzyme is constitutively expressed in many cells and tissues but with wide variation in activity with the liver showing the highest activity (Duch et al., 1984). GTPCH-1 is expressed in endothelial cells and its local enzyme function plays an important role in determining BH_4 levels in the endothelium.

1.5.1 GTPCH-1 structure

Crystal structure analysis has shown that GTPCH-1 exits as a homodecamer composed of two pentamers aligned face-to-face, assembled from five dimers arranged into a ring-like structure (Figure 1.10) (Nar et al., 1995b). Each active site is located at the interface of 3 subunits on the outer surface, 2 from 1 pentamer and 1 from the other; there are thus 10 equivalent active sites per functional unit (Nar et al., 1995a). As the committing and rate-limiting enzyme for BH_4 synthesis, GTPCH-1 is subject to direct regulation at transcriptional and posttranscriptional levels.

1.5.2 Regulation of GTPCH-1 gene expression

Several cytokines (TNF-α, INF-γ, IL-1) and lipopolysaccharide (LPS) alone or in combination with cytokines are known to increase GTPCH-1 transcription, enzyme activity, and BH_4 levels in human endothelial cells (Katusic et al., 1998). Insulin may also upregulate GTPCH-1 expression in endothelial cells via a phosphatidylinositol-3-kinase (PI3K) dependent pathway (Ishii et al., 2001). Increases in GTPCH-1 mRNA levels are also found in endothelial cells stimulated with statins (or HMG-CoA reductase inhibitors) (Hattori et al., 2003).

1.5.3 Post-translational modification of GTPCH-1

The transcriptional control of GTPCH-1 activity, however, is not the only mechanism increasing enzyme activity in endothelial cells. GTPCH-1 is also subject to post-translational modification by phosphorylation. Studies from our own libratory have shown that laminar shear stress stimulates GTPCH-1 phosphorylation at Serine 81 by Casein Kinase 2 in human aortic endothelial cells

Figure 1.10 Crystal structures of GTPCH-1 and GFRP. Panel A shows one-half of the GTPCH-1 homodecamer. Each of the 5 subunits is represented by a different color. GTP is shown bound to each of the subunits on the outer faces as depicted by the white arrow. Panel B shows the same structure rotated 90°. Figures are from the protein database (http://www.pdb.org/pdb/explore/explore.do?structureId=1N3R and (Rebelo et al., 2003)). Panel C shows crystal structure of GTPCH-1 homodecamer in complex with two homopentamers of the GTP cyclohydrolase feedback regulatory protein (GFRP) and is adapted from (Maita et al., 2004).

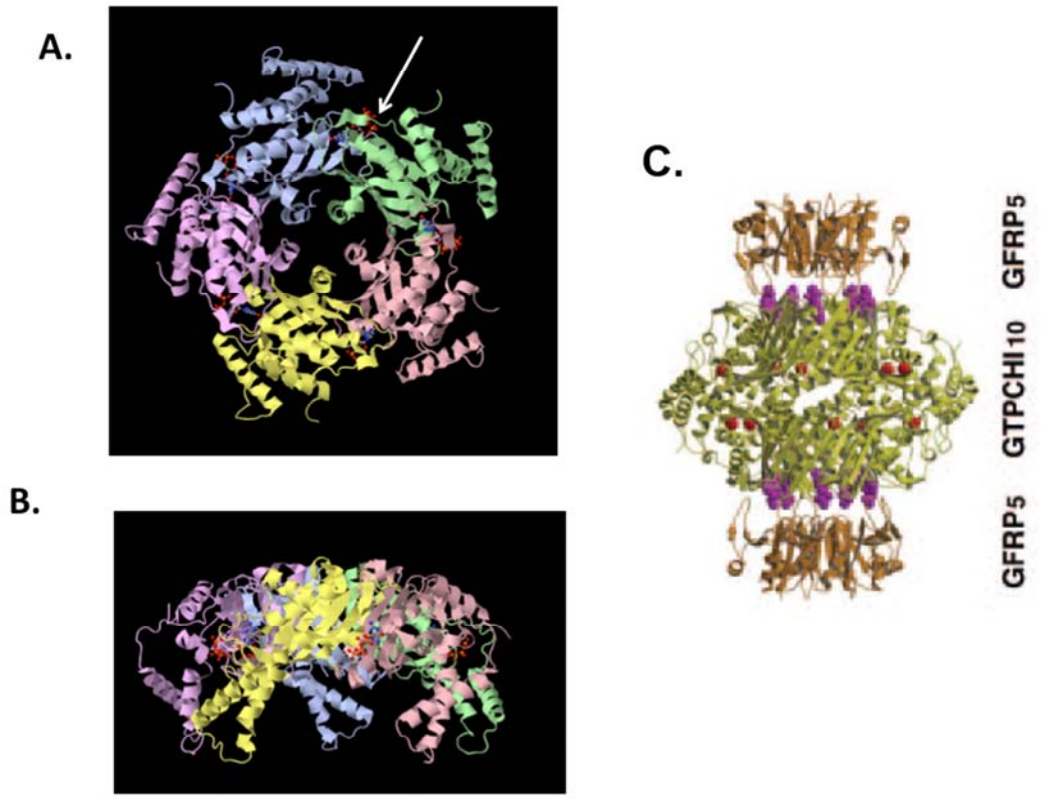

(HAECs) (Widder et al., 2007). Phosphorylation of the enzyme is accompanied by a 30-fold increase in the activity of GTPCH-1. Interestingly, oscillatory shear stress only modestly affects these parameters. This study identified a novel phosphorylation site on GTPCH-1 and provided evidence that phosphorylation of the enzyme dramatically modulates its enzymatic function. In other cell types, for example, rat mesangial cells, angiotensin II and platelet-derived growth factor are reported to increase GTPCH-1 activity by phosphorylation via a protein kinase C-dependent mechanism (Lapize et al., 1998).

1.5.4 GTPCH-1 protein interactions

GTPCH-1 activity is governed by interactions with GTPCH-1 feedback regulatory protein (GFRP). GFRP exists as a homopenatmer and one GTPCH decamer forms a complex with two GFRP pentamers (Figure 1.10) (Yoneyama et al., 1997). The activity of GTPCH-1 is regulated both negatively and positively by BH_4 and phenylalanine, which are bound at the interface of the two proteins. Studies using purified proteins suggest that binding of phenylalanine at this site increases GTPCH-1 activity, while binding of BH_4 inhibits its activity (Yoneyama and Hatakeyama, 1998). GFRP expression has been documented in various cell types and is highly expressed in hepatocytes (Milstien et al., 1996), but whether GFRP has a biologically important role in regulating GTPCH-1 activity in endothelial cells remains to be determined.

1.6 Summary

Current research indicates that maintenance of adequate BH_4 levels in the

endothelium is critical in regulating the balance of NO and $O_2^{\cdot-}$ production by NOS. Cellular BH_4 levels are under the control of GTPCH-1 and the redox state in the cell. Strategies to maintain BH_4 availability may include measures to increase BH_4 biosynthesis or to reduce BH_4 oxidation, and have shown beneficial effects in various animal models of vascular diseases.

GTPCH-1 plays a key role in modulating BH_4 biosynthesis; however, very little is understood about the mechanisms by which GTPCH-1 is regulated by phosphorylation and interaction with its regulatory protein as well as the interplay between these two properties in intact cells and in vivo. A better understanding of cellular regulation of endogenous BH_4 biosynthesis, particularly of GTPCH-1 activity, would lead to new therapeutic approaches other than exogenous BH_4 supplementation.

Mechanical forces have an enormous impact on endothelial biology and the development of vascular diseases. It remains unclear how GTPCH-1 activity and BH_4 levels are regulated by different shear patterns both in vitro and in vivo, and whether this plays a role in the predisposition of atherosclerosis at sites of flow disturbance in the circulation.

1.7 Objectives of this dissertation

Based on the above-mentioned studies that highlight the important role of endothelial BH_4 levels in regulating the balance of NO and $O_2^{\cdot-}$ production by NOS, this dissertation sought to explore the mechanisms of endothelial GTPCH-1 regulation and BH_4 biosynthesis and their roles in atherosclerosis at areas of

disturbed flow. This dissertation also attempted to explore therapeutic approaches to augment levels of cellular BH_4, especially at sites of disturbed flow where BH_4 levels are insufficient to promote proper NOS function.

The first objective of this dissertation was to understand the interplay between GTPCH-1 phosphorylation and GFRP and their roles in regulating BH_4 levels and NO production in the endothelium. This interplay was studied under the settings of different shear forces to understand how this regulates BH_4 levels and NOS uncoupling. The second objective of this dissertation was to determine whether BH_4 is reduced at areas of disturbed flow and if this is responsible for augmented atherosclerosis at these sites. The final objective of this dissertation was to identify novel pharmacological agents to promote dissociation of GFRP and GTPCH-1. We postulate that agents such as these will increase endogenous production of BH_4, and will prevent a decline in BH_4 and NOS uncoupling in the setting of disturbed flow.

Chapter 2:

The interplay between GTPCH-1 phosphorylation and GFRP and their roles in regulating endothelial BH_4 levels and NO production[1]

[1]A portion of this chapter is published in: Li L, Rezvan A, Salerno JC, Husain A, Kwon K, Jo H, Harrison DG, Chen W.(2010) GTP cyclohydrolase I phosphorylation and interaction with GTP cyclohydrolase feedback regulatory protein provide novel regulation of endothelial tetrahydrobiopterin and nitric oxide. *Circ Res.* **106(2)**:328-36 (Li et al., 2010).

2.1 Introduction

Our laboratory has previously found that laminar shear stress dramatically increases BH_4 levels and enzymatic activity of GTPCH-1, whereas oscillatory shear only modestly affects BH_4 levels and GTPCH-1 activity in human aortic endothelial cells (HAECs) (Widder et al., 2007). Notably, for the first time we discovered that laminar, but not oscillatory shear, stimulates phosphorylation of GTPCH-1 on Ser 81 (S81) by Casein Kinase II alpha prime (CK2α') subunit. We raised phospho-specific antibodies for GTPCH-1 and showed an increase of phosphorylation in a time-dependent manner responsive to laminar shear stress.

It is known that CK2 is usually constitutively active (Litchfield, 2003) and phosphorylates a large number of substrates when their phosphorylation sites are exposed upon release from their binding partners (Wang et al., 2000). This would suggest that GTPCH-1 binding proteins might modulate its activity by influencing its phosphorylation. Two known binding partners for GTPCH-1 are Activator of Hsp90 ATPase (Aha1) and GTP cyclohydrolase I feedback regulatory protein (GFRP). GFRP has been reported to interact with GTPCH-1 and both inhibit and stimulate GTPCH-1 activity in vitro depending on the presence of either BH_4 or phenylalanine (Yoneyama and Hatakeyama, 1998). Aha1 has been shown to participate in the Hsp90 chaperone cycle by stimulating the low intrinsic ATPase activity of Hsp90 (Panaretou et al., 2002). However, the roles of Aha1 and GFRP in modulating GTPCH-1 activity and BH_4 levels in the endothelium remain unclear.

GTPCH-1 undergoes negative feedback regulation by its end product BH_4 via interaction with GFRP. Negative feedback is a ubiquitous mechanism that

maintains the end-product of many enzymes within a very narrow range, and if fully functional in the case of GTPCH-1, should prevent large changes in intracellular BH_4. However, we found that laminar shear stress promotes phosphorylation of GTPCH-1 at S81 and markedly increases its enzymatic activity and BH_4 levels by 30-fold in HAECs (Widder et al., 2007). This finding would suggest that laminar shear, and perhaps S81 phosphorylation of GTPCH-1, disrupts the negative feedback conferred by GFRP in endothelial cells.

This study was therefore performed to understand the role of GFRP in modulating GTPCH-1 phosphorylation, BH_4 levels and NO production in endothelial cells. I also determined how GTPCH-1 phosphorylation affects its enzyme activity and its association with GFRP and whether this interaction is affected by shear stress. I compared the effects of unidirectional laminar shear to oscillatory shear stress in attempt to understand differences of GTPCH-1 regulation by GFRP in responses to these two mechanical stimuli. My findings illustrate a new, previously unknown mechanism for regulation of GTPCH-1 activity in endothelial cells, which involves its phosphorylation and interaction with GFRP.

2.2 Materials and methods

2.2.1 Recombinant DNA Plasmids

Human GTPCH-1 cDNA was obtained form GeneCopoeia (Cat.No.EX-X0381-M07) and was cloned into the pCMV-HA vector (Clontech) and the pEGFP-C1 vector (Clontech) to create pCMV-HA/GTPCH-1 and pEGFP/GTPCH-1 constructs, respectively. Serine 81 in pCMV-HA/GTPCH-1 was

changed to an alanine and an aspatate to produce the GTPCH-1 mutants S81A and S81D respectively using the QuikChange II Site-Directed Mutagenesis Kit (Stratagene). Prokaryotic expression of wild-type, S81D and S81A GTPCH-1 was accomplished by cloning these into the pET-30a(+) vector (EMDBiosciences, Madison, WI). The human GFRP cDNA was synthesized by Genscript (Piscataway, NJ) and cloned into the pDsRed-Monomer-C1 vector (Clontech), the pGEX-5X-3 vector (GE Healthcare) and the pET-15b vector (EMDBiosciences, Madison, WI) to create pDsRed/GFRP, pGEX-5X-3/GFRP and pET-15b/GFRP constructs, respectively. Rluc8 cDNA was amplified from the construct pcDNA3.1-Rluc8, which was kindly provided by Andreas Loening and Sanjiv Gambhir (Stanford University, Stanford, CA). PCR product for Rluc8 coding region was inserted in-frame into pEGFP/GTPCH-1 replacing the EGFP cDNA to generate Rluc8/GTPCH-1. The Venus/GFRP construct was prepared from the construct pcS2-Venus kindly provided by Atsushi Miyawaki (RIKEN BrainScience Institute, Wako-city, Japan). A PCR product for the Venus coding sequence was substituted in-frame into pDsRed/GFRP replacing the DsRed cDNA. DNA sequencing was used to confirm construct sequences (Agencourt Biosciences, Beverly, MA).

2.2.2 Cell Culture, Transfection Procedure and Shear Apparatus

Human Aortic Endothelial Cells (HAEC) were purchased from Lonza (Walkersville, MD) and used between the 3rd and 6th passages. Plasmids were transfected in HAECs using PrimeFect II (Lonza). HAECs were transfected with small interfering (si)RNA against GFRP (sense: GCCUUGGGAAACAACUUUUtt)

or transfected with a non-silencing control sequence (Applied Biosystems/Ambion, Austin, TX) as described previously (Widder et al., 2007). Laminar (15 dynes/cm^2) and oscillatory shear (±15 dynes/cm^2) were applied using a cone-in-plate viscometer with a 0.5˚ angle in an incubator at 37˚C in 5% CO_2 for 14 hours (McNally et al., 2003).

2.2.3 Antibodies and western blot analysis

Antibodies against eNOS and P-S1177 eNOS were purchased from BD Biosciences (San Jose, CA). Antibodies against CK2α', HA-tag and His-Tag were purchased from Santa Cruz Biotechnology (Santa Cruz, CA) and Cell Signaling Technology (Danvers, MA), respectively. An anti-Actin antibody (Sigma-Aldrich) was used for protein loading control. The Phospho-S81 GTPCH-1 antibody was described previously (Widder et al., 2007). An anti-GTPCH-1 rabbit polyclonal antibody was generated against a synthesized peptide, MEKPRGVRCTNGFPERE, which corresponds to amino acid residues 1-17 of rat GTPCH-1 (GenBank accession number NP 077332). An anti-GFRP rabbit polyclonal antibody was generated against a synthesized peptide, DPELMQHLGASKRRAL, which corresponds to amino acid residues 25-40 of human GFRP (GenBank accession number NP 005249). Anti-GFRP IgG was purified from rabbit serum and tested using both purified GFRP and mouse liver lysates for western blotting. Cells were washed twice in cold PBS and scraped in 1X RIPA lysis buffer (Millipore, Billerica, MA) supplemented with Complete Protease Inhibitor Cocktail Tablet (Roche). Thirty μg of supernatant was separated by 12.5% SDS-PAGE and transferred to nitrocellulose membranes

(Amersham Biosciences, UK). Membranes were probed using antibodies described above. Immunoreactive bands were visualized by enhanced chemiluminescence detection (GE Healthcare). Densitometry was performed with Quantity One software (Bio-Rad Laboratories).

2.2.4 Real-time PCR analysis

Endothelial cDNA was amplified using 7500 Fast Real Time PCR system (Applied Biosystems). Taqman primers for human GFRP were purchased from Applied Biosystems (Assay ID Hs00193360_m1). The resulting mRNA levels were normalized to the levels of human GAPDH mRNA.

2.2.5 BH_4, GTPCH-1 activity, NO and $O_2^{\bullet-}$ measurements

Endothelial BH_4 levels and GTPCH-1 activity were measured by high-performance liquid chromatography (HPLC) as previously described (Widder et al., 2007). For analysis of wild type GTPCH-1, S81D activity, a kinetic microplate assay was utilized as previously described in the presence of GTP and BH_4 (Kolinsky and Gross, 2004). Endothelial cell NO production was measured by electron spin resonance (ESR) using the specific colloid probe Fe^{2+} diethyldithiocarbamate ($Fe[DETC]_2$) as described (Hart et al., 2005). $O_2^{\bullet-}$ production in HAECs was measured by quantifying formation of 2-hydroxyethidium from dihydroethidium (10 μM) by HPLC. This product specifically reflects the reaction of $O_2^{\bullet-}$ with dihydroethidium and has been validated previously (Fink et al., 2004).

2.2.6 GST and His Pull-down Assays

To detect association of GST-GFRP with His-tagged GTPCH-1, the ProFound Pull-Down GST Protein:Protein Interaction Kit (Pierce, Rockford, IL) was employed. E. coli (strain BL21) was transformed with pGEX-5X-3/GFRP and cultured overnight in LB medium. The culture was then diluted 1:100 with pre-warmed LB and incubated at 37°C with vigorous shaking. Recombinant GST-GFRP was obtained by isopropyl-β-d-thiogalactopyranoside (IPTG, 0.5 mmol/L) induction for 4 h at 30°C. Two mg of E. Coli lysate was incubated with 150 μg of purified His-GTPCH-1 recombinant protein in a buffer containing 10 μmol/L BH_4, 100 μmol/L GTP and 100 μmol/L ascorbic acid (Buffer A) or 1mmol/L L-phenylalanine (Buffer B). Protein complexes were eluted according to the manufacturer's instructions and then separated on 12.5% gel by SDS–PAGE, followed by Western blot analysis using anti-His tag and anti-GFRP antibodies.

For His pull-down assay, 50 μg of purified His-tagged GTPCH-1 recombinant protein was incubated with 50 μl of Ni-NTA (nickel-nitrilotriacetic acid) magnetic agarose beads (Qiagen, Valencia, CA) in protein binding buffer, according to the manufacturer's protocol. The beads and attached protein were separated from the buffer by using a magnetic separator, and then incubated with E.Coli lysate containing GST-GFRP fusion protein in buffer A. After washing once with the interaction buffer, the beads were heated in SDS-PAGE sample buffer and proteins analyzed by SDS-PAGE followed by western blotting using anti-His tag and anti-GFRP antibodies.

2.2.7 Immunoprecipitation and Immunoblotting

Cells were harvested in 1X RIPA lysis buffer (Millipore) supplemented with Complete Protease Inhibitor Cocktail Tablet (Roche). Supernatants (400 μg total protein) were pre-cleared with 20 μL of protein A/G Plus agarose beads (Santa Cruz Biotechnology) for 6 h at 4˚C and incubated overnight at 4˚C with 20 μL of protein A/G Plus agarose beads and 3 μL of anti-DsRed polycolonal antibody (Clontech), or an equal amount of non-immune rabbit IgG as a control. After four washes in phosphate-buffered saline buffer (PBS), the immunoprecipitated proteins were separated by SDS-PAGE, transferred to nitrocellulose membranes, and immunoblotted with anti-HA (Cell Signaling Technology) or our custom made anti-GFRP antibodies.

2.2.8 Spectral FRET imaging

HAECs were transfected with genes encoding AcGFP-GTPCH-1 and DsRed-GFRP using the transfection method described above. The imaging system used here was a Zeiss 510 Meta confocal microscope, and the system was controlled using the LSM software. A 63 × oil NA 1.4 objective lens was used for the studies described here. The Zeiss 510 system collects lambda stacks - a series of x–y images that sample emission wavelengths from a range of small wavelength bands (10.7 nm). A mathematical algorithm defines the spectral signature for each pixel of the scanned confocal image, which allows digital separation of the component signals. The spectral FRET images were obtained by using a spectral FRET macro program embedded in the LSM software.

2.2.9 BRET Assay

HAECs were transfected with genes encoding Rluc8-GTPCH-1 and Venus-GFRP using the transfection method described above. Forty-eight hours after transfection, cells were detached with Trypsin/EDTA and washed once with PBS. BRET assays were performed in 96-well isoplates (Perkin–Elmer, Boston, MA) using approximately 100,000 cells resuspended in 180 µL of PBS. Coelenterazine h substrate (Invitrogen) was added at a final concentration of 5 µM, and luminescent readings at 460 and 528 nm wavelengths were collected immediately thereafter using a Synergy™ HT Multi-Mode Microplate Reader (Biotek, Winooski, VT). The BRET ratio was determined as described previously (Pfleger et al., 2006). In preliminary experiments, evidence for specific interaction was established by showing that transfection with increasing amounts of acceptor (Venus-GFRP) plasmid to a constant amount of donor (Rluc8-GTPCH-1) plasmid led to a linear increase in BRET ratio which saturated at a ratio of approximately 0.1 (Figure 2.1). A donor:acceptor ratio of 1:4 was used as this represented the mid-point of the saturation curve. Co-expression of empty Rluc8 and Venus-GFRP led to a minimal BRET signal (Figure 2.1).

2.2.10 CK2α' Kinase Assay

CK2α' was immunoprecipitated from cell extracts by an anti-CK2α' antibody (Santa Cruz Biotechnology) and enzyme activity was measured using a Casein Kinase 2 Assay Kit (Millipore) according to the manufacture's instructions. Kinase activity was calculated by subtracting the mean of the background control samples without enzyme from the mean of samples with enzyme.

Figure 2.1 BRET saturation curve for constitutive interaction between GTPCH-1 and GFRP. Increasing amounts of Venus-GFRP was co-expressed with a constant amount of Rluc8-GTPCH-1 in HAECs. BRET ratios are plotted as a function of the ratio of Venus-GFRP over Rluc8-GTPCH-1 DNA. The Rluc8 empty vector was used as a negative control.

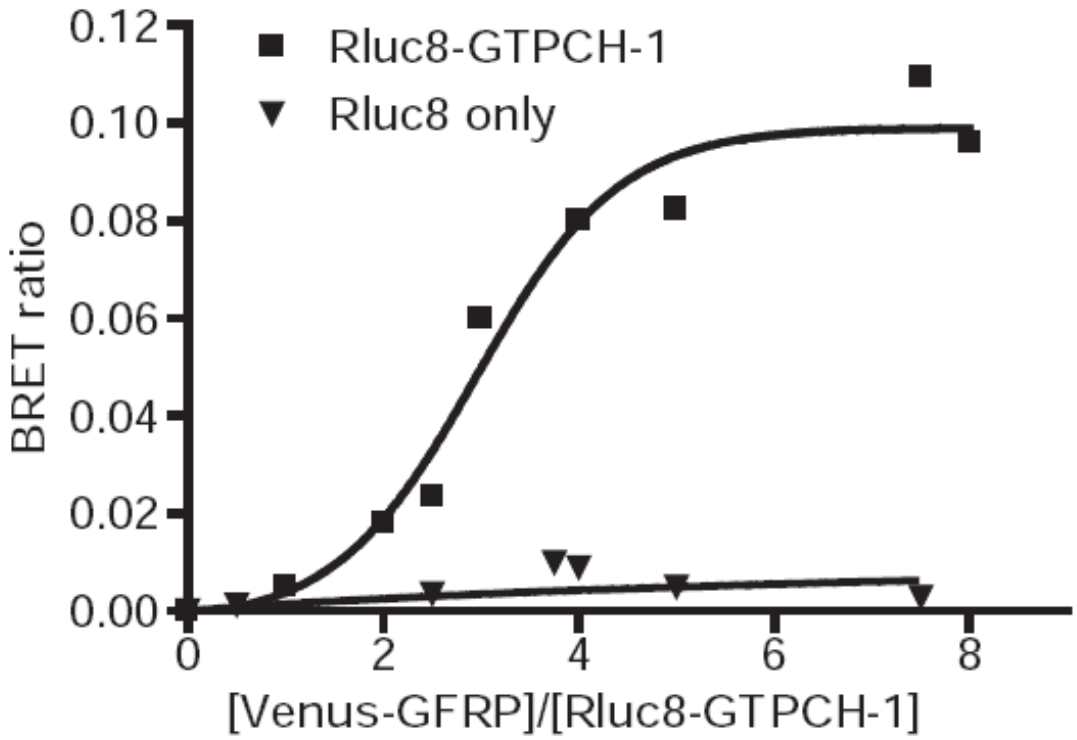

2.2.11 Statistical Analysis

All values are means ± standard error of the means (SEM). The data were compared between groups by t test when comparison between two groups was performed and by ANOVA for multiple comparisons. When significance was indicated by ANOVA, the Bonferroni post hoc test was used to make selected comparisons and the Dunnett post hoc test was used when one group was served as a control. A value of $p<0.05$ was considered significant.

2.3 Results

2.3.1 Interaction of GTPCH-1 with Activator of Hsp90 ATPase (Aha1) and its role in modulating endothelial BH_4 levels

GTPCH-1 was found to interact with Aha1 by using a yeast 2-hybrid screening and this interaction was validated by GST pull-down assay (Swick and Kapatos, 2006). It has been shown that Aha1 binds to the middle domain of Hsp90, contributing to client protein activation (Lotz et al., 2003). Because association of Hsp90 with eNOS activates eNOS to release NO (Garcia-Cardena et al., 1998), we speculate that Aha1 may recruit GTPCH-1 into the eNOS/Hsp90 complex to support endothelial NO production through the local synthesis of BH_4. We hypothesize that laminar shear may dissociate GTPCH-1 from the eNOS/Hsp90/Aha1 complex to allow its phosphorylation by CK2. I found that HAECs express Aha1 by Western blot and confirmed that GTPCH-1 binds to Aha1 in HAECs by co-IP. Interestingly, the interaction between HA-tagged GTPCH-1 and endogenous Aha1 and Hsp90 was reduced in cells exposed to laminar shear compared to cells under static conditions

(Figure 2.2A). However, down-regulation of Aha1 by siRNA transfection did not affect HAEC BH_4 levels (Figure 2.2B and 2.2C), suggesting that Aha1 has a minimal role in modulating GTPCH-1 activity and BH_4 levels in endothelial cells.

2.3.2 Effect of GFRP on GTPCH-1 S81 phosphorylation and activity in HAECs

While GFRP has been shown to both inhibit and stimulate GTPCH-1 activity in vitro depending on interactions with either BH_4 or phenylalanine (Harada et al., 1993), the role of GFRP in the endothelium in modulating BH_4 levels and NO production remains unclear. Using real-time PCR, I found GFRP mRNA is abundant in HAECs. To determine the role of GFRP in regulating GTPCH-1 activity and BH_4 levels in HAECs, I examined the consequences of specific disruption of GFRP in the endothelial cells using siRNA. GFRP siRNA decreased GFRP mRNA by 80%, but did not change levels of GTPCH-1 protein, eNOS protein or eNOS S1177 phosphorylation (Figure 2.3A and 2.3B). Importantly, siRNA inhibition of GFRP expression increased GTPCH-1 S81 phosphorylation in a manner similar to that induced by unidirectional laminar shear (Figure 2.3C and 2.3D). I also found that down-regulation of GFRP by siRNA markedly increased HAEC BH_4 levels and GTPCH-1 enzyme activity (Figure 2.3E and 2.3F). Of note, following down-regulation of GFRP, shear no longer increased BH_4 levels or GTPCH-1 activity. This finding suggests that GFRP is critical for the increase in endothelial BH_4 and GTPCH-1 activity induced by laminar shear. Finally, down-regulation of GFRP by siRNA substantially increased endothelial cell production of NO (Figure 2.3G). In contrast to these effects of GFRP siRNA, non-silencing RNA had no

Figure 2.2 Interaction of GTPCH-1 and Aha1 and the effect of Aha1 in modulating BH4 levels in HAECs. A, Co-IP of transfected HA-GTPCH-1 and endogenous Aha1 and Hsp90 in HAECs. HAECs transfected with HA-GTPCH-1 were exposed to laminar shear for 14 hours and the cell lysates were subjected to immunoprecipitation using anti-HA (IP: HA) antibody and Western blot using antibodies against Aha1 and Hsp90. B, Aha1 protein levels in HAECs detected by Western blot after transfection of siRNA against Aha1 and a non-silencing RNA. C, BH4 levels in HAECs after transfection of siAha1 determined by HPLC. (n=5).

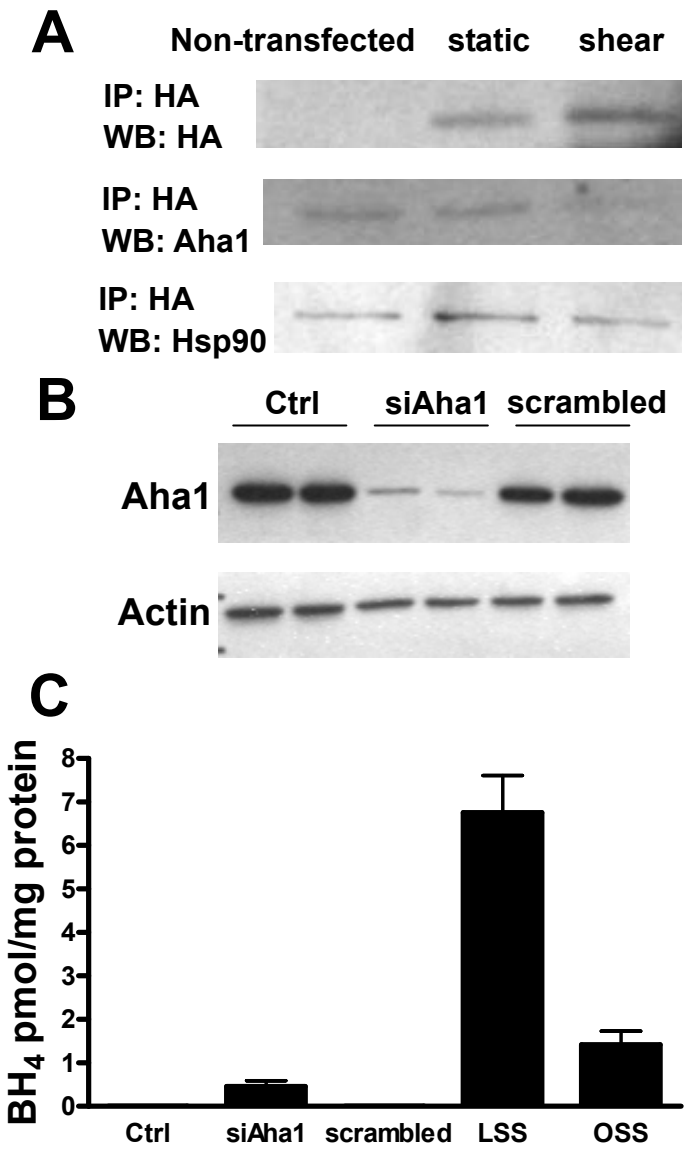

Figure 2.3 Effect of GFRP down-regulation by siRNA in modulating endothelial GTPCH-1 S81 phosphorylation and activity, BH_4 levels and NO production. HAECs were transfected with either a non-silencing siRNA or GFRP siRNA, or not transfected. A, GFRP mRNA levels measured using real-time PCR (n=4). B, Protein levels determined by western blotting for GTPCH-1, phospho-S1177 eNOS and total eNOS in HAECs transfected with either a non-silencing siRNA or GFRP siRNA, or not transfected. Actin was used as a loading control. C, Representative western blot for S81 phospho-GTPCH-1 in HAECs exposed to 14 hours of laminar sheer stress and in cells transfected with siRNA against GFRP or a non-silencing control siRNA. D, Densitometry values for phospho/total GTPCH-1 (n=3). E, BH_4 levels determined using HPLC (n=4-5). F, GTPCH-1 activity measured by HPLC (n=6-7). G, NO production measured using ESR (n=6).

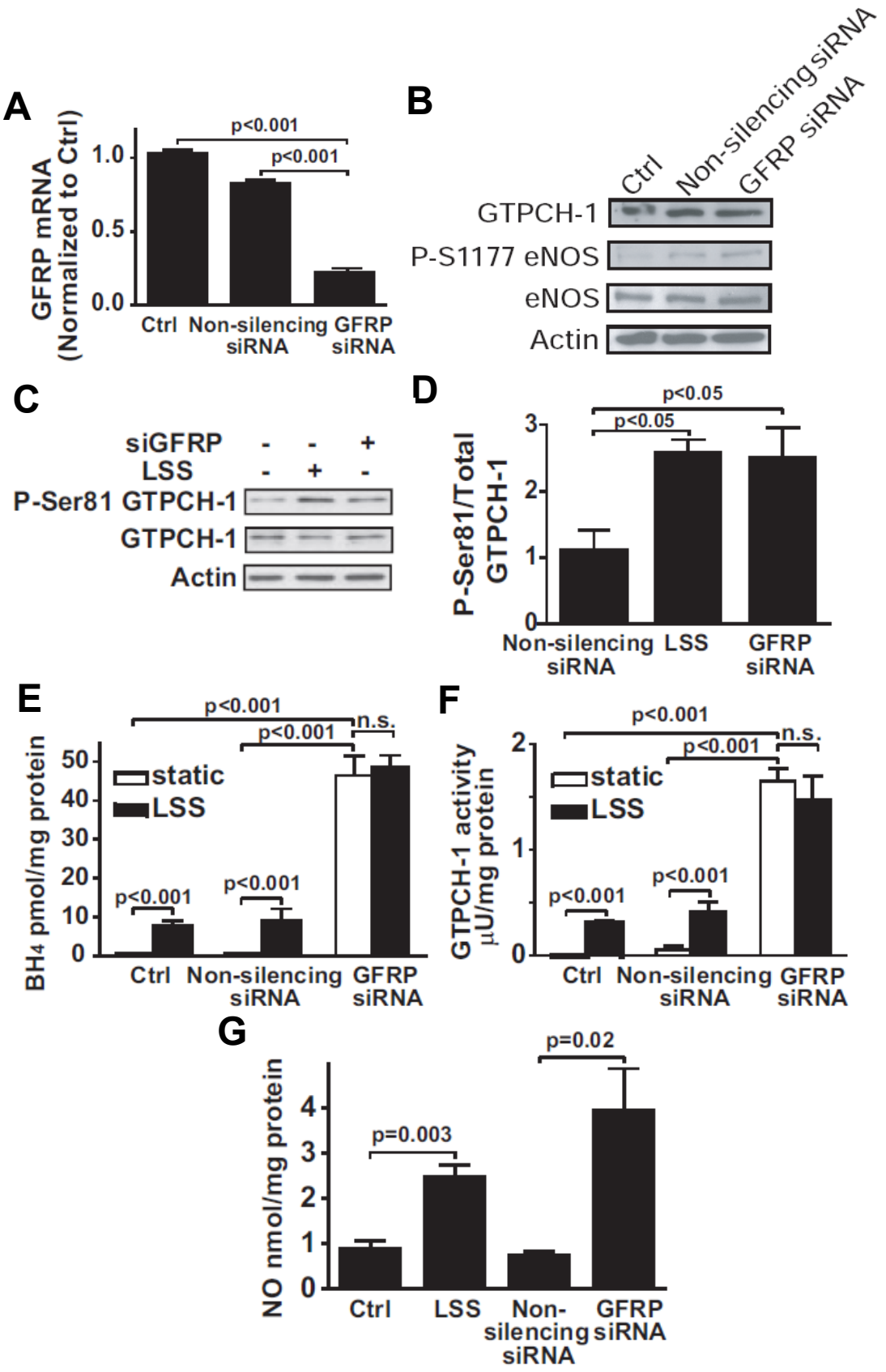
A
GFRP mRNA (Normalized to Ctrl)
1.0
0.5
0.0
p<0.001
p<0.001
Ctrl
Non-silencing siRNA
GFRP siRNA
B
Ctrl
Non-silencing siRNA
GFRP siRNA
GTPCH-1
P-S1177 eNOS
eNOS
Actin
C
siGFRP - - +
LSS - + -
P-Ser81 GTPCH-1
GTPCH-1
Actin
D
P-Ser81/Total GTPCH-1
3
2
1
0
p<0.05
p<0.05
Non-silencing siRNA
LSS
GFRP siRNA
E
BH4 pmol/mg protein
50
40
30
20
10
0
static
LSS
p<0.001
p<0.001
p<0.001
n.s.
Ctrl
Non-silencing siRNA
GFRP siRNA
F
GTPCH-1 activity μU/mg protein
2
1
0
static
LSS
p<0.001
p<0.001
p<0.001
n.s.
Ctrl
Non-silencing siRNA
GFRP siRNA
G
NO nmol/mg protein
4
3
2
1
0
p=0.003
p=0.02
Ctrl
LSS
Non-silencing siRNA
GFRP siRNA

effect on GTPCH-1 activity, BH_4 levels or NO production. Thus, GFRP plays an inhibitory role in regulation of human endothelial cell GTPCH-1 enzyme activity, BH_4 levels and NO production in part by mediating S81 phosphorylation.

To further examine the role of GFRP in modulation of endothelial cell GTPCH-1 phosphorylation and activity, I overexpressed GFRP in HAECs and exposed these cells to either static or shear conditions. Overexpression of GFRP alone almost completely abolished the increase in GTPCH-1 S81 phosphorylation caused by laminar shear (Figure 2.4A and 2.4B). Likewise, GFRP overexpression also suppressed the increase in BH_4 levels, GTPCH-1 enzyme activity and NO production caused by laminar shear (Figure 2.4C through 2.4E). I also co-transfected HAECs with GFRP and GTPCH-1. As expected, transfection of HAECs with GTPCH-1 alone significantly increased BH_4 levels, whereas co-transfection of GTPCH-1 with GFRP prevented this effect (Figure 2.4F and 2.4G). These findings further support the concept that GFRP negatively regulates GTPCH-1 phosphorylation and BH_4 levels at baseline and in response to laminar shear stress in human endothelial cells.

2.3.3 Interaction of GTPCH-1 and GFRP in endothelial cells

I used three approaches to study the interaction between GTPCH-1 and GFRP in human endothelial cells: co-immunoprecipitation (co-IP), fluorescence resonance energy transfer (FRET) and a bioluminescence resonance energy transfer (BRET).

To study the interaction of these two proteins by using co-IP, I overexpressed HA-tagged human GTPCH-1 and DsRed-tagged human GFRP in HAECs and

Figure 2.4 Effect of GFRP overexpression on endothelial GTPCH-1 S81 phosphorylation and BH_4 levels. A, Representative western blot for S81 phospho-GTPCH-1 in HAECs transfected with GFRP cDNA or a vector control cDNA and exposed to 14 hours of laminar sheer stress or static conditions. B, Densitometry values for phospho/total GTPCH-1 (n=4). C, BH_4 levels in HAECs transfected with GFRP cDNA or a vector control cDNA and exposed to either laminar shear or static condition for 14 hours (n=4-5). D, GTPCH-1 activity measured by HPLC (n=5-6). E, NO production measured using ESR (n=5-6). F, Western blots for overexpressed GTPCH-1 and GFRP in HAECs co-transfected with HA-GTPCH and DsRed-GFRP. Western blot analysis was performed using antibodies against HA and DsRed, respectively. G, BH_4 levels in HAECs co-transfected with HA-GTPCH and DsRed-GFRP (n=4-5).

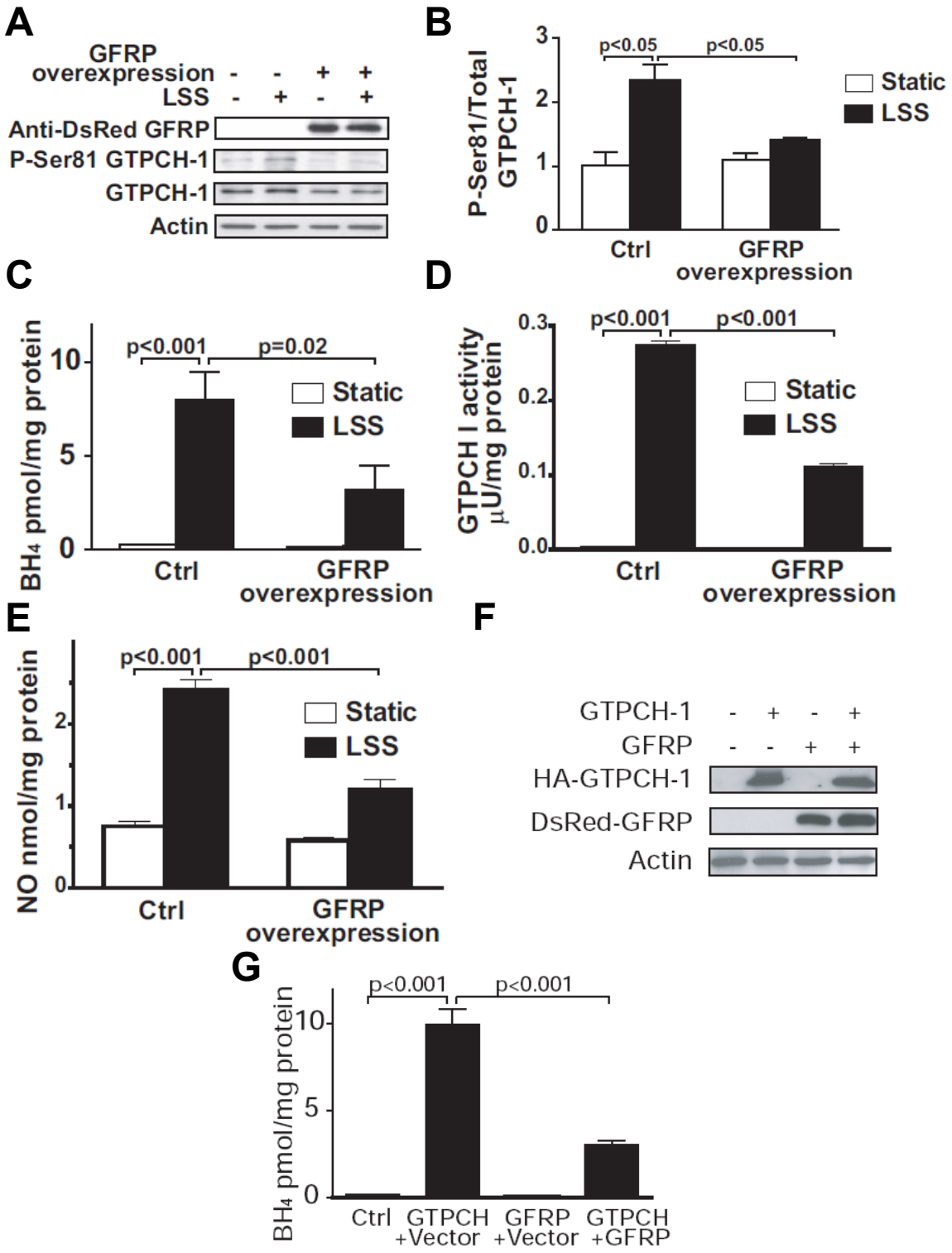
A
GFRP overexpression - - + +
LSS - + - +
Anti-DsRed GFRP
P-Ser81 GTPCH-1
GTPCH-1
Actin
B
P-Ser81/Total GTPCH-1
p<0.05
p<0.05
Static
LSS
Ctrl
GFRP overexpression
C
BH4 pmol/mg protein
p<0.001
p=0.02
Static
LSS
Ctrl
GFRP overexpression
D
GTPCH I activity μU/mg protein
p<0.001
p<0.001
Static
LSS
Ctrl
GFRP overexpression
E
NO nmol/mg protein
p<0.001
p<0.001
Static
LSS
Ctrl
GFRP overexpression
F
GTPCH-1 - + - +
GFRP - - + +
HA-GTPCH-1
DsRed-GFRP
Actin
G
BH4 pmol/mg protein
p<0.001
p<0.001
Ctrl
GTPCH +Vector
GFRP +Vector
GTPCH +GFRP

obtained successful overexpression of both proteins. HA-GTPCH-1 was co-immunoprecipitated from HAECs by an anti-DsRed antibody, indicating the interaction of GTPCH-1 and GFRP in HAECs (Figure 2.5A and 2.5B).

The FRET technique has become a state-of-the-art tool to demonstrate interactions if the distance between two proteins is less than 10 nm. A common difficulty for FRET acquisition and analysis is that the spectral overlap of the donor and acceptor often leads to a substantial fluorescence background that interferes with the detection of the FRET signals. In the method that we have adapted, spectral FRET allows the removal of the donor and acceptor spectral bleedthrough to the FRET signal. The spectral signatures for the donor and acceptor references are first obtained and linear unmixing is then used to separate the contributions of donor or acceptor signals in each pixel of an acquired FRET image, generating a net FRET image (Zimmermann, 2005). When imaging a real FRET sample, usually only a percentage of perfect FRET occurs and real FRET is a mix of perfect FRET and no FRET in a certain percentage. The FRET efficiency (in %) is calculated from FRET Intensity / (FRET + Donor + Acceptor intensities) x 100.

In this study, I employed confocal FRET microscopy to detect the interaction between GTPCH-1 and GFRP, using Aequorea coerulescens green fluorescent protein (AcGFP) and red fluorescence protein (DsRed). I prepared the first fusion protein of AcGFP-GTPCH-1 as the donor and the second fusion protein of DsRed-GFRP as the acceptor (Figure 2.6A). The FRET images allow me to directly visualize the protein-protein interactions and also quantify the extent of

Figure 2.5 Interaction of GTPCH-1 and GFRP in HAECs by co-immunoprecipitation. A, HAECs were co-transfected with HA-GTPCH-1 and DsRed-GFRP constructs and the cell lysates were subject to Western blot using antibodies against HA-tag and GFRP. B, HAECs co-transfected with HA-GTPCH-1 and DsRed-GFRP constructs were subjected to immunoprecipitation using anti-DsRed (IP:DsRed) antibody. IgG was used as a control for co-IP.

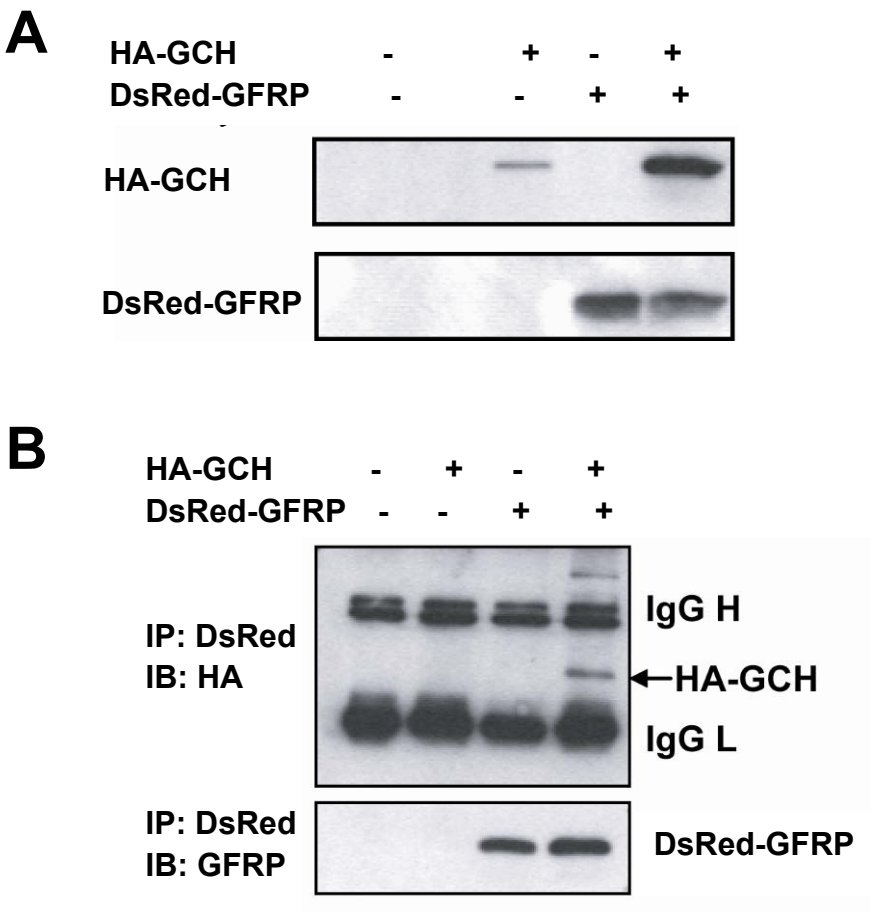

Figure 2.6 Colocalization and FRET imaging of GFP-tagged GTPCH-1 and DsRed-tagged GFRP. A, Illustration of FRET methodology for studying the interaction between GTPCH-1 and GFRP. B, Colocalization of GFP-tagged GTPCH-1 and DsRed-tagged GFRP. Confocal microscopy of HAECs transfected with the fusion constructs indicated. Recordings were performed at the excitation and emission setting for GFP and DsRed. C, Representative laser scanning microscope FRET images of cells expressing the GFP-GTPCH-1 and DsRed-GFRP constructs acquired with a Zeiss LSM 510 META confocal microscope. In the experiment, GFP-GTPCH-1 functioned as a donor and DsRed-GFRP as an acceptor. Shown on the top of the columns are various FRET channels. HAECs were co-transfected with both constructs and FRET images were subsequently taken after 24 hours of culture. The Representative pseudocolor images illustrating FRET efficiency is shown on the right.

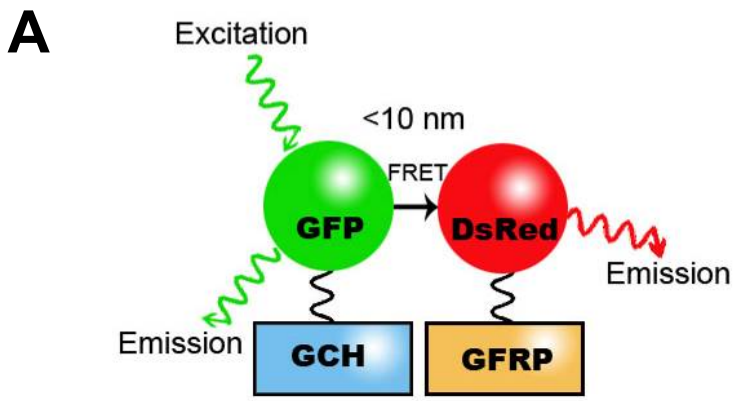
A
Excitation
<10 nm
FRET
GFP
DsRed
Emission
Emission
GCH
GFRP

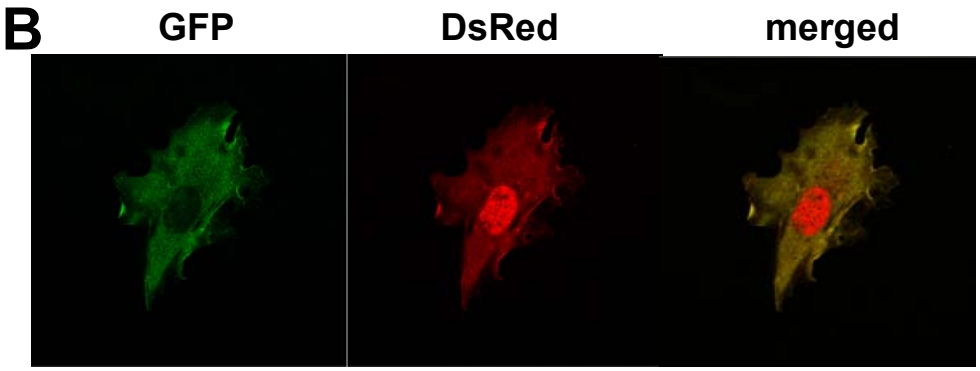
B
GFP
DsRed
merged

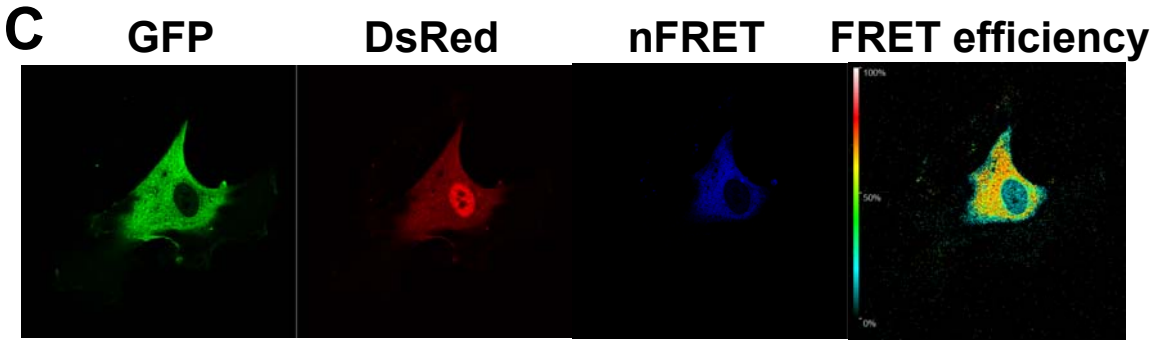
C
GFP
DsRed
nFRET
FRET efficiency
100%
50%
0%

interactions. Expression of GFP-GTPCH-1 in HAECs produced a fluorescence pattern characteristic of cytoplasmic localization, whereas DsRed-GFRP was present both in the nucleus and the cytoplasm. Confocal microscopy of cells co-transfected with GFP-GTPCH-1 and DsRed-GFRP revealed a marked co-localization of the GFP and DsRed fluorescence in the cytoplasm (Figure 2.6B).

Besides co-localization analysis, FRET imaging can be performed to calculate and generate an image of the FRET efficiency, with green showing the low efficiency and red suggesting the high efficiency (Figure 2.6C). As shown in the FRET efficiency image, GTPCH-1 interacts with GFRP with a relatively higher FRET efficiency in the cytoplasm, which is consistent with the co-localization analysis of GTPCH-1 and GFRP. In addition to the overall efficiency picture, I can also obtain quantitative FRET efficiencies from different regions of interest on the image. The average FRET efficiency from 20 regions of interest indicates that the interaction between GTPCH-1 and GFRP in HAECs is 0.619. Efficiencies of 0.4 to 0.6 have been reported in other FRET studies (Chen et al., 2006; Thaler et al., 2005), so the efficiency of 0.619 between GTPCH-1 and GFRP suggests a high extent of interaction.

To analyze the interaction of GTPCH-1 and GFRP using BRET, HAECs were co-transfected with plasmids encoding Renilla luciferase (Rluc8)-GTPCH-1 and Venus-GFRP fusion proteins. When Rluc8-GTPCH-1 and Venus-GFRP were co-expressed and Rluc8 was excited with the substrate coelenterazine h, I detected a robust BRET signal with a value of 0.094 ± 0.012, supporting the concept that

GTPCH-1 binds to GFRP in human endothelial cells (Figure 2.1).

2.3.4 Effect of GTPCH-1 S81 phosphorylation on its enzymatic activity and interaction with GFRP

The above experiments in 2.3.2 show that GFRP inhibits GTPCH-1 phosphorylation and activity in HAECs and I next performed additional experiments to determine whether the opposite hypothesis was true: that GTPCH-1 phosphorylation reduces its binding to GFRP and escapes from the negative feedback regulation by its end production BH_4 via interaction with GFRP. The rationale for this hypothesis is that phosphorylation of GTPCH-1 induced by laminar shear stress markedly increases its enzymatic activity by about 30-fold in HAECs, suggesting that phosphorylation of GTPCH-1 might disrupt the negative feedback inhibition exerted by GFRP.

To explore the effect of phosphorylation on GTPCH-1 activity and its regulation by GFRP, we mutated S81 to aspartate to mimic phosphorylation (S81D) and alanine to block phosphorylation (S81A), respectively and studied the properties of these mutants. Transfection with S81D caused a significantly higher increase in BH_4 levels and GTPCH-1 activity than transfection with either wild type or S81A in HAECs (Figure 2.7A and 2.7B). Transfection with empty vector had no effect on BH_4 levels. Exposure of cells to shear increased BH_4 levels and GTPCH-1 activity in cells transfected with the wild type enzyme, but did not in cells transfected with either S81D or S81A mutant constructs (Figure 2.7A and 2.7B), consistent with the concept that these mutants could not be phosphorylated in response to shear.

Figure 2.7 Effect of GTPCH-1 S81 phosphorylation on endothelial BH_4 levels, GTPCH-1 activity and NO production in HAECs. A, HAECs were either not transfected or transfected with plasmids encoding HA-tagged WT, S81D or S81A GTPCH-1. Forty-eight hours later, cells were either left in static conditions or exposed to unidirectional laminar shear for 14 hours. BH_4 levels were determined by HPLC (n=3-4). The left portion shows a western blot illustrating endogenous and overexpressed GTPCH-1 using an anti-GTPCH-1 antibody. B, GTPCH-1 activity in HAECs after transfection and exposure to shear stress was measured by HPLC (n=3). C, NO production by HAECs transfected with either wild type, S81D or S81A GTPCH-1 measured by ESR 48 hours after transfection (n=3). The right portion of panel C shows representative $Fe[DETC]_2$ ESR spectra for NO production. D, Saturation curves examining the rate of dihydroneopterin trisphosphate (H_2NTP) from purified WT and S81D GTPCH-1 proteins expressed prokaryotically in the presence and absence of GFRP (n=3).

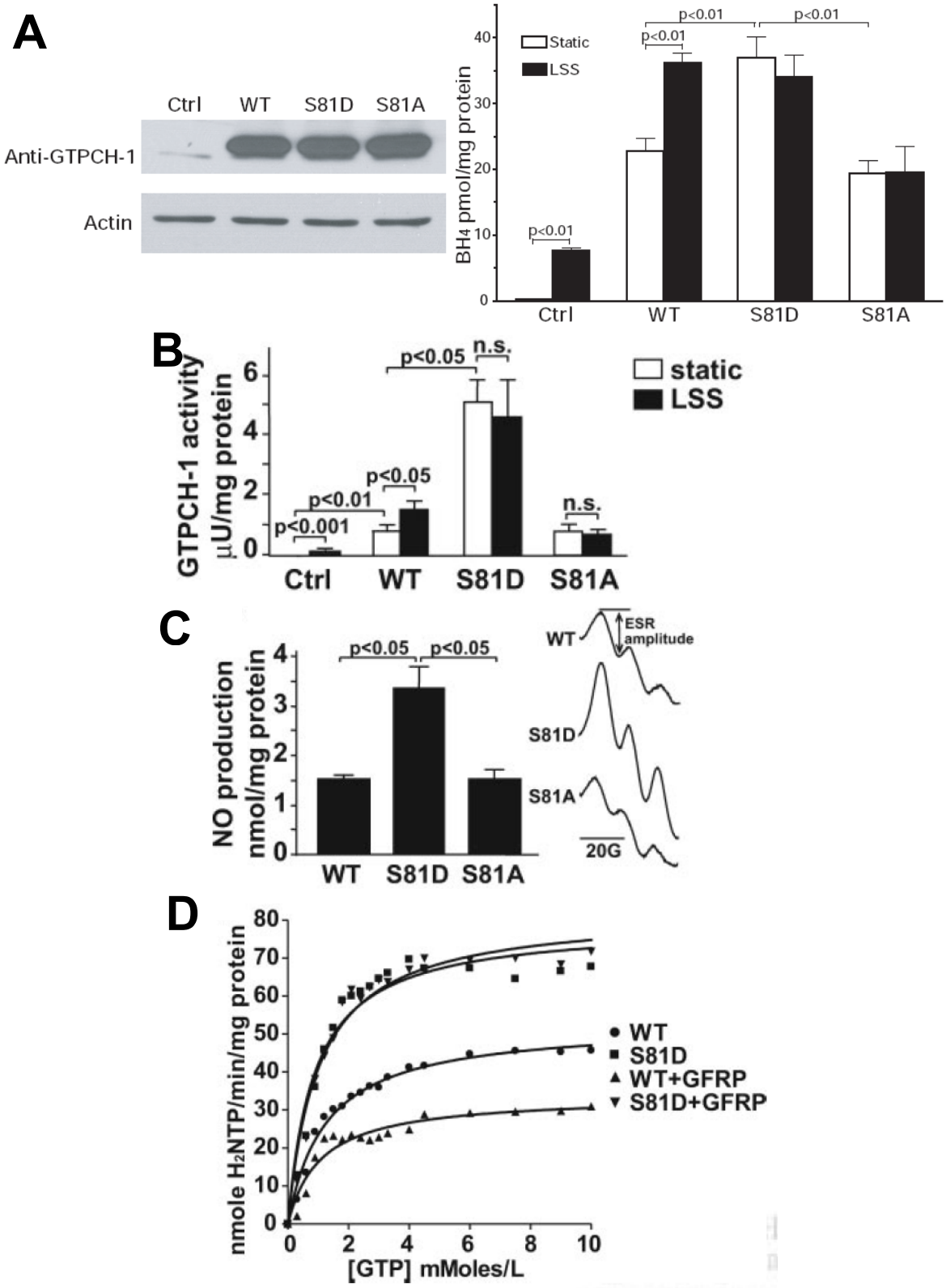
A
Ctrl
WT
S81D
S81A
Anti-GTPCH-1
Actin
Static
LSS
BH4 pmol/mg protein
p<0.01
p<0.01
p<0.01
p<0.01
Ctrl
WT
S81D
S81A
B
GTPCH-1 activity
μU/mg protein
static
LSS
p<0.05
n.s.
p<0.05
p<0.01
p<0.001
n.s.
Ctrl
WT
S81D
S81A
C
NO production
nmol/mg protein
p<0.05
p<0.05
WT
S81D
S81A
ESR
amplitude
20G
D
nmole H2NTP/min/mg protein
[GTP] mMoles/L
WT
S81D
WT+GFRP
S81D+GFRP

Importantly, cells transfected with the S81D mutant produced significantly more NO than cells transfected with either wild type or S81A GTPCH-1 (Figure 2.7C).

Because GFRP is known to inhibit GTPCH-1 activity in the presence of BH_4 in vitro (Harada et al., 1993), we examined the effect of GFRP on activity of purified wild type and S81D GTPCH-1 that had been expressed prokaryotically and purified. The Vmax of purified S81D was increased by approximately 2-fold compared to the wild type enzyme (Figure 2.7D and Table 2.1). Surprisingly, while Vmax of the wild type enzyme was reduced by half due to the addition of an equimolar concentration of GFRP, the Vmax of S81D was resistant to inhibition by GFRP (Figure 2.7D and Table 2.1). Moreover, GFRP binding increased the apparent Km of GTPCH-1, which also contributes to inhibition and increases the cooperativity of substrate binding. These effects were not seen in the S81D mutant. To summarize these results, GTPCH-1 phosphorylation at S81 increases its enzyme activity and its production of BH_4 and thus augments NO production in human endothelial cells. This is likely due, in part, to its resistance to feedback inhibition by GFRP.

We next considered the hypothesis that phosphorylated GTPCH-1 has reduced binding to GFRP, which might explain its resistance to GFRP inhibition. To test this hypothesis, I employed pull-down assays using prokaryotically expressed wild type, S81D and S81A GTPCH-1 fusion proteins containing a 6-His tag and a glutathione S-transferase (GST)-tagged GFRP fusion protein. These experiments demonstrated that S81D exhibited reduced interaction with GFRP compared to wild type GTPCH-1 while S81A showed enhanced interaction both in the presence of

Table 2.1 Kinetic properties of WT and S81D GTPCH-1 in the presence and absence of GFRP

	Wild type	S81D	WT + GFRP	S81D + GFRP
Vmax nmol/min/mg protein	51.7 ± 2.4	84.3 ± 6.9*	32.3 ± 0.8†	85 ± 5.1
Km (mmol/L)	1.1 ± 0.2	1.1 ± 0.2	0.8 ± 0.2	1.1 ± 0.2

* $p<0.001$ vs. Wild type, †$p<0.01$ vs. Wild type (n=3)

BH_4 and GTP and in separate experiments, in the presence of phenylalanine (Figure 2.8A through 2.8C). To examine binding of wild type and mutant GTPCH-1 with GFRP in intact endothelial cells, I transfected HAECs with plasmids encoding DsRed-tagged GFRP and HA-tagged GTPCH-1 wild type and mutant enzymes. GFRP was immunoprecipitated using an anti-DsRed antibody and the co-precipitated GTPCH-1 was detected using an anti-HA antibody. In keeping with the results from the pull-down assays, the cellular association of S81D with GFRP was reduced by approximately one half compared to wild type and S81A GTPCH-1 as determined by densitometry (Figure 2.8D and 2.8E). Thus, these results suggest that GTPCH-1 phosphorylation at S81 reduces its binding to GFRP and attenuates its feedback inhibition by GFRP.

2.3.5 Effects of GTPCH-1 S81 phosphorylation and GFRP down-regulation on eNOS uncoupling in response of oscillatory shear stress

We have previously shown that in contrast to laminar shear, oscillatory shear induced a minimal increase in BH_4 levels in HAECs (Widder et al., 2007). Such a paucity of BH_4 in response to oscillatory shear might cause eNOS uncoupling. In keeping with this, oscillatory shear increased $O_2^{\bullet-}$ production by approximately two-fold in control cells. In contrast, transfection of HAECs with GTPCH-1 WT, S81D and S81A constructs all blocked the increase of $O_2^{\bullet-}$ caused by oscillatory shear, but the greatest effect was observed with S81D (Figure 2.9A). Moreover, the NOS inhibitor L-NAME blocked $O_2^{\bullet-}$ production in untransfected cells, indicating eNOS uncoupling; whereas transfection with any of the GTPCH-1 constructs

Figure 2.8 Effect of GTPCH-1 S81 phosphorylation on its interaction with GFRP. A, B and C, Pull-down assays using glutathione S-transferase (GST)-tagged GFRP to immunoprecipitate His-tagged WT, S81D, and S81A GTPCH-1 (A) and His-tagged WT, S81D, and S81A GTPCH-1 to precipitate GST-GFRP (B) in the presence of BH4 and GTP, and in the presence of L-phenylalanine (C). D, Analysis of GFRP and GTPCH-1 binding in intact cells by co-IP. Cells were co-transfected with DsRed-GFRP and HA-GTPCH-1 constructs and subjected to immunoprecipitation using anti-DsRed (IP:DsRed) antibody. Input amounts of GFRP and HA-tagged GTPCH-1 are shown at the bottom. E, Densitometry values for GTPCH-1 divided by GFRP from co-IP (n = 4 to 5).

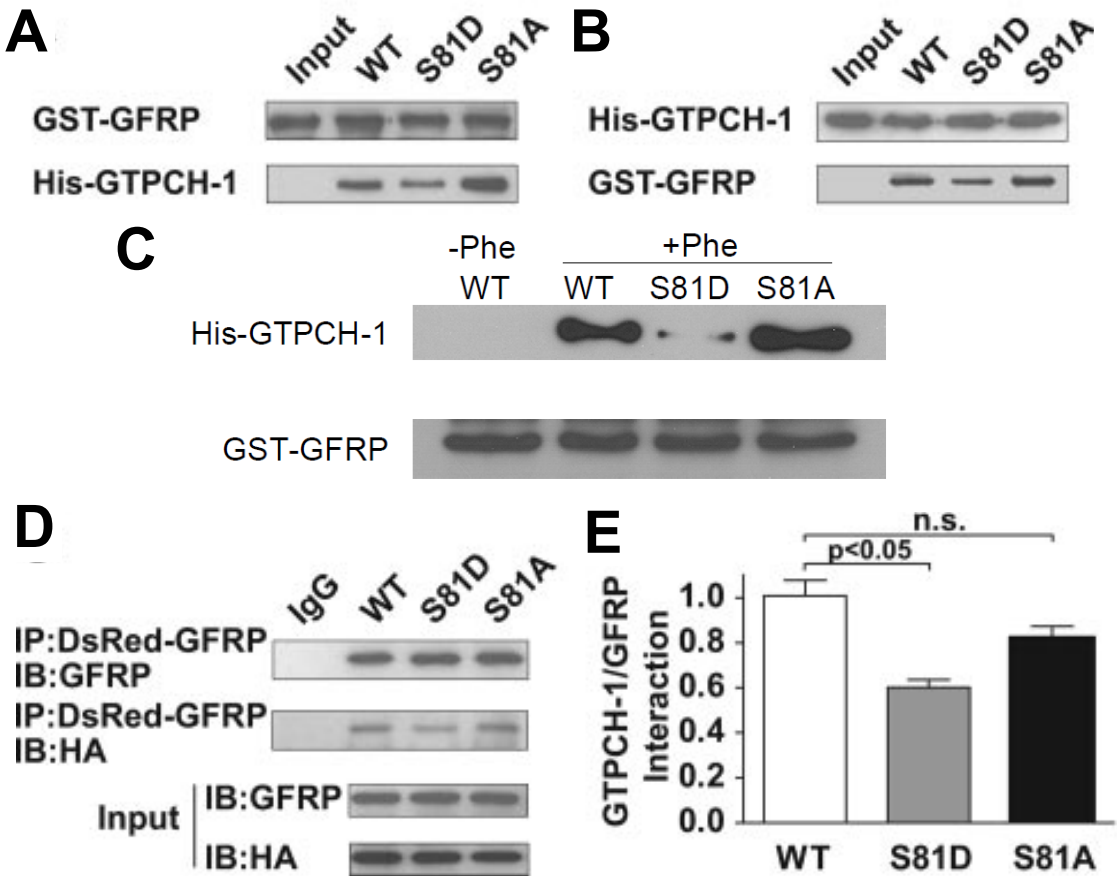

Figure 2.9 Effects of GTPCH-1 phosphorylation and GFRP down-regulation on eNOS coupling in HAECs exposed to oscillatory shear stress. HAECs were either not transfected or transfected with plasmids encoding HA-tagged WT, S81D or S81A GTPCH-1. Forty-eight hours later, cells were either left in static conditions or exposed to oscillatory shear for 14 hours. Comparison of wild type and S81 modified GTPCH-1 on $O_2^{\bullet-}$ production (A) (n=5-6) and NO production (B) (n=5). Effect of GFRP down-regulation by siRNA on $O_2^{\bullet-}$ production (C) (n=4-6) and NO production (D) (n=5).

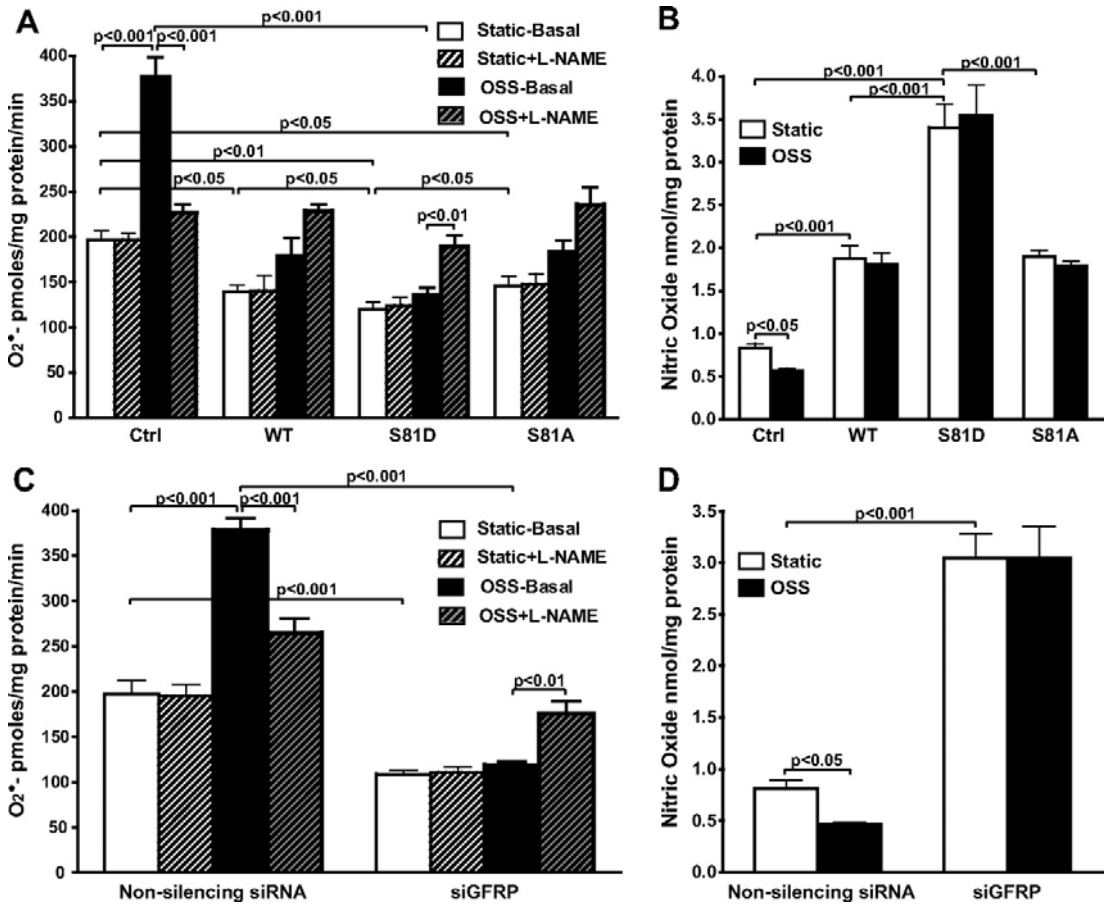

reversed this phenomenon such that L-NAME increased $O_2^{\bullet-}$ production, suggesting that they were able to recouple eNOS in the setting of oscillatory shear stress (Figure 2.9A). All the constructs prevented the decline of NO production in response to oscillatory shear stress, but S81D had the greatest effect on overall NO levels (Figure 2.9B). Down-regulation of GFRP using siRNA also prevented eNOS uncoupling and reduction of NO in cells exposed to oscillatory shear (Figure 2.9C and 2.9D). These results indicate that GTPCH-1 levels, GTPCH-1 phosphorylation status and GFRP levels play critical roles in regulating eNOS uncoupling in response to oscillatory shear stress.

2.3.6 Comparison of the effects of laminar vs. oscillatory shear stress on CK2α' activity and association of GFRP with GTPCH-1

We previously demonstrated that laminar, but not oscillatory, shear stress stimulated GTPCH-1 phosphorylation at S81 by CK2α' (Widder et al., 2007); however, the mechanism by which shear induces S81 phosphorylation is unknown. In initial experiments I found that CK2α' activity was similar in HAECs exposed to no shear, laminar or oscillatory shear (Figure 2.10A). Thus, CK2α' is not directly affected by either laminar or oscillatory shear stress. I next sought to determine if GFRP, which, as shown above, prevents GTPCH-1 phosphorylation, is released from GTPCH-1 to allow phosphorylation in response to laminar shear. I used two different approaches to examine the interaction of GTPCH-1 and GFRP in static and sheared cells: co-IP and BRET. Co-IP of HA-GTPCH-1 and DsRed-GFRP from static and sheared HAECs showed that the amount of GTPCH-1 co-precipitated with

Figure 2.10 Comparison of laminar vs. oscillatory shear stress on the association of GTPCH-1 and GFRP and the role of GTPCH-1 phosphorylation in its dissociation from GFRP. A, CK2α' kinase activity measured from CK2α' immunoprecipitates in HAECs exposed to various shear conditions (n=6). B, Cells co-transfected with DsRed-GFRP and HA-GTPCH-1 constructs were exposed to various shear conditions and subjected to immunoprecipitation using anti-DsRed (IP:DsRed) antibody. IgG was used as a control for co-IP. Input amounts of GFRP and GTPCH-1 are shown below. C, Densitometry values for GTPCH-1 normalized to GFRP from co-IP (n=5-6). D, BRET ratio of GTPCH-1 interaction with GFRP in HAECs exposed to various shear conditions (n=5-11). E, Co-IP of DsRed-GFRP and HA-GTPCH-1 from HAECs exposed to static condition or laminar shear in the presence and absence of a CK2 inhibitor, TBB (30 μM). Representative western blots for S81 phospho–GTPCH-1 and total GTPCH-1 are shown at the bottom. F, Densitometry values for GTPCH-1 normalized to GFRP from co-IP (n=5). G, Co-IP of DsRed-GFRP and HA-tagged S81A GTPCH-1 from HAECs exposed to static condition or laminar shear. H, Densitometry values for GTPCH-1 normalized to GFRP from co-IP (n=4).

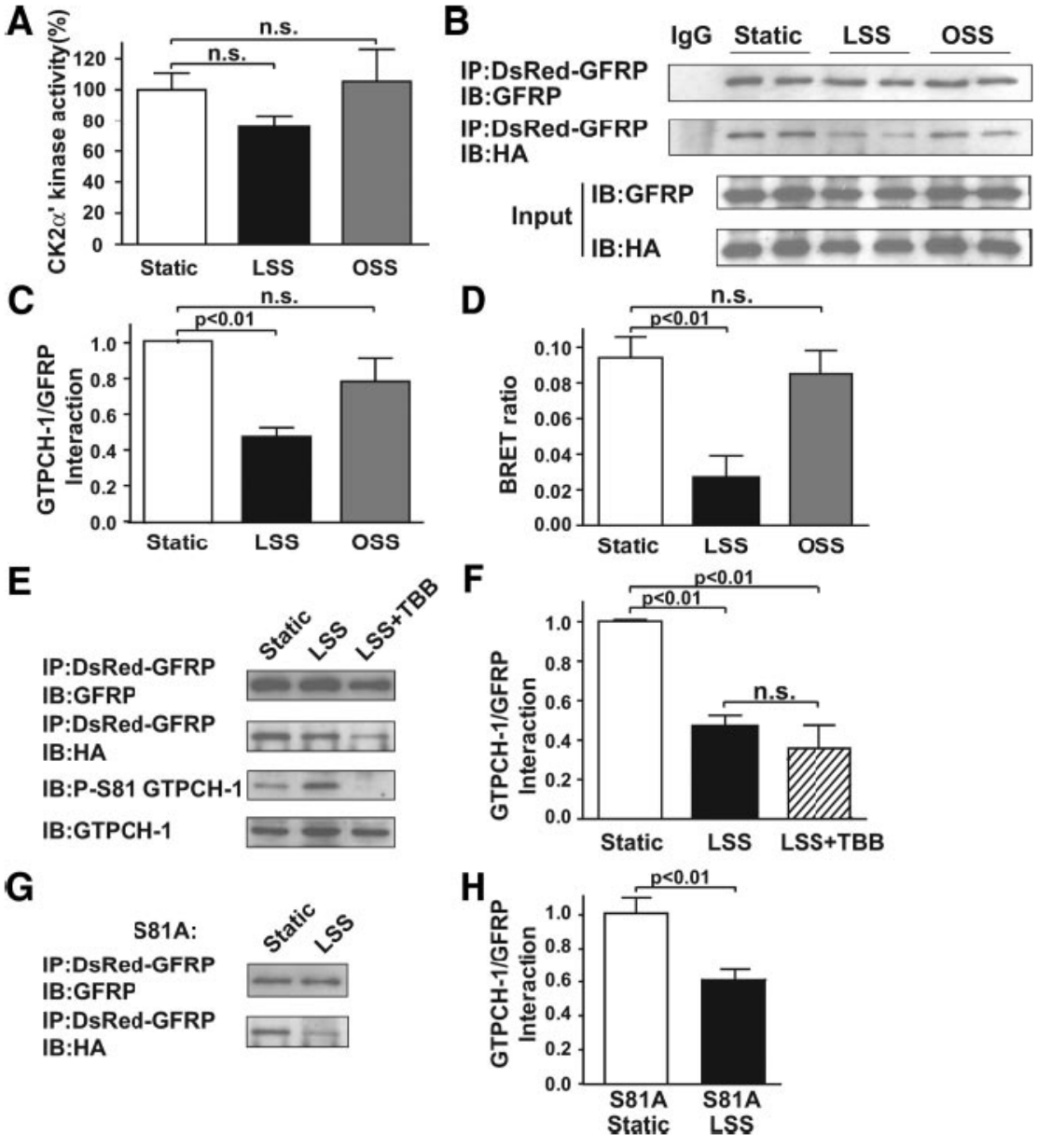
A
CK2α' kinase activity(%)
n.s.
n.s.
Static
LSS
OSS
B
IgG
Static
LSS
OSS
IP:DsRed-GFRP
IB:GFRP
IP:DsRed-GFRP
IB:HA
Input
IB:GFRP
IB:HA
C
GTPCH-1/GFRP Interaction
n.s.
p<0.01
D
BRET ratio
n.s.
p<0.01
E
Static
LSS
LSS+TBB
IP:DsRed-GFRP
IB:GFRP
IP:DsRed-GFRP
IB:HA
IB:P-S81 GTPCH-1
IB:GTPCH-1
F
GTPCH-1/GFRP Interaction
p<0.01
p<0.01
n.s.
G
S81A:
Static
LSS
IP:DsRed-GFRP
IB:GFRP
IP:DsRed-GFRP
IB:HA
H
GTPCH-1/GFRP Interaction
p<0.01
S81A Static
S81A LSS

GFRP decreased after cells were exposed to laminar but not oscillatory shear (Figure 2.10B and 2.10C). The BRET ratio was significantly lower in cells that were exposed to laminar, but not oscillatory shear, than cells under static conditions (Figure 2.10D). These results demonstrate that laminar shear causes the dissociation of GTPCH-1 and GFRP. Taken together with my experiments in which GFRP was either reduced by siRNA or overexpressed, this dissociation likely allows phosphorylation of GTPCH-1 at S81 and thus activates the enzyme.

In additional experiments, I sought to determine if phosphorylation was either the cause or result of dissociation of GTPCH-1 and GFRP in the setting of laminar shear stress. Treatment of cells with 4,5,6,7-tetrabromobenzotriazole (TBB), a specific CK2 inhibitor that prevents GTPCH-1 phosphorylation (Widder et al., 2007), did not affect dissociation of GFRP and GTPCH-1 as detected by co-IP (Figure 2.10E and 2.10F). Similarly, shear also reduced the interaction of GFRP and the phosphorylation resistant S81A GTPCH-1 mutant (Figure 2.10G and 2.10H). These results indicate that S81 phosphorylation is likely the result of GFRP and GTPCH-1 dissociation and does not initiate dissociation of these proteins.

2.3.7 Exploring the mechanism by which laminar shear induces dissociation of GTPCH-1 and GFRP

The above experiments demonstrated that laminar shear disrupts the interaction of GTPCH-1 and GFRP, thereby allowing CK2 to phosphorylate GTPCH-1. However, the mechanism by which laminar shear causes dissociation of these two proteins remains unclear. I first examined two stimuli that mimic laminar shear

stress in signal transduction and the effect on NO production – treatment with vascular endothelial growth factor (VEGF) and statins. VEGF was found to have a stimulatory effect on eNOS message, protein expression, eNOS phosphorylation and NO production in rat glomeruli (Wang et al., 2004). Time- and dose-dependent upregulation of eNOS protein by statins has been observed in both cell culture and animal studies (Laufs et al., 1998). I found that treatment of HAECs with VEGF or statins for 24 hours did not increase BH_4 levels, as laminar shear does (data not shown). A major difference between laminar shear and the above-mentioned two treatments is that endothelial cells change shape and re-align themselves according to the flow. Re-alignment of the cells in response to laminar shear involves signaling pathways of Akt/PI3K, MAPK/p38 and Rho/ROCK (Wojciak-Stothard and Ridley, 2003), we therefore sought to determine if these kinases play a role in regulating GTPCH-1 binding with GFRP, its enzymatic activity and BH_4 levels in response to shear. By using pharmacological inhibitors of p38 and ROCK, I found that p38 and ROCK plays a minimal role in modulating BH_4 levels in HAECs in response to laminar shear (Figure 2.11A). In contrast, pharmacological inhibition of PI3K using Wortmannin or LY294002 completely abolished shear induced effect on BH_4 levels in HAECs (Figure 2.11B). Of note, PI3K inhibitor also prevented shape change and re-alignment of endothelial cells stimulated by laminar shear (Figure 2.11C). These results indicate that PI3K is required for laminar shear induced increase of BH_4 levels and actin cytoskeleton rearrangement in response to shear. It remains unknown whether endothelial shape change in response to shear

Figure 2.11 Roles of p38, ROCK and PI3K in laminar shear induced increase in BH_4 levels in HAECs. A, Total biopterin levels in HAECs after exposure to laminar shear for 14 hours with the treatment of 10 μM SB 203850 (SB, p38 inhibitor) and 5 μM Y-27632 (Y, ROCK inhibitor) measured by HPLC (n=5). B. Total biopterin and BH_4 levels in HAECs after exposure to laminar shear for 14 hours with the treatment of 100 nM Wortmannin (PI3K inhibitor) and 10 μM LY294002 (LY, PI3K inhibitor) measured by HPLC (n=5). C, Morphology of HAECs before and after exposure to laminar shear for 14 hours with the treatment of 100 nM Wortmannin. Images were obtained using bright field microscopy.

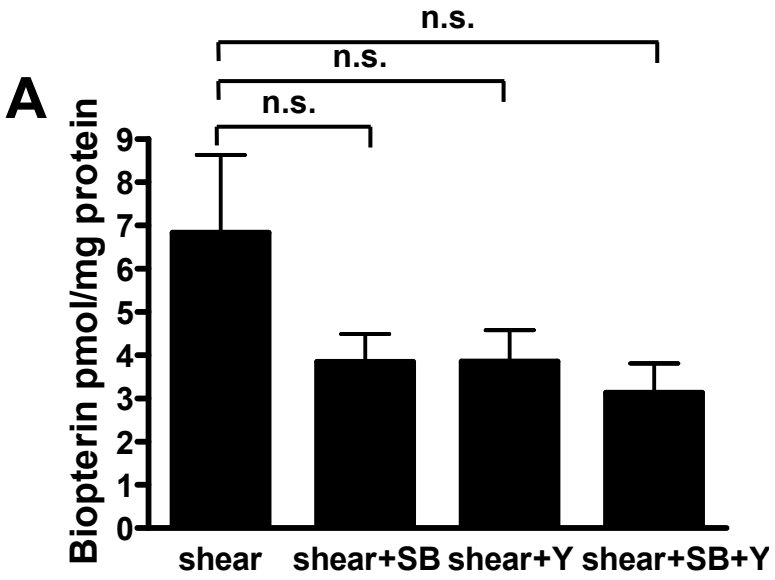
A
n.s.
n.s.
n.s.
Biopterin pmol/mg protein
0
1
2
3
4
5
6
7
8
9
shear
shear+SB
shear+Y
shear+SB+Y

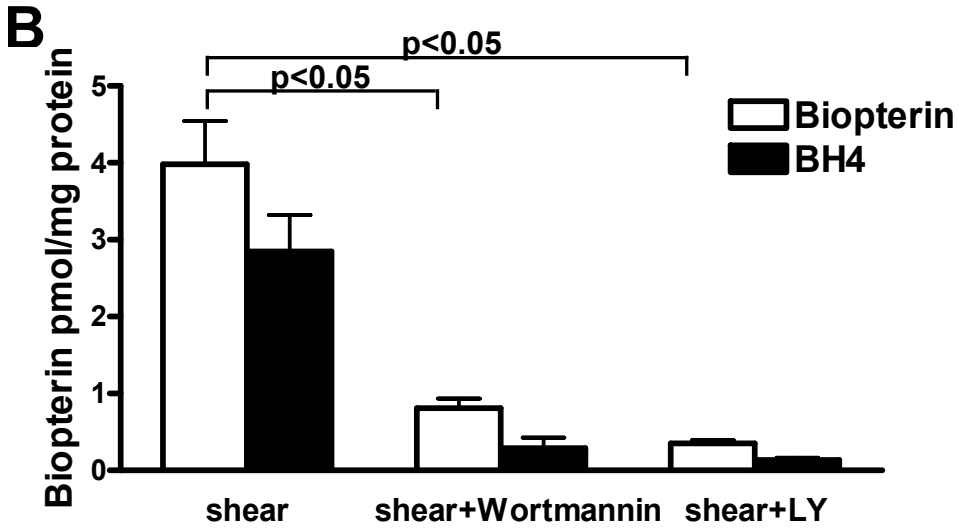
B
p<0.05
p<0.05
Biopterin
BH4
Biopterin pmol/mg protein
0
1
2
3
4
5
shear
shear+Wortmannin
shear+LY

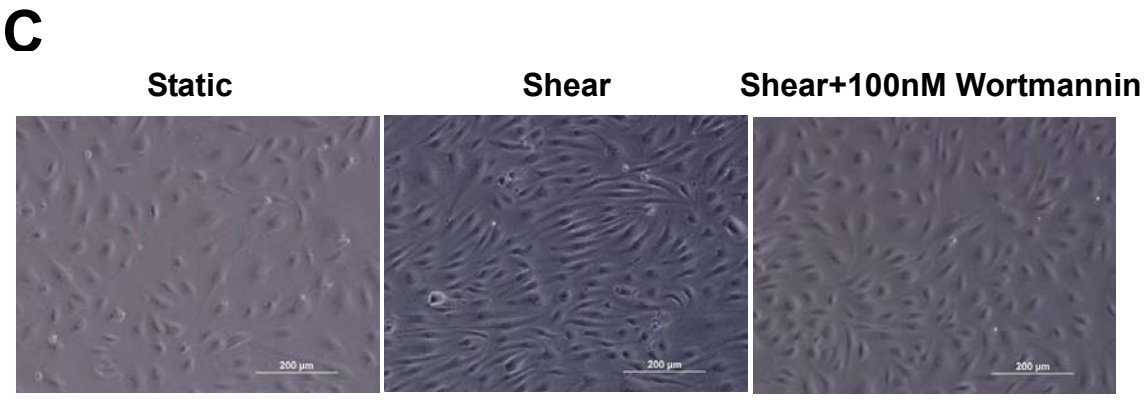
C
Static
Shear
Shear+100nM Wortmannin

is required for shear induced dissociation of GTPCH-1 and GFRP and increase in BH_4 levels.

2.4 Discussion

Recently, our laboratory has demonstrated that unidirectional laminar shear stress stimulates endothelial GTPCH-1 phosphorylation by CK2α' and that this is associated with a marked increase in GTPCH-1 catalytic activity and BH_4 production (Widder et al., 2007). My current study provides additional insight into mechanisms underlying GTPCH-1 phosphorylation and modulation of its activity by the regulatory protein, GFRP. My data demonstrate that GFRP regulates GTPCH-1 S81 phosphorylation. Reduction of GFRP levels using siRNA induced GTPCH-1 phosphorylation and dramatically increased endothelial cell GTPCH-1 activity, BH_4 levels and NO production. In contrast, overexpression of GFRP inhibited GTPCH-1 phosphorylation and reduced endothelial cell levels of BH_4 stimulated by laminar shear stress. A phospho-mimetic mutant of GTPCH-1, S81D, was shown to have increased activity compared to the wild type enzyme and in contrast to the wild type enzyme, was resistant to negative feedback inhibition by GFRP. Importantly, I demonstrated that the phospho-mimetic mutant enzyme exhibited reduced binding to GFRP. My data also showed that both transfection of S81D GTPCH-1 and down-regulation of GFRP rescued eNOS uncoupling induced by oscillatory shear stress in HAECs. I also found that unidirectional laminar shear stress, which induces GTPCH-1 phosphorylation, decreased its association with GFRP. GTPCH-1 phosphorylation is likely a consequence, rather than a cause of

its dissociation from GFRP, because this phenomenon was not prevented by pharmacological inhibition of CK2 or by mutation of GTPCH-1 to prevent its phosphorylation.

Taken together, my findings are compatible with the scheme illustrated in Figure 2.12A. GTPCH-1 exists as a homodecamer in complex with two homopentamers of GFRP. We propose that unidirectional laminar shear initially promotes dissociation of GFRP and GTPCH-1. This permits access of CK2α' to GTPCH-1, allowing phosphorylation of one or more S81 residues. The phosphorylation of S81 reduces re-association of GFRP and GTPCH-1, allowing further phosphorylation of other S81 residues. The fully phosphorylated GTPCH-1 exhibits markedly increased activity in part because it has reduced affinity for GFRP and is not inhibited by GFRP, which leads to increased BH_4 levels and eNOS coupling. My current in situ data do not allow discrimination between the direct effect of augmentation of GTPCH-1 activity by phosphorylation and the indirect effect of phosphorylation on altering association with GFRP; however, our studies of purified wild type and S81D GTPCH-1 would suggest that both are important.

My current findings provide further insight into differences between the effects of unidirectional laminar and oscillatory shear on endothelial cell function (Figure 2.12B). In humans and experimental animal models, areas of oscillatory shear, such as bifurcations and branching points of arterial trees, are associated with enhanced atherosclerotic lesion formation, while areas of well developed laminar shear have reduced atherosclerosis (De Keulenaer et al., 1998). Over the long-term,

Figure 2.12 Proposed mechanism for shear regulation of GTPCH-1. A, Proposed mechanism for phosphorylation and modulation of GTPCH-1 activity by shear stress. Laminar shear promotes dissociation of GTPCH-1 from the regulatory protein GFRP, which allows GTPCH-1 phosphorylation by CK2. The fully phosphorylated enzyme has diminished binding affinity to GFRP and is not inhibited by GFRP, leading to a fully functioning enzyme. B, Proposed effects of laminar and oscillatory shear on GTPCH-1 regulation, BH_4 levels and NOS coupling. Laminar shear stress causes dissociation of GTPCH-1 and GFRP, which allows phosphorylation of GTPCH-1 by CK2. Phosphorylation of GTPCH-1 dramatically increases its enzyme activity and leads to increased cellular BH_4 levels. This enhances endothelial cell BH_4, which serves as a critical co-factor for eNOS, which is also increased in response to shear. Consequently, eNOS is coupled and produces NO to promote vasorelaxation. In contrast, oscillatory shear has no effect on the association of GTPCH-1 and GFRP, thus inhibiting GTPCH-1 phosphorylation and preventing activation of the enzyme. BH_4-deficient eNOS produces $O_2^{\bullet -}$ instead of NO upon stimulation of the enzyme.

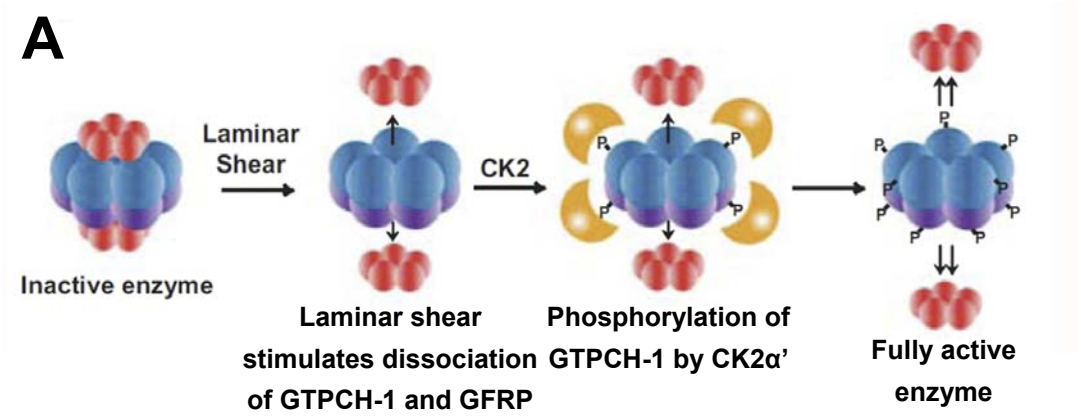
A
Laminar Shear
CK2
Inactive enzyme
Laminar shear stimulates dissociation of GTPCH-1 and GFRP
Phosphorylation of GTPCH-1 by CK2α'
Fully active enzyme

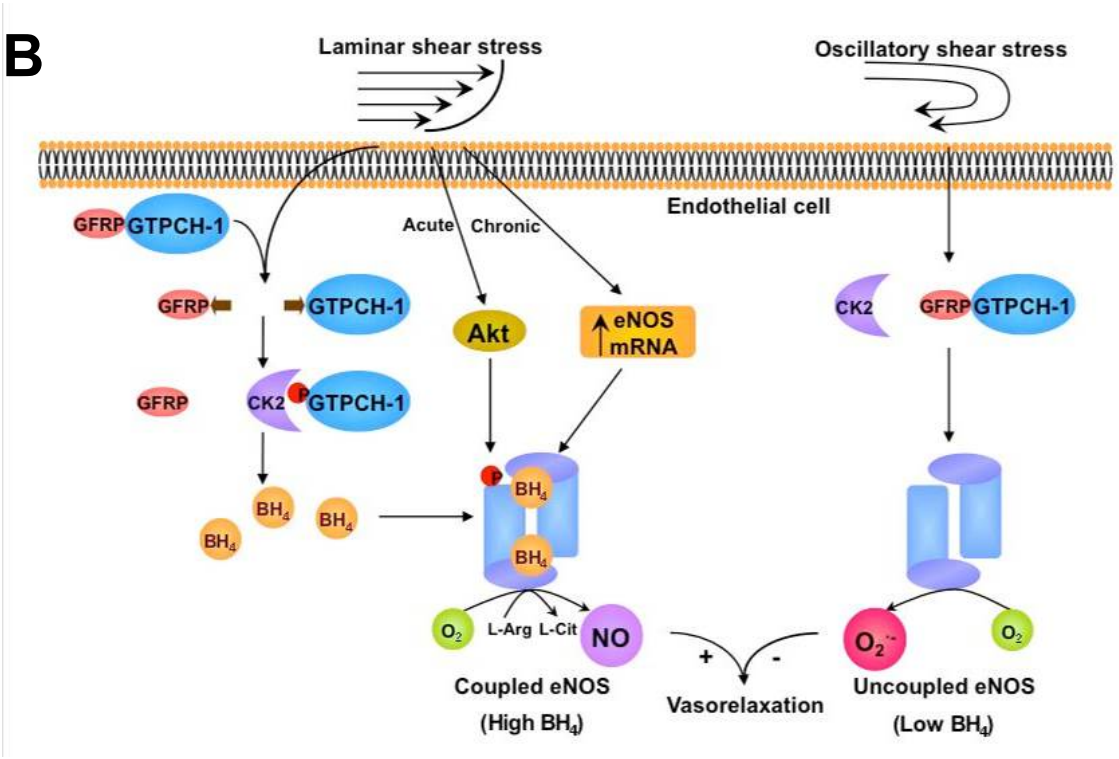
B
Laminar shear stress
Oscillatory shear stress
Endothelial cell
GFRP GTPCH-1
Acute
Chronic
Akt
eNOS mRNA
CK2
BH4
O2
L-Arg L-Cit
NO
O2·-
+
-
Vasorelaxation
Coupled eNOS (High BH4)
Uncoupled eNOS (Low BH4)

laminar shear enhances NO production and reduces endothelial cells production of reactive oxygen species, while oscillatory shear has the opposite effects (De Keulenaer et al., 1998). In the present study, I demonstrated that eNOS was uncoupled in HAECs exposed to oscillatory shear, compatible with the concept that BH_4 levels were insufficient to sustain eNOS catalysis in the setting of oscillatory shear. My studies suggest that both GTPCH-1 phosphorylation and GFRP down-regulation can rescue eNOS uncoupling in the setting of oscillatory shear.

To explore the mechanism by which laminar shear stimulates GTPCH-1 phosphorylation whereas oscillatory shear does not, I employed two separate methods to show that laminar shear dissociates GFRP and GTPCH-1, while oscillatory shear does not. My data indicate that the continued association of these two proteins in the setting of oscillatory shear would inhibit GTPCH-1 phosphorylation and thus prevents activation of the enzyme. The precise mechanism by which laminar shear causes dissociation of GFRP and GTPCH-1 remains undefined. In preliminary studies, I found that the onset of GTPCH-1 phosphorylation begins approximately 4-5 hours after initiation of shear stress (data not shown). This temporally corresponds to the time that endothelial cell shape changes in response to shear. It is therefore interesting to speculate that endothelial cell cytoskeletal reorganization could alter the respective subcellular localizations of GTPCH-1 and GFRP and promote their dissociation. In keeping with this, I found that PI3K inhibitors blocked both endothelial cell shape change and the increase in BH_4 levels in response to laminar shear, indicating that cell cytoskeletal

rearrangement might play a role in the mechanism for shear induced dissociation of GTPCH-1 and GFRP and phosphorylation of GTPCH-1. A very recent study showed that GTPCH-1 interacts with a Rho-GTPase (Du et al., 2009b), which is activated by shear is known to modulate cytoskeletal reorganization (Tzima, 2006). Moreover, endothelial GTPCH-1 has been shown to be associated with the caveolae and inhibited by caveolin-1 (Peterson et al., 2009). It is also possible that changes in caveolar-trafficking or caveolin-1 phosphorylation, both known to occur in response to shear, could alter this subcellular localization and perhaps interaction with GFRP. Additional studies are needed to address this issue.

My data indicate that phosphorylation of GTPCH-1 on S81 by CK2α' is a key biochemical mechanism for the activation of this enzyme. Mutation of S81 to an aspartate that mimics phosphorylation (S81D) recapitulates the effect of phosphorylation to enhance its enzyme activity and BH_4 levels when studied in the context of intact cells, but only increased activity of purified protein by two-fold. Strikingly, when exposed to its regulatory protein, GFRP, S81D enzyme activity was unaffected, while the wild-type enzyme activity was appreciably inhibited by GFRP in the presence of BH_4. To summarize, GTPCH-1 phosphorylation on S81 is a crucial mechanism to enhance its activity not only because it increases its intrinsic enzyme activity but also makes it resistant to GFRP inhibition. In keeping with this, Swick et al. (Swick and Kapatos, 2006), using a yeast two hybrid approach, found that amino-terminal 42 residues of GTPCH-1 is required for its binding to GFRP. Since S81 of GTPCH-1 resides in a regulatory arm of the enzyme, it is likely that

this site phosphorylation leads to a conformational change of this arm containing amino acids 1–42, which might cause reduced affinity of GTPCH-1 to GFRP. However, how phosphorylation on S81 affects the enzyme structure and its interaction with GFRP remains unknown and needs additional studies.

Comparison of results in endothelial cells with purified enzyme experiments is somewhat complicated by the contribution to GTPCH-1 regulation in cells of binding of ligands such as phenylalanine and BH_4 to sites on both catalytic GTPCH-1 domains and regulatory GFRP domains. These effects are buffer dependent and probably account for the greater effects of S81 phosphorylation observed in cells (Kolinsky and Gross, 2004). While GFRP is generally considered to inhibit GTPCH-1 in the presence of BH_4 (Werner et al., 2002), the ubiquitously present amino acid phenylalanine reverses the inhibition of GTPCH-1 without causing the dissociation of GFRP in vitro. My experiments using siRNA show that in intact endothelial cells, the predominant role of GFRP is marked inhibition of GTPCH-1 activity. In keeping with an inhibitory role of GFRP, Nandi et al. (Nandi et al., 2008) showed that its overexpression attenuated LPS and cytokine-stimulated BH_4 and NO production in an endothelial cell line.

My results also reveal a novel mechanism for GFRP modulation of GTPCH-1 activity, by inhibiting its phosphorylation. Interestingly, in contrast to our conclusions, a very recent study showed no evidence for regulation of human GTPCH-1 by mouse GFRP when the former was expressed in murine fibroblasts (Tatham et al., 2009). It is conceivable that mouse GFRP might not effectively

interact with human GTPCH-1 and thus does not regulate its activity or that this interaction is unimportant in fibroblasts. My current studies clearly indicate a role of GFRP in modulation of both basal and laminar shear stimulated GTPCH-1 activity in human endothelial cells. Previous studies have reported that pro-inflammatory stimuli on endothelial cells and rat liver down-regulates GFRP mRNA levels, which is associated with a dramatic elevation in GTPCH-1 activity and BH_4 levels (Gesierich et al., 2003; Kalivendi et al., 2005; Werner et al., 2002). Kalivendi et al. (Kalivendi et al., 2005) reported that treatment with hydrogen peroxide increased GFRP mRNA levels in HAECs, leading to BH_4 depletion in the cell. These findings in combination with ours suggest that GFRP could be regulated by oxidative stress and provide important regulation of BH_4 production in physiological and pathological conditions.

Our previous data indicate that CK2α' is responsible for GTPCH-1 phosphorylation in response to laminar shear. Pharmacological inhibition of CK2 and siRNA inhibition of CK2α' eliminated S81 phosphorylation and the increase in GTPCH-1 activity caused by shear (Widder et al., 2007). My current finding that GTPCH-1 is phosphorylated when it dissociates from GFRP is in accord with the action of CK2 on other substrates. CK2 is considered constitutively expressed and active, and its ability to phosphorylate target substrates is often modulated by other proteins that bind to these targets (Litchfield, 2003). As an example, the NFkB subunit p65 is known to be phosphorylated by CK2 when it is released from the inhibitory subunit IkB (Wang et al., 2000). My finding that shear does not

modulate CK2α' activity is in keeping with the concept that it simply gains access to GTPCH-1 upon GFRP dissociation. In preliminary studies, I was unable to demonstrate binding of CK2α' with GTPCH-1 (data not shown), perhaps due to the transient nature of this association.

In summary, I find that phosphorylation of GTPCH-1 is critical in activation of this enzyme, because this not only enhances its intrinsic activity but also reduces the feedback inhibition by its regulatory protein, GFRP. My results establish a pivotal role of GFRP in regulating GTPCH-1 S81 phosphorylation and activity, BH_4 levels and NO production in human endothelial cells. These data also demonstrate that the constitutive interaction of GTPCH-1 and GFRP can be regulated by laminar shear stress, which dynamically modulates GTPCH-1 phosphorylation and enzyme activity. The interplay between GTPCH-1 and GFRP shown in my study defines a novel mechanism of GTPCH-1 control in the endothelium.

Chapter 3:

Regulation of GTPCH-1 phosphorylation and BH_4 levels by disturbed flow in vivo and their roles in augmented atherosclerosis at sites of disturbed flow[1,2]

[1]A portion of this chapter is published in: Li L, Rezvan A, Salerno JC, Husain A, Kwon K, Jo H, Harrison DG, Chen W.(2010) GTP cyclohydrolase I phosphorylation and interaction with GTP cyclohydrolase feedback regulatory protein provide novel regulation of endothelial tetrahydrobiopterin and nitric oxide. *Circ Res.* **106(2)**:328-36 (Li et al., 2010).

[2]A portion of this chapter is accepted for publication: Li L, Chen W, Rezvan A, Jo H, Harrison DG. Tetrahydrobiopterin deficiency and Nitric Oxide Synthase uncoupling contribute to atherosclerosis induced by disturbed flow. *Arterioscler Thromb Vasc Biol.*

3.1 Introduction

Disturbances of blood flow, such as low and oscillatory shear stress, often exist at branch points and curved regions of the circulation such as the aortic arch (Ku et al., 1985b; Suo et al., 2007). Human and experimental atherosclerosis occurs preferentially at these sites of flow alteration. In contrast, laminar shear stress, which exists in straight portions of arteries, inhibits atherosclerotic lesion formation (VanderLaan et al., 2004). One mechanism involved in shear regulation of atherosclerosis is the endothelial production of NO. Laminar shear stress acutely stimulates endothelial production of NO and over the long term enhances eNOS gene expression (Kawashima and Yokoyama, 2004). NO inhibits atherosclerosis by suppressing inflammation, inhibiting platelet aggregation and leukocyte adhesion, and preventing smooth muscle cell proliferation (Li and Forstermann, 2000).

BH_4 is a critical cofactor for all three isoforms of NOS, and is involved in the reduction of the heme iron of the enzyme to ultimately form an iron-oxy species that hydroxylates L-arginine to produce NO. In the absence of BH_4, the NOS enzymes produce $O_2^{\cdot-}$ rather than NO, a situation referred to as NOS uncoupling (Vasquez-Vivar et al., 2003). BH_4 deficiency and NOS uncoupling have been shown to be present in experimental vascular disease models of hypercholesterolemia and atherosclerosis (Channon, 2004), and in humans with hypercholesterolemia (Stroes et al., 1997).

The rate-limiting enzyme for *de novo* synthesis of BH_4 is GTPCH-1. GFRP is an important modulator of GTPCH-1 enzyme activity and BH_4 promotes inhibition of GTPCH-1 by GFRP in a negative feedback fashion (Yoneyama and Hatakeyama,

1998). We have demonstrated that in human endothelial cells, laminar shear stress stimulates GTPCH-1 phosphorylation and this dramatically increases endothelial cell BH_4 levels by reducing the binding of GTPCH-1 and GFRP (Widder et al., 2007). In contrast, oscillatory shear only modestly affects GTPCH-1 activity and BH_4 levels. In Chapter 2, I demonstrated that GTPCH-1 phosphorylation and interaction with GFRP play a critical role in modulating endothelial cell GTPCH-1 activity, BH_4 levels, and NO production. I also found that this mechanism is distinctively regulated by two different mechanical stimuli, laminar and oscillatory shear. Notably, oscillatory shear induces NOS uncoupling in HAECs and this can be prevented by enhanced GTPCH-1 phosphorylation or reduced GFRP levels, suggesting that GTPCH-1 regulation by phosphorylation and interaction with GFRP might play an important role in disturbed flow induced atherosclerosis.

The purpose of this study was therefore to determine whether different shear profiles have different effects on GTPCH-1 phosphorylation and BH_4 levels in vivo, and whether these effects differentially influence the development of atherosclerosis. We hypothesize that oscillatory shear in vivo can lead to a reduction in GTPCH-1 phosphorylation and a concomitant deficiency in BH_4 levels, resulting in NOS uncoupling and augmented atherosclerosis. We therefore sought to determine whether atherosclerosis induced by disturbed flow is due to low levels of BH_4 and NOS uncoupling, and to determine if increasing BH_4 prevents endothelial dysfunction, plaque inflammation and atherosclerosis. To perform these studies, I used an in vivo model of disturbed flow by inducing partial carotid ligation (Nam et

al., 2009). I ligated the external, internal and occipital branches of the left carotid artery (LCA), while leaving the superior thyroid artery intact. This has been shown to result in low and oscillatory shear stress in the LCA and accelerates atherosclerosis in ApoE$^{-/-}$ mice on a hyperlipidemic diet. This model facilitates the examination of therapeutic interventions by creating rapid atherosclerotic lesion formation.

3.2 Materials and methods

3.2.1 Reagents and materials

BH_4 and 5,6,7,8-tetrahydro-D-neopterin (NH_4) were from Schircks Laboratories (Switzerland). All other biochemicals were purchased in the highest available grade from Sigma-Aldrich (St Louis, MO). Live/Dead Fixable Near-IR stain and PE-TR rat anti-mouse CD45 antibody were from Invitrogen (Carlsbad, CA). PE Cy7 rat anti-mouse F4/80 antibody was from eBiosciences (San Diego, CA). All other antibodies for flow cytometry were from BD Biosciences (San Jose, CA). The eNOS antibody used for Western blot was from BD Biosciences (San Jose, CA).

3.2.2 Animals studied

The Institutional Animal Care and Use Committee at Emory University approved all experimental protocols. C57Bl/6 and ApoE$^{-/-}$ mice were obtained from Jackson Laboratories. Partial ligation of left common carotid artery (LCA) was carried out at 8 weeks of age as previously described (Nam et al., 2009) to create low and oscillatory shear stress in the LCA. The right common carotid artery (RCA) was not ligated and used as a control with laminar shear.

To augment vascular levels of BH_4, this pterin was added to the drinking water to provide an approximate dose of 10 mg/kg per day. To minimize oxidation of BH_4 in the drinking water, 0.04% vitamin C was also added. In preliminary experiments, I found that this prevented BH_4 oxidation for up to 24 hours. As a vehicle control, mice not receiving BH_4 received only vitamin C in the drinking water. In some experiments, mice were also treated with 10 mg/kg NH_4 per day. Treatment with BH_4, NH_4 or vehicle was started three days before the carotid ligation. Mice were fed a high fat diet containing 45% kcal% fat (OpenSource Diets, New Brunswick, NJ) immediately following ligation until sacrificed.

3.2.3 Plasma lipid analysis

Blood was collected by cardiac puncture into syringes containing heparin. Plasma was obtained through centrifugation of blood for 15 minutes at 5500 g and 4°C, and then stored at -20°C until each assay was performed. Lipid analysis was performed commercially (Cardiovascular Specialty Laboratories, Atlanta, GA). All lipid determinations were performed using a Beckman CX7 chemistry analyzer and reagents from Beckman Diagnostics (Fullerton, CA) for total cholesterol and triglycerides.

3.2.4 BH_4 measurements by HPLC

Tissue biopterins (BH_4 and more oxidized species) were measured by HPLC as previously described (Widder et al., 2007). Carotids were homogenized with lysis buffer (50mM Tris-HCl, 1mM DTT, 1mM EDTA) and oxidized by exposure to 1% I_2 and 2% KI at room temperature for 1 hour under dark conditions. Ascorbic acid

was added to stop the reaction, and the mixture was then centrifuged for 10 minutes at 12,000 g. Biopterins in the supernatant were quantified by HPLC on a C18 column with fluorescence detection.

3.2.5 Measurement of vascular $O_2^{\bullet-}$ production

Carotid superoxide production was quantified by measuring formation of 2-hydroxyethidium from dihydroethidium (DHE) by HPLC. This product specifically reflects the reaction of $O_2^{\bullet-}$ with DHE as previously validated (Fink et al., 2004). To localize $O_2^{\bullet-}$ within the vascular wall, I employed DHE staining. As previously described (Nam et al., 2009), frozen sections (30 μm) obtained from LCA and RCA of partially ligated mice were stained in 2 μmol/L DHE for 30 min at 37°C. Slides were mounted with DAKO mounting media and immediately imaged with a Zeiss LSM 510 META confocal microscope.

3.2.6 Western blot analysis for eNOS dimers/monomers

Low-temperature Western blot was performed to detect eNOS dimers and monomers as described previously (Klatt et al., 1995).

3.2.7 Assessment of atherosclerosis by Oil red O staining

Mice were sacrificed and perfused at physiological pressure with saline containing heparin. The left and right carotid arteries were removed en bloc with the trachea and esophagus. For frozen sections, tissue was embedded in Tissue-Tek optimum cutting temperature medium, frozen in liquid nitrogen, and stored at -80°C until stained. Oil red O staining was carried out using frozen sections as previously described (Nam et al., 2009) and nuclei were stained with hematoxylin. Images

were captured with a Zeiss epifluorescence microscope. Images were analyzed with Image J software to quantify lesion size as previously described (Nam et al., 2009). For en face oil red O staining to examine intercostal artery lesions, the aortas were removed, cleaned, and opened longitudinally with the luminal surface facing up. Aortas were rinsed with 60% isopropanol for 1 min. Staining was then performed with filtered Oil red O solution (Cayman Chemical, Ann Arbor, Michigan) for 30 min. Vessels were then rinsed with 60% isopropanol and pinned to black wax to reveal the entire luminal surface area. Images were obtained using a camera connected to a Zeiss dissecting microscope.

3.2.8 Vascular isometric tension studies

Endothelium-dependent and independent vasodilatation was examined using carotid rings obtained from LCA and RCA of partially ligated ApoE$^{-/-}$ mice as previously described (Nam et al., 2009). Isometric tension was measured using Multi Wire Myograph System Model 610M (DMT). After equilibrating for at least 30 minutes, the rings were preconstricted using phenylephrine. After a stable contraction was achieved, the rings were exposed to acetylcholine to assess endothelium-dependent vasodilation. Endothelium-independent relaxation to sodium nitroprusside (SNP) was also examined.

3.2.9 Flow cytometry for measurement of vascular inflammatory cells

Mouse carotids were minced with fine scissors and digested using collagenase type IX (125 U/ml), collagenase type I (450 U/ml), and hyaluronidase I (60 U/ml) dissolved in PBS containing calcium and magnesium for 1 hr at 37°C, with agitation

every 20 minutes. Digested samples were then homogenized using an 18 gauge needle yielding single cell suspensions. Cells were then centrifuged at 1,200 rpm and resuspended in FACS buffer. Cells were stained for 30 min at 4°C with antibodies and then washed and resuspended in FACS buffer. Antibodies used for staining were FITC rat anti-mouse CD4, PE-TR rat anti-mouse CD45, PerCP-Cy5.5 rat anti-mouse CD3, V450 rat anti-mouse CD8, APC rat anti-mouse CD44, APC Cy7 rat anti-mouse CD62L, FITC rat anti-mouse CD45, PerCP-Cy5.5 rat anti-mouse cd11c, APC rat anti-mouse cd11b, PE rat anti-mouse CD86, PE Cy7 rat anti-mouse F4/80, and Live/Dead Fixable Near-IR stain. Absolute cell counting was performed by adding a known quantity of calibration beads to a known sample volume. After staining, cells were analyzed immediately on a LSR-II flow cytometer with DIVA software (BD Biosciences). Data were analyzed using FlowJo software (Tree Star, Inc.).

3.2.10 Cytokine measurements

Mouse carotids were placed into each well of a 96-well plate containing 60 μL DMEM with 10% fetal calf serum, 100 U/ml penicillin, and 100 μg/mL streptomycin and maintained at 37°C under 5% CO_2 for 16 hours. During this time, a combination of phorbol myristate acetate (PMA, 10 μmol/L) and ionomycin (2 μmol/L) was added to stimulate vascular cytokine production. Following this, levels of cytokines TNF-α, IFN-γ, and IL-2 in the media were measured using cytokine bead array kit (BD Biosciences).

3.2.11 Statistical Analysis

Data are expressed as mean ± standard error of the mean. When two groups were compared, unpaired t tests were employed. ANOVA was employed for multiple comparisons and when significance was indicated, a two-tailed Bonferroni post hoc test was used to make selected comparisons. When one group was served as a control, the Dunnett post hoc test was used. A value of $p<0.05$ was considered significant.

3.3 Results

3.3.1 Effect of disturbed flow on GTPCH-1 phosphorylation and BH_4 levels in vivo

To determine if different shear profiles have varying effects on GTPCH-1 phosphorylation and BH_4 levels in vivo, I used an in vivo model of disturbed flow by inducing partial carotid ligation. This procedure reduced GTPCH-1 S72-phosphorylation by 50% compared to RCA in the same mouse as detected using a newly developed antibody to mouse GTPCH-1 phospho-S72, which is homologous to human phospho-S81 (Figure 3.1A and 3.1B). In accordance to impaired GTPCH-1 phosphorylation in the LCA, partial ligation also decreased total biopterin production in the LCA (Figure 3.1C). There was also evidence of BH_4 oxidation in the LCA, as indicated by decreased ratio of BH_4 to BH_2, likely due to increased reactive oxygen species production caused by oscillatory shear stress (Nam et al., 2009) (Figure 3.1C). Taken together, these markedly decreased BH_4 levels at regions of disturbed flow in vivo. Moreover, these results show that shear forces modulate GTPCH-1 phosphorylation and BH_4 production in intact vessels.

Figure 3.1 Effect of disturbed flow on GTPCH-1 phosphorylation and BH_4 levels in vivo. A, The LCA of C57BL/6 mice was partially ligated as described in the methods section. The LCA and RCA were then collected two days post-ligation and subjected to Western blot analysis. B, Densitometry values of phospho-S72 GTPCH-1 in the LCA vs. RCA in non-ligated and ligated mice (n=5). C, LCA and RCA were collected 4 days post-ligation for the measurement of total biopterin and BH_4 levels (n=5).

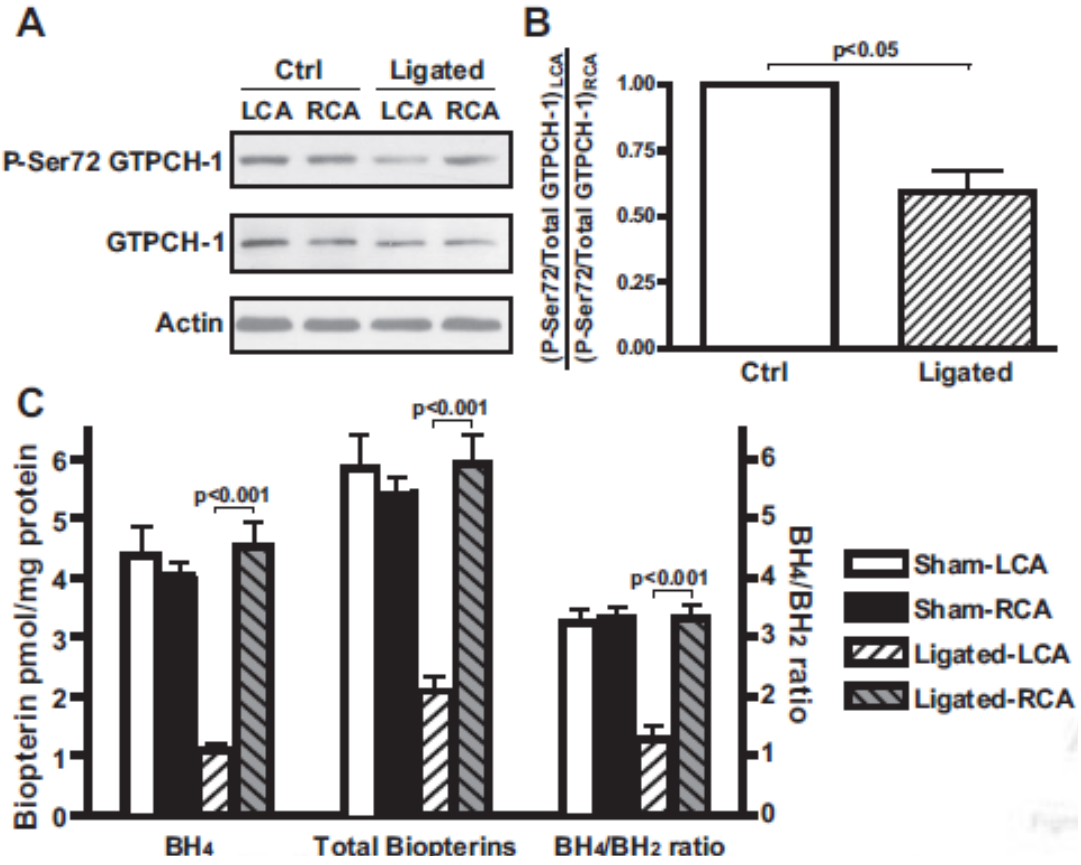

3.3.2 Disturbed flow induced by partial carotid ligation causes NOS uncoupling

I have shown that partial carotid ligation reduces total biopterin production and increases BH_4 oxidation to BH_2 in the LCA of the C57bl/6 mice. Next, I confirmed that this also occurred in $ApoE^{-/-}$ mice fed a high fat diet. In these animals, total biopterin and BH_4 were reduced in the LCA after 1 week of ligation (Figure 3.2A through 3.2C). Notably, the BH_4/BH_2 ratio in the LCA was lower than the RCA, indicating the higher oxidative stress in the LCA induced by disturbed flow (Figure 3.2D). We hypothesized that these defects in BH_4 synthesis and stability could cause NOS uncoupling. In keeping with this, in $ApoE^{-/-}$ mice that were ligated and treated with vehicle alone for one week, vascular $O_2^{\bullet-}$ production by the LCA was increased two-fold compared to the RCA. The NOS inhibitor NG-L-nitro-arginine methyl ester (L-NAME) inhibited $O_2^{\bullet-}$ production in the LCA, suggesting NOS was uncoupled and was a source of $O_2^{\bullet-}$ (Figure 3.3A). To localize $O_2^{\bullet-}$ production within the vessel wall, I also employed DHE staining. DHE staining was significantly increased not only in the endothelium, but also in the medium and adventitia of the LCA in vehicle treated animals (Figure 3.3B). Consistent with these results, low-temperature Western blot for eNOS revealed that in vehicle treated animals, carotid ligation decreased the level of intact eNOS dimers while increasing eNOS monomers, indicating uncoupling of eNOS (Figure 3.3C and 3.3D).

3.3.3 Effect of BH_4 treatment on NOS uncoupling and vascular $O_2^{\bullet-}$ production at areas of disturbed flow

I treated mice with BH_4 in the drinking water to examine if increasing BH_4

Figure 3.2 Pterin levels in the carotids that underwent partial ligation for one week. The left carotid arteries of ApoE$^{-/-}$ mice were partially ligated and mice were treated with an approximate dose of 10 mg/kg per day BH_4 in the drinking water or vehicle for 1 week. Total biopterin (Panel A), BH_2 (Panel B), BH_4 (Panel C) levels and the ratio of BH_4/BH_2 (Panel D) in the carotids were shown (n=5). Values were compared using two-way ANOVA and selected comparisons were made using a Bonferroni post hoc test.

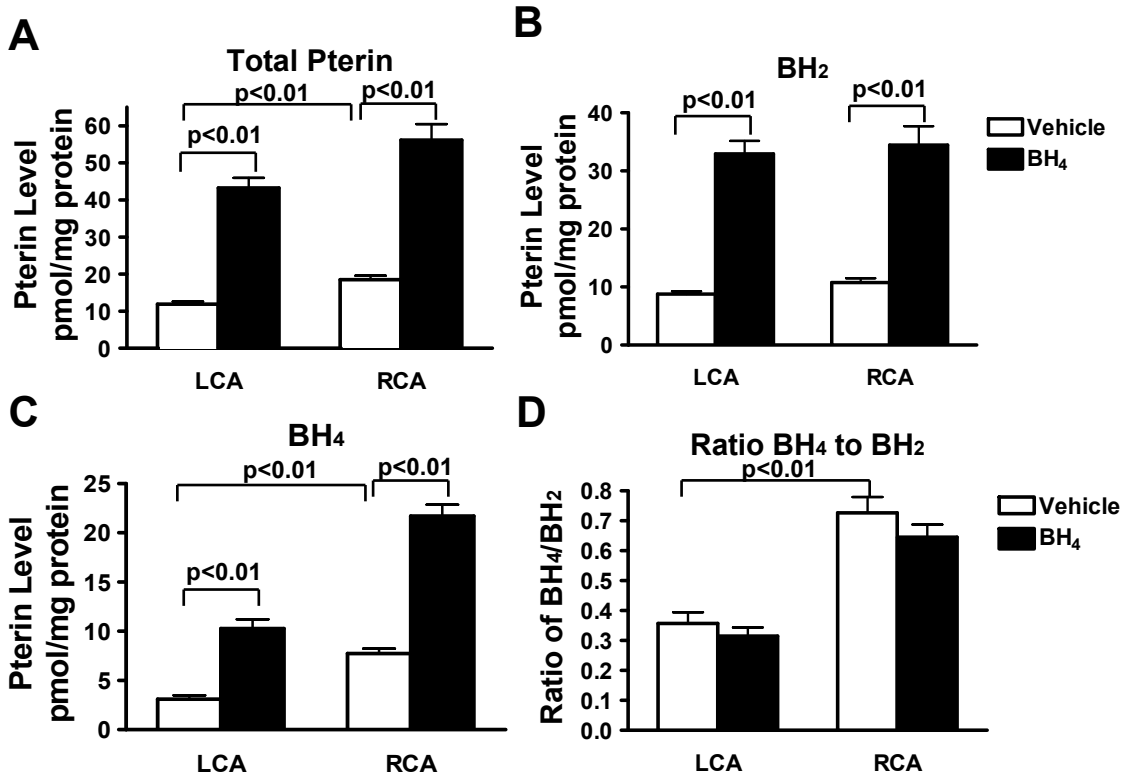

Figure 3.3 Identification of NOS uncoupling at areas of disturbed flow. ApoE$^{-/-}$ mice underwent partial carotid ligation and were fed a high fat diet for one week. Mice were further randomized to receive either oral BH_4 or vehicle in the drinking water. A, During incubation with DHE ex vivo, vessels were co-incubated with and without L-NAME and formation of 2-hydroxyethidium was subsequently measured by using HPLC (n=6). B, Representative images of DHE fluorescence (red) in frozen sections of carotid arteries. Autofluorescence of the elastic laminas is green. C, Representative western blot for eNOS dimer/monomer in the carotids using a low-temperature gel. D, Densitometry ratios for eNOS dimers and monomers (n=3).

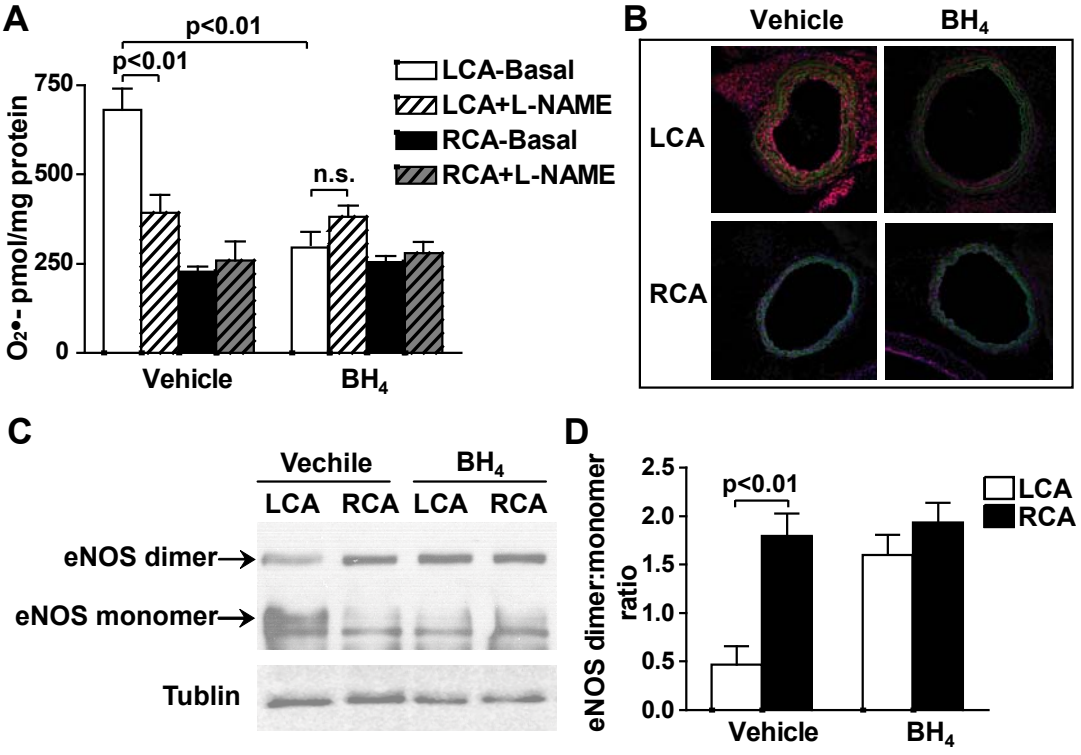

levels can reverse NOS uncoupling and decrease $O_2^{\bullet-}$ levels at areas of disturbed flow. BH_4 treatment for 1 week increased the total biopterin and BH_4 levels in the LCA to the values observed in the normal RCA (Figure 3.2A and 3.2C). This confirmed that oral BH_4 supplementation increased vascular BH_4 levels. BH_4 treatment also reduced $O_2^{\bullet-}$ production in the LCA while not affecting RCA levels. Moreover, in BH_4 treated mice, L-NAME increased $O_2^{\bullet-}$ production, suggesting that BH_4 treatment was able to recouple NOS in the setting of disturbed flow (Figure 3.3A). Using DHE staining, I found that BH_4 treatment markedly reduced $O_2^{\bullet-}$ production in all three layers of the vessel wall (Figure 3.3B). In keeping with this, BH_4 treatment inhibited disturbed flow-induced reduction of eNOS dimers and the increase of eNOS monomers (Figure 3.3C and 3.3D). Taken together, these results indicate that NOS uncoupling markedly enhances vascular $O_2^{\bullet-}$ production at areas of disturbed flow and that this can be ameliorated by BH_4 treatment.

3.3.4 Effect of NOS uncoupling on atherosclerosis induced by partial carotid ligation

I next sought to determine the role of NOS uncoupling in the severity of atherosclerosis at sites of disturbed flow. Nam et al. (Nam et al., 2009) have previously shown that partial carotid ligation in $ApoE^{-/-}$ mice fed a high fat diet causes accelerated atherosclerosis within 3 weeks. In keeping with this, Oil red O staining showed that the LCA of vehicle treated mice developed severe atherosclerosis. In striking contrast, BH_4 treatment for 3 weeks virtually eliminated atherosclerotic lesion formation in the LCA (Figure 3.4A and 3.4B). The unligated

Figure 3.4 Role of NOS uncoupling in atherosclerosis induced by partial carotid ligation. ApoE$^{-/-}$ mice underwent partial carotid ligation, were fed a high fat diet and were treated with BH_4, 5,6,7,8-tetrahydro-D-neopterin (NH_4) or vehicle for 3 weeks. A, Representative images of Hematoxylin and Oil red O staining of the carotid frozen sections. B, Quantification of the intimal lesion areas using Image J (n=6).

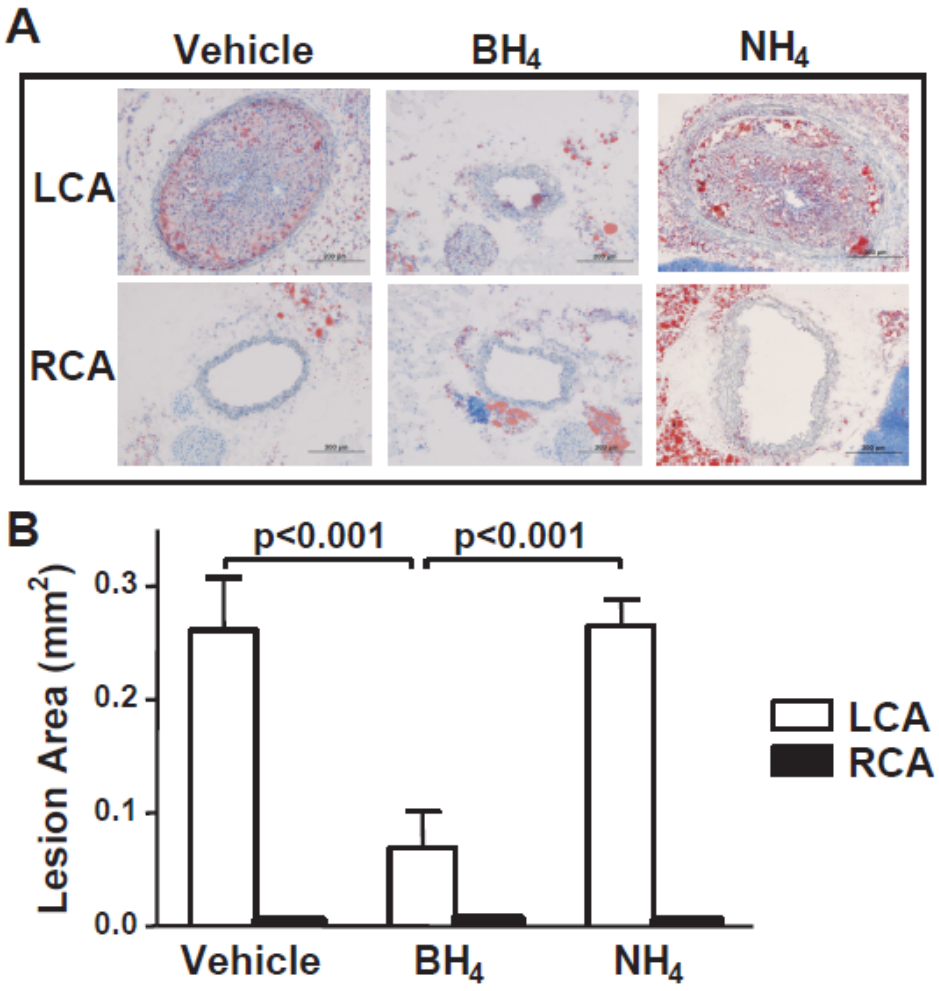

RCA did not develop atherosclerotic lesions in this time frame. BH_4 treatment for 3 weeks did not affect plasma cholesterol levels of the $ApoE^{-/-}$ mice fed a high fat diet for 3 weeks. To exclude the possibility that the benefit of BH_4 was due to a non-specific anti-oxidant effect, I also treated mice with 5,6,7,8-tetrahydro-D-neopterin (NH_4). NH_4 has a similar redox potential to BH_4, but does not sustain NOS catalysis. In contrast to BH_4 treatment, oral treatment with NH_4 did not affect atherosclerosis development (Figure 3.4A and 3.4B). Taken together, these findings indicate that NOS uncoupling plays a major role in promoting atherosclerosis at sites of disturbed flow and that this is markedly reduced by oral administration of BH_4. The benefit of BH_4 is likely due to improved NOS catalysis rather than direct anti-oxidant properties.

Prior studies of $ApoE^{-/-}$ mice have shown that atherosclerosis normally develops preferentially develops at the origin of the brachiocephalic and intercostal arteries, areas were shear stresses are low (Chien, 2008; VanderLaan et al., 2004). In keeping with these prior observations, we found that high fat feeding induced small lesions in the brachiocephalic artery and in some of the intercostal artery branches of the aorta. These were reduced by BH_4 treatment (Figure 3.5).

3.3.5 Effect of NOS uncoupling on endothelial dysfunction induced by partial ligation

Endothelial dysfunction is an early marker for atherosclerosis (Davignon and Ganz, 2004). A defect in BH_4 results in NOS uncoupling and reduces production of NO, leading to impaired endothelium-dependent vasodilation. We therefore sought

Figure 3.5 Effect of BH_4 treatment on atherosclerosis in the brachiocephalic and intercostal arteries of ApoE$^{-/-}$ mice fed a high fat diet. Animals also received BH_4 or vehicle in the drinking water for 3 weeks. A. Representative images of Hematoxylin and Oil red O staining of the brachiocephalic artery frozen sections. B. Quantification of the intimal lesion areas using Image J (n=5-6). Values were compared using an unpaired t-test. C. Representative images of en face Oil Red O staining of the aorta. Intercostal arteries were indicated by the yellow arrows. D. Quantification of the intercostal lesion area presented as percentage of entire aorta (n=5). Values were compared using an unpaired t-test.

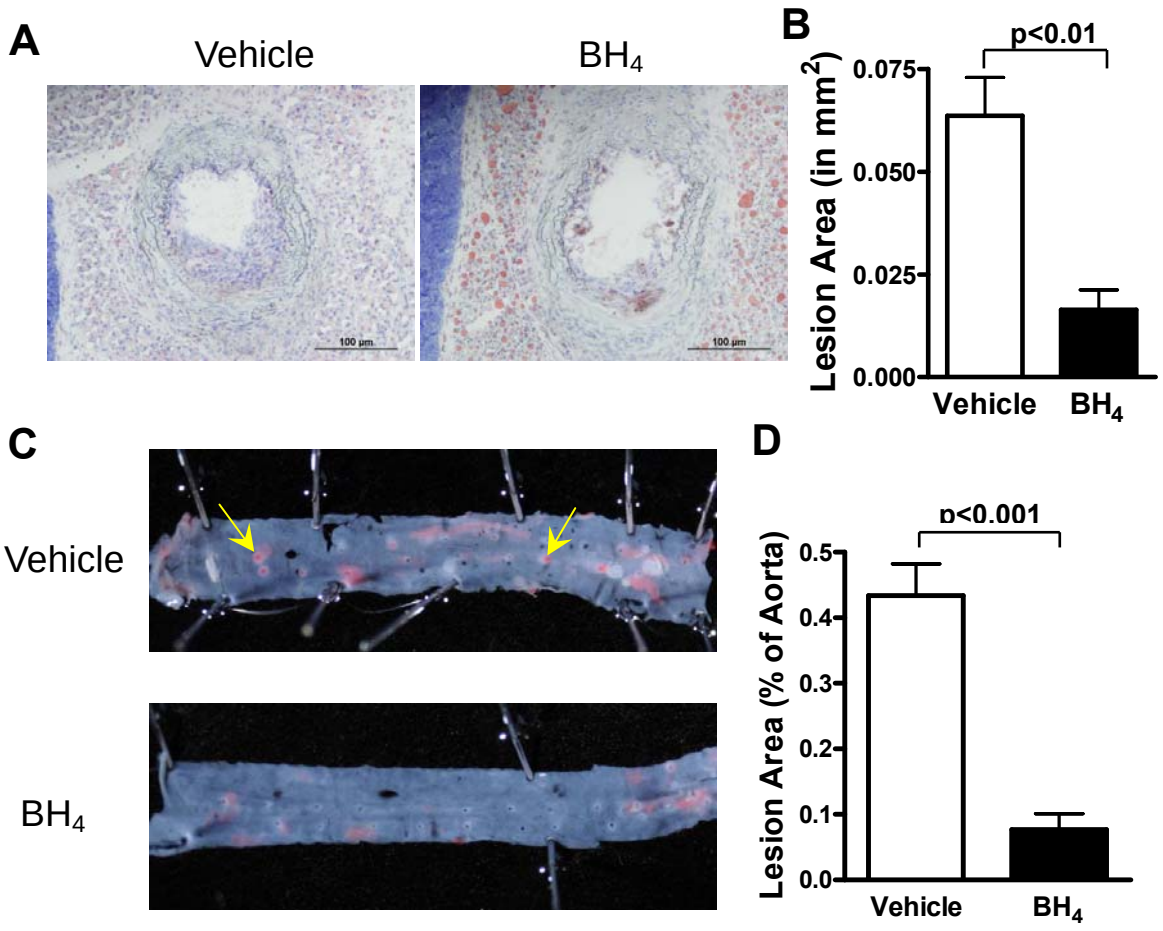

to determine if the endothelial dysfunction observed at sites of disturbed flow was due to NOS uncoupling. Carotid rings were obtained from LCA and RCA of partially ligated ApoE$^{-/-}$ mice fed a high fat diet for one week. Carotid rings were pre-constricted with phenylephrine and the relaxation evoked by increasing concentrations of acetylcholine was examined. In the unligated RCA, acetylcholine elicited potent relaxations reaching 90% of the pre-constricted tension at EC_{50} of 10^{-8} mol/L (Table 3.1). LCA segments from vehicle treated mice exhibited significantly blunted relaxations to acetylcholine both in terms of peak relaxation and the EC_{50}. BH_4 treatment normalized the peak relaxation to acetylcholine and improved but did not normalize EC_{50} (Figure 3.6A and Table 3.1). Endothelium-independent relaxation in response to the NO donor sodium nitroprusside (SNP) was identical among all the groups (Figure 3.6B). Thus, the alteration of endothelium-dependent vasodilatation observed at areas of disturbed flow is largely related to BH_4 deficiency and NOS uncoupling.

3.3.6 Role of NOS uncoupling in infiltration of activated immune cells at sites of disturbed flow

Inflammatory cells, including T cells, antigen-presenting dendritic cells and macrophages are present in atherosclerotic lesions and are thought to promote the progression of atherosclerosis and plaque instability by releasing inflammatory cytokines (Hansson, 2005). I therefore examined the role of NOS uncoupling in this inflammatory response at regions of disturbed flow. Using flow cytometry, I found that partial ligation of the LCA for one week caused marked infiltration of

Table 3.1 EC_{50} and peak relaxation values of LCA and RCA of $ApoE^{-/-}$ mice treated with vehicle or BH_4 in response to acetylcholine.

Experimental groups	EC_{50} Log M[Ach]	Peak relaxation (%)
Vehicle-LCA	-5.82 ± 0.64*	58.1 ± 14.0†
Vehicle-RCA	-8.33 ± 0.64	95.3 ± 3.1
BH_4-LCA	-6.80 ± 0.34¶	92.0 ± 3.3
BH_4-RCA	-8.09 ± 0.34	93.1 ± 4.8

* $p<0.001$ vs. RCA, †$p<0.01$ vs. RCA, ¶ $p<0.05$ vs. Vehicle-LCA (n=6-8).

Figure 3.6 Role of NOS uncoupling in endothelial dysfunction induced by partial carotid ligation. ApoE$^{-/-}$ mice underwent partial carotid ligation and were fed a high fat diet for one week. The animals were randomized to receive oral BH_4 or vehicle following carotid ligation. Arterial rings were obtained from LCA and RCA of these mice for vascular ring activity measurements. A, Rings were pre-constricted with phenylephrine and responses evoked by increasing concentrations of acetylcholine for endothelium-dependent relaxation (n=6-8). B, Responses to increasing concentrations of sodium nitroprusside (SNP) were studied to assess endothelium-independent relaxation (n=6-8).

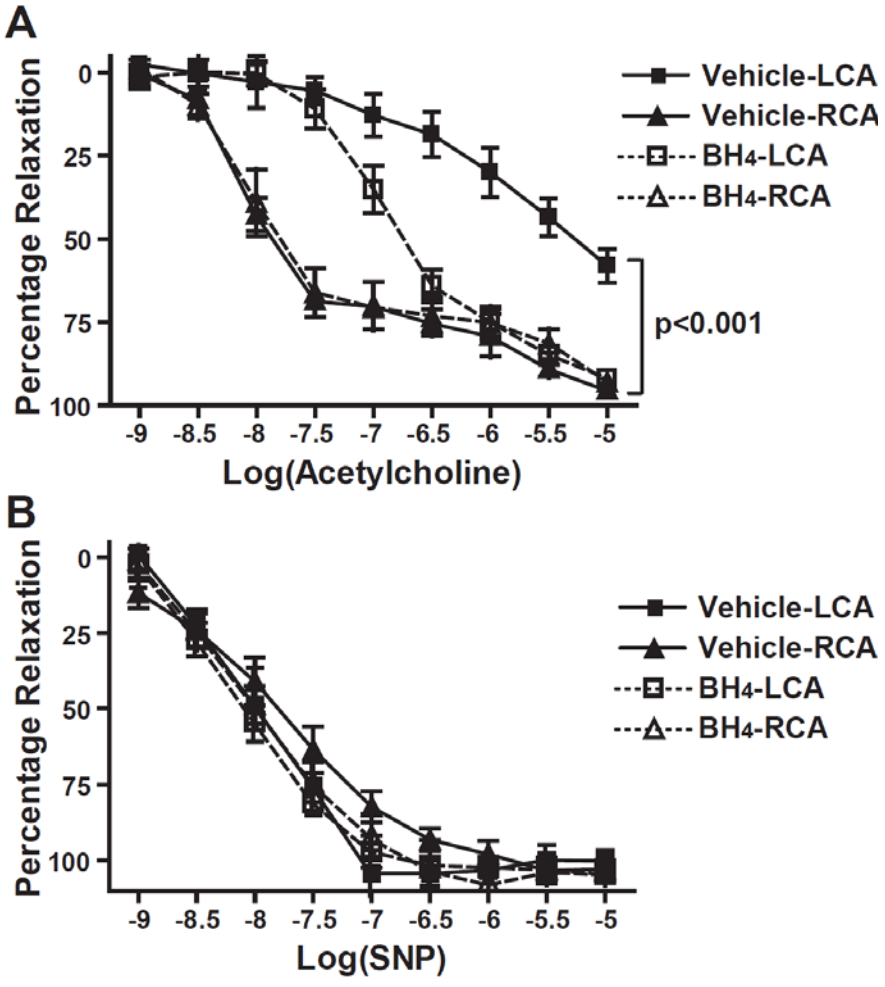

total leukocytes and T cells, characterized by the surface markers, CD45+ and CD3+, respectively. BH_4 treatment reduced the number of leukocytes and T cells in the LCA (Figure 3.7A through 3.7D). Within the T cell population, I found that BH_4 treatment reduced both CD4+ and CD8+ cells in the LCA (Figure 3.7E and 3.7F). In addition to reducing the total number of T cells in the LCA, BH_4 also decreased the number of activated T cells, as indicated by a reduced number of CCR5+ and $CD44^{High}$ cells (Figure 3.7G and 3.7H). Immune cells in the RCA were virtually undetectable. Of note, BH_4 treatment had no effect on levels of total leukocytes, T cells, CD4+ cells, CD8+ cells or activated T cells in the peripheral blood or spleen (Figure 3.8A through 3.8F).

Vascular monocyte infiltration and differentiation into macrophages is one of the hallmarks of atherosclerosis. I therefore examined vascular levels of monocytes and macrophages, characterized by surface markers, CD11b+ and F4/80+, respectively, at areas of disturbed flow. In the LCA of vehicle treated animals, both CD11b+ and F4/80+ cells were markedly increased compared to the RCA. BH_4 treatment reduced infiltration of these cells by approximately one half (Figure 3.9A through 3.9D). Taken together, these data suggest that vascular leukocyte and monocyte infiltration at sites of disturbed flow is in part due to NOS uncoupling and that this inflammatory response can be reduced by BH_4 treatment.

3.3.7 Role of NOS uncoupling in ex vivo cytokine production of the carotid exposed to disturbed flow

It is known that activated immune cells in the plaque produce cytokines (TNF-α,

Figure 3.7 Role of NOS uncoupling in infiltration of T cells and T cell activation induced by partial carotid ligation. ApoE$^{-/-}$ mice were fed a high fat diet and underwent partial carotid ligation for one week. Animals also received BH_4 or vehicle in the drinking water. Two carotids from the same treatment group were pooled to obtain adequate cell numbers for flow cytometry. Flow cytometry was performed to detect CD45 (A) and CD3 (B) in the carotids. Absolute numbers of vascular CD45+ (C) and CD3+ cells (D) were quantified using using counting beads and FlowJo software (n=6-8). Numbers of CD4+ (E), CD8+ (F), CD4+CCR5+ (G), and CD4+CD44^{High} (F) cells are shown (n=6-8).

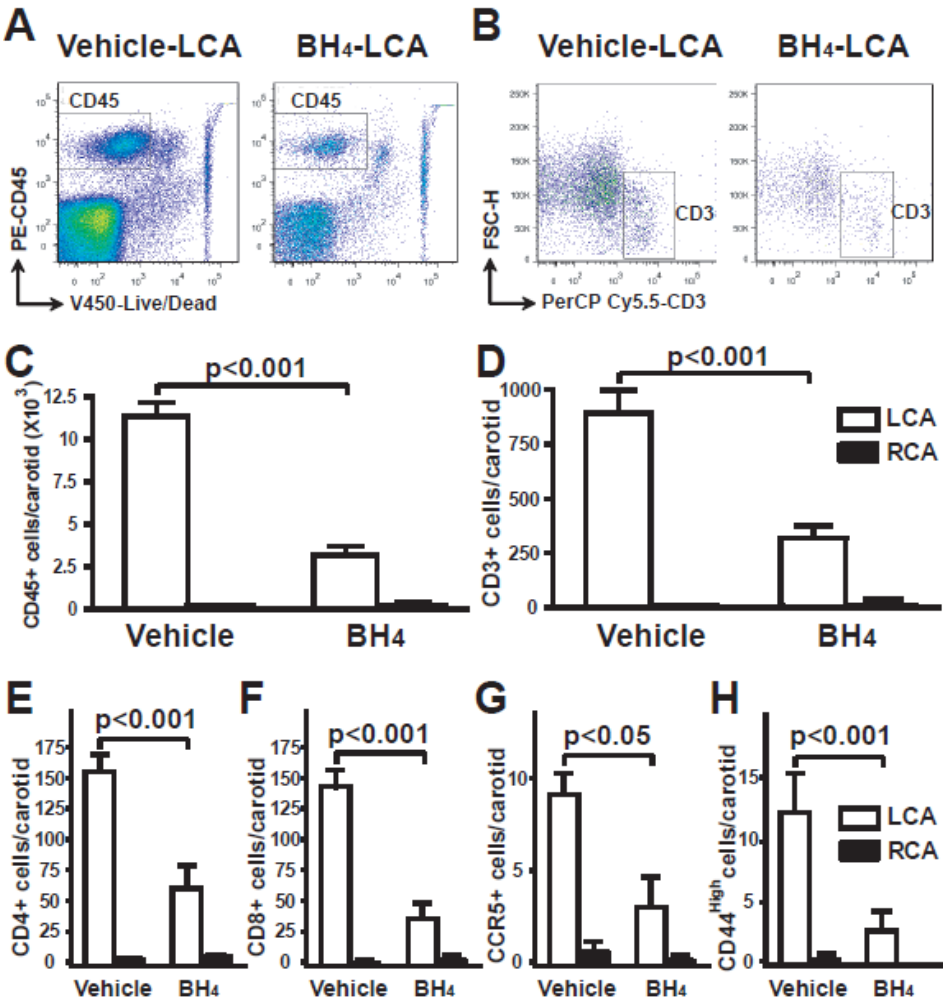

Figure 3.8 Effect of BH_4 treatment on T cell numbers and activation in the peripheral blood and spleen after partial carotid ligation. $ApoE^{-/-}$ mice were fed a high fat diet and underwent partial carotid ligation for one week. Animals also received BH_4 or vehicle in the drinking water. Percentages of CD45+ (A), CD3+ (B), CD4+ (C), CD8+ (D), CD4+CCR5+ (E), and $CD4+CD44^{High}$ (F) cells were shown (n=6).

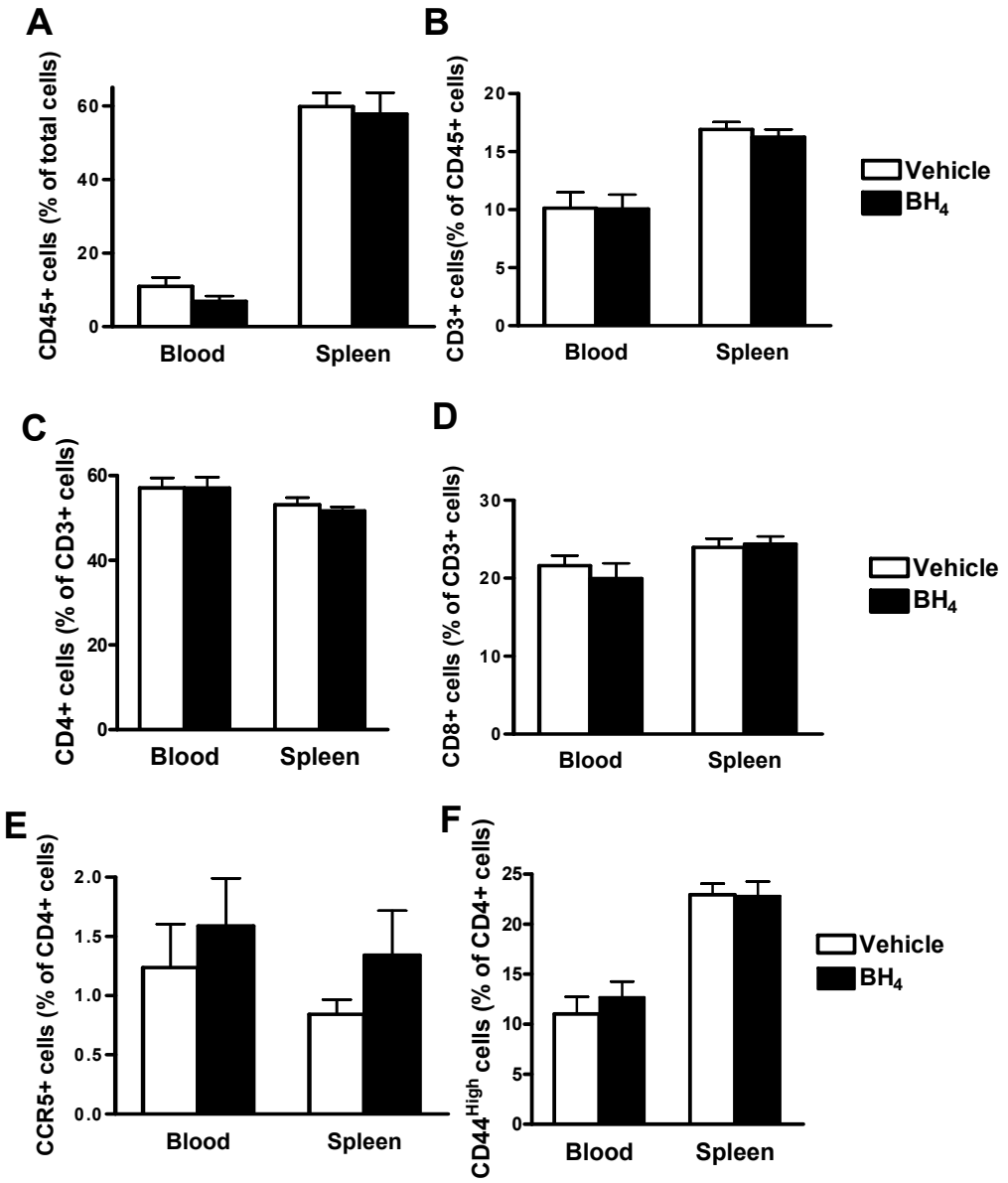

Figure 3.9 Role of NOS uncoupling in infiltration and activation of monocytes and macrophages induced by partial carotid ligation. ApoE$^{-/-}$ mice were fed a high fat diet and underwent partial carotid ligation for one week. Animals also received BH_4 or vehicle in the drinking water. Flow cytometry was performed to detect CD11b (A) and F4/80 (B) in the carotids. Absolute numbers of CD11b+ (C) and F4/80+ cells (D) in the carotids were shown (n=6-8).

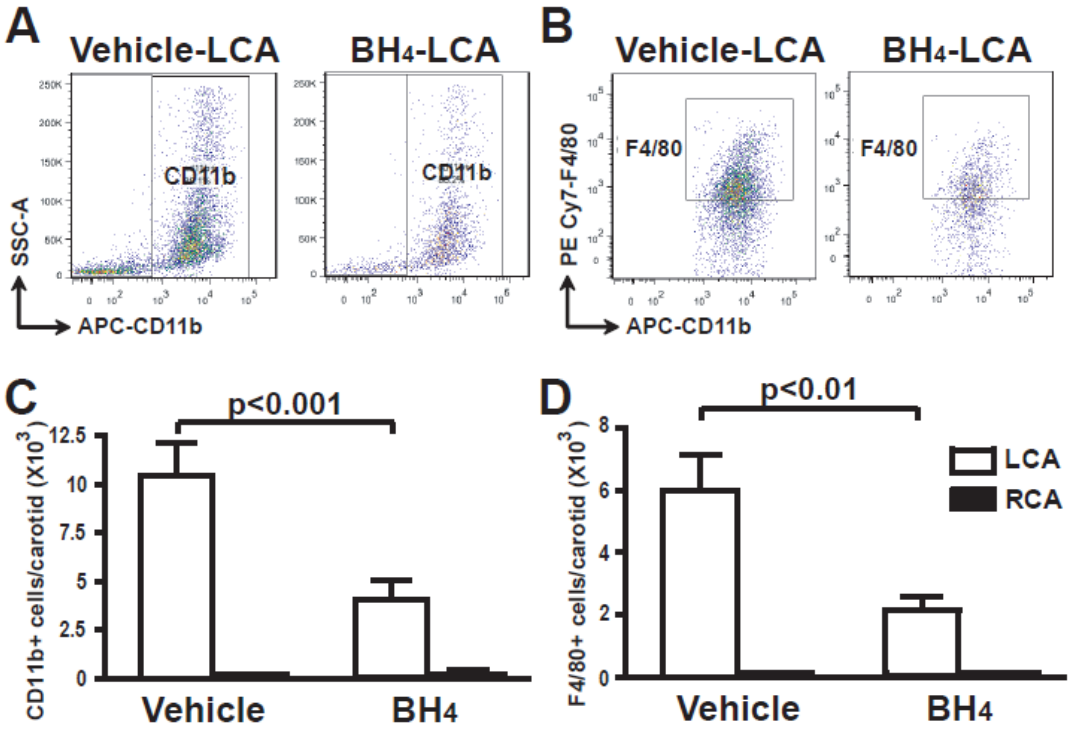

INF-γ, etc.) that promote further inflammation, induce plaque progression, and stimulate matrix proteases and ROS production. To examine the role of NOS uncoupling in cytokine levels in the LCA, I measured carotid cytokine production by incubating isolated mouse carotid ex vivo and stimulating it with a combination of phorbol myristate acetate (PMA) and ionomycin. The cytokines released into the media were then measured. I found that BH_4 treatment dramatically decreased levels of cytokines, including TNF-α, INF-γ, and IL-2 in the LCA of $ApoE^{-/-}$ mice that were partially ligated for 1 week (Figure 3.10A through 3.10C). These data further demonstrate NOS uncoupling promotes the inflammatory cascade that contributes to atherosclerosis at areas of disturbed flow and that this is suppressed by BH_4 treatment.

3.4 Discussion

In the present study, I demonstrate that disturbed flow produced by partial carotid ligation reduces GTPCH-1 phosphorylation, decreases total biopterin production, and augments BH_4 oxidation in vivo. I further show that these perturbations of BH_4 homeostasis lead to NOS uncoupling and contribute to the accelerated lesion development at regions of altered shear stress, including areas of disturbed flow induced by partial carotid ligation and naturally formed in the arterial tree. In addition to promoting lesion development, my findings indicate that BH_4 deficiency and NOS uncoupling contribute to vascular $O_2^{\bullet -}$ production and endothelial dysfunction associated with atherosclerosis at sites of disturbed flow. Finally, my data indicate that BH_4 deficiency and NOS uncoupling likely contribute

Figure 3.10 Role of NOS uncoupling in ex vivo cytokine production of the carotid induced by partial ligation. ApoE$^{-/-}$ mice that underwent partial carotid ligation were fed a high fat diet and treated with BH_4 or vehicle for one week. Isolated mouse carotids were incubated in DMEM medium containing 10 μmol/L PMA and 2 μmol/L ionomycin for 16 hours. TNF-α (A), IFN-γ (B), and IL-2 (C) in the culture media were measured by cytokine bead array (n=7-8).

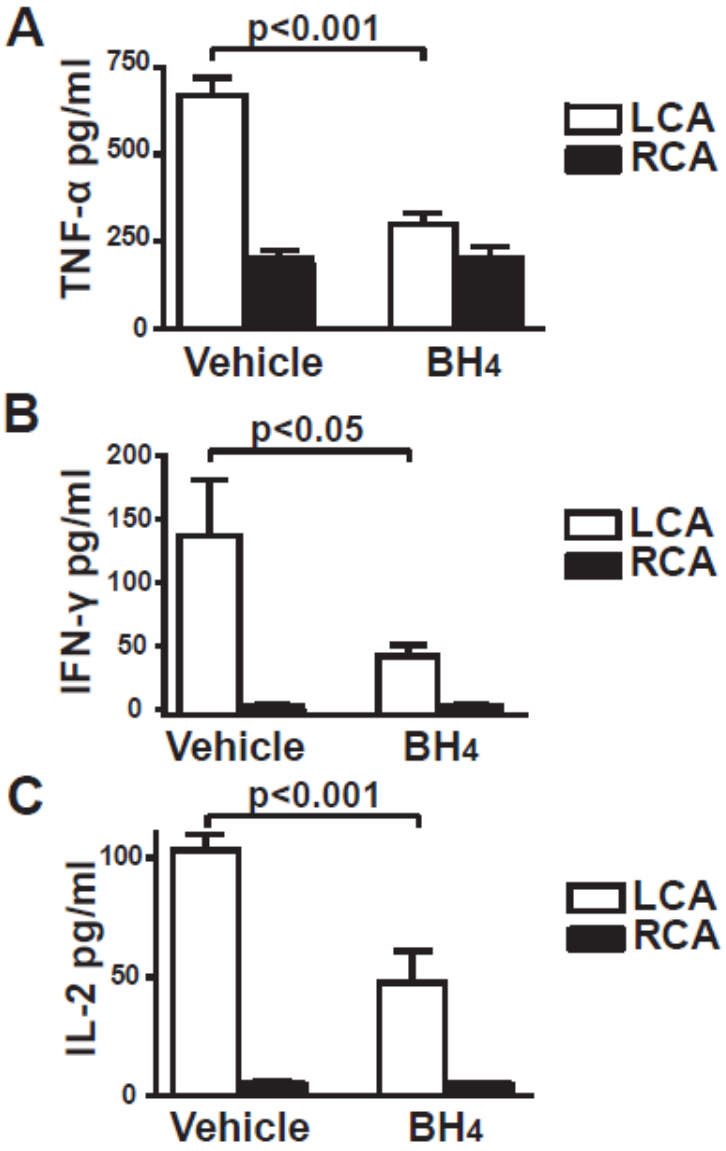

to the vascular inflammation and abnormal cytokine milieu induced by disturbed flow without affecting systemic immune cell numbers.

Evidence from animal models and human studies suggests that atherosclerosis preferentially develops at areas where blood flow is known to be disturbed, including the lesser curvature of the aortic arch, the infrarenal aorta, the carotid bulb and the proximal coronary arteries (Suo et al., 2007). Flow separations occur at these sites, reducing wall shear stress. In addition, flow reversal occurs at some of these sites, leading to oscillatory shear. Low and oscillatory shear stress promote atherosclerotic lesion development through a number of molecular and cellular mechanisms, including attenuation of NO-dependent atheroprotection, promotion of oxidative stress and inflammation, induction of vascular smooth muscle cell (VSMC) migration, and enhancement of low-density lipoprotein cholesterol (LDL) uptake (Chatzizisis et al., 2007). Oscillatory shear stress has been shown to activate the NADPH oxidases and cause eNOS uncoupling. I have shown that oscillatory shear can reduce BH_4 levels and cause eNOS uncoupling by at least two mechanisms. One is that oscillatory shear causes oxidation of BH_4; the other being that it reduces the synthesis of BH_4 by reducing GTPCH-1 phosphorylation and activation. My findings indicate that the reduction in NO and concomitant increase in $O_2^{\bullet -}$ caused by NOS uncoupling likely play a critical role in the accelerated lesion formation caused by disturbed flow in vivo.

In the present study, I employed a model of rapid developing atherosclerosis caused by partial carotid ligation in $ApoE^{-/-}$ mice fed a high fat diet (Nam et al.,

2009). This intervention leads to both low and oscillatory shear stress in the carotid proximal to the site of ligation. The resulting lesions share many characteristics of complex human atherosclerotic lesions, including lipid deposition, inflammation and fibrosis. This model allows examination of interventions such as BH_4 administration over a short period, but does not provide insight into any long term benefits of BH_4 therapy. In keeping with my studies, Schmidt et al. (Schmidt et al., 2010) have shown that oral BH_4 reduces atherosclerosis in the aortic root over 12 weeks. Likewise, Hattori et al. (Hattori et al., 2007) have shown a benefit of BH_4 treatment on plaque development in $ApoE^{-/-}$ mice over 10 weeks of high fat feeding. Of note, in the study of Hattori et al. (Hattori et al., 2007), BH_4 therapy seemed to have a striking effect on lesion development in the lesser curvature of aorta, where shear stress has been shown to be oscillatory.

BH_4 exhibits modest anti-oxidant effects, and therefore could have prevented atherosclerosis via its ability to scavenge ROS. We and others have previously shown that BH_4 reacts with strong oxidants, including peroxynitrite, thiyl and carbonate radicals (Laursen et al., 2001; Patel et al., 2002). To exclude the possibility that the effect of BH_4 was mediated by oxidant scavenging, I performed additional experiments with NH_4, an anti-oxidant structurally similar to BH_4 but without cofactor activity for NOS. My data demonstrate that NH_4 did not protect against disturbed flow induced atherosclerosis, suggesting that the effect of BH_4 was primarily mediated by its ability to sustain NOS catalysis.

In the present study, I found that BH_4 treatment decreased $O_2^{\bullet -}$ production not

only in the endothelium, but also in the media and adventitia. This might have been due to its ability to sustain catalysis of NOS isoforms in all these cell layers. In additional to eNOS, neuronal NOS (nNOS) is expressed in rat and human vascular smooth muscle cells (Boulanger et al., 1998; Buchwalow et al., 2002). Expression of inducible NOS (iNOS) in the vessel wall can also occur in the setting of oxidative stress and inflammation (Gunnett et al., 2005). Upmacis et al. (Upmacis et al., 2007) reported the contribution of iNOS uncoupling in vascular dysfunction in atherosclerosis by showing profound biopterin oxidation and protein tyrosine nitration in $ApoE^{-/-}$ mice on an atherogenic diet. Importantly, Wilcox et al. (Wilcox et al., 1997) showed that atherosclerosis is associated with expression of all forms of NOS in the intima and adventitia. It is also conceivable that ROS produced by uncoupled NOS could activate other sources of superoxide, such as the NADPH oxidase, in a feed forward fashion, and that these could contribute to ROS production throughout the vessel wall.

In keeping with improved NOS catalysis, endothelium-dependent vasodilatation of the ligated carotid arteries was partially enhanced by BH_4 treatment. It is of interest that in normal vessels, the dose response curve to acetylcholine seemed biphasic, rather than sigmoidal. This response is similar to that observed by others (Schrader et al., 2007; Stec et al., 2008). Of interest, BH_4 treatment normalized the relaxation to higher doses of acetylcholine and thus the peak response to acetylcholine, while having a partial beneficial effect on the responses to the lower doses and thus partially shifted EC_{50}s. It is conceivable that this might reflect a

differential effect of BH_4 on different mechanisms of carotid artery relaxation.

It is well known that inflammation plays a key role in the pathogenesis of atherosclerosis (Hansson, 2005). Flow disturbances promote endothelial expression of leukocyte adhesion molecules and chemokines, such as VCAM-1 and MCP-1. These could in turn induce monocyte rolling, adhesion and transmigration into the sub-endothelial space, promoting early lesion development. Monocytes differentiate into macrophages that present antigens and trigger T cell activation within the lesion. Of note, the T cells present in the lesions caused by disturbed flow seemed to have the phenotype of effector T cells, in that they express CCR5 and are $CD44^{High}$. These activated T cells produce Th1 cytokines, such as TNF-α and INF-γ, which further lead to inflammation and lesion progression. My data indicate that NOS uncoupling has a dramatic impact on these inflammatory events. I found that BH_4 treatment reduced vascular accumulation of T cells and macrophages. Increased oxidative stress at areas of disturbed flow can also cause oxidative damage to lipids, DNA or proteins and generate various inflammatory molecules, which can be processed as antigens by macrophages and dendritic cells to active T cells and induce inflammation. It is likely that BH_4 treatment decreases the antigen load by substantially reducing oxidative stress in the vessel wall induced by disturbed flow, thereby suppressing the inflammatory cascade. In addition to preventing the accumulation of these cells, BH_4 treatment also markedly reduced the ability of vascular segments to elaborate Th1 cytokines, such as TNF-α, INF-γ, and IL-2. In keeping with my findings, Ali et al. (Ali et al., 2008) showed that

increased endothelial BH_4 reduces vein graft neointimal hyperplasia and atherosclerosis through a reduction in vascular inflammation via the MCP-1/CCR2 signaling pathway. A very recent study also showed that BH_4 treatment and gene transfer of GTPCH-1 reduced the infiltration of T cells, macrophages and monocytes in the vessel in a hypercholesterolemia induced atherosclerosis model (Schmidt et al., 2010). Taken together, these data indicate that recoupling of NOS has dramatic effects in reducing vascular inflammation in the setting of rapid atherosclerosis development.

In summary, my findings demonstrate that NOS uncoupling is a key mechanism by which disturbed flow induces accelerated atherosclerosis. I find that oral BH_4 supplementation prevents NOS uncoupling and improves endothelial function in the carotid exposed to disturbed flow induced by partial carotid ligation. The reduction in oxidative stress elicited by BH_4 treatment is associated with diminished monocyte adhesion and T cell activation as well as blunted cytokine production from the vessel wall. Taken together, these indicate that BH_4 treatment, by correcting NOS uncoupling and rectifying the oxidative status at areas of disturbed flow, targets the underlying mechanism of atherosclerosis progression by inhibiting inflammation. These results highlight a pivotal role of BH_4 deficiency and NOS uncoupling in atherosclerosis progression, particularly under the patterns of low and oscillatory shear flow, and indicate that modulation of vascular BH_4 levels could be a therapeutic target for preventing atherosclerosis at branches and curvatures in the arterial tree.

Chapter 4:

Identification of inhibitors of GTPCH-1 and GFRP interaction and development of a time-resolved fluorescence resonance energy transfer assay to monitor GTPCH-1 and GFRP interaction

4.1 Introduction

GTP Cyclohydrolase I (GTPCH-1) converts GTP to dihydroneopterin triphosphate (H_2NTP) and is the first and rate-determining enzyme in the pathway for *de novo* synthesis of BH_4. BH_4 is an essential cofactor that controls the activity of all three NOS isoforms and the aromatic amino acid hydroxylases. Since BH_4 levels commonly restrict the activity of enzymes that rely on it as a cofactor, GTPCH-1 activity can govern the synthesis of NO and other key cell signaling molecules and neurotransmitters.

A well-characterized mechanism for control of GTPCH-1 activity is through its interaction with GFRP. In vitro, GFRP mediates both end-product inhibition by BH_4 and this inhibition is reversed by phenylalanine (Harada et al., 1993). Of note, in the presence of BH_4, GFRP induces a decrease in GTPCH-1 enzymatic activity. This diminishes Vmax of GTPCH-1, as shown by our own laboratory and others (Figure 2.7 and Table 2.1) (Harada et al., 1993).

As demonstrated in Chapter 2, using both siRNA inhibition and overexpression of GFRP, I found that GFRP inhibits GTPCH-1 activity in human aortic endothelial cells. I also demonstrated that laminar shear stress increases GTPCH-1 activity, and this is associated with the dissociation of GTPCH-1 and GFRP and an increase in phosphorylation of GTPCH-1. Unidirectional laminar shear promotes dissociation of GTPCH-1 and GFRP, while oscillatory shear stress does not. We therefore speculate that dissociation of GTPCH-1 and GFRP increases GTPCH-1 enzyme activity, in part by promoting its phosphorylation by CK2α'. In keeping

with this, I find lower levels of BH_4 in carotid arteries exposed to disturbed flow caused by partial carotid ligation than in control vessels (Figure 3.1). My data also indicate that these regions of the circulation are markedly predisposed to atherosclerotic lesion formation. Currently, there is no specific treatment to reduce atherosclerosis at sites of disturbed flow. We propose that agents that disrupt the binding of GTPCH-1 and GFRP would increase BH_4 levels at these sites and thus could reduce atherosclerosis.

Further understanding of the mechanism by which GTPCH-1 interacts with GFRP would facilitate the development of peptide or small molecule inhibitors of GTPCH-1 and GFRP interaction. X-ray crystallography of human GTPCH-1 reveals that each of the 10 identical monomers folds into an N-terminal extended α-helix (h1) and two antiparallel helices (h2, h3), separated from a compressed C-terminal domain made up of four antiparallel β-sheets (b1-b4) divided by two antiparallel helices (h4, h5) that terminate in a C-terminal helix (h6) (Figure 4.1) (Swick and Kapatos, 2006). In the crystal structure of the biopterin-induced inhibitory complex of GTPCH-1 and GFRP reported by Maita et al. (Maita et al., 2004), h5, the loop between h5 and b3, b4 and h6, all of which are in the C-terminal region of GTPCH-1, are in direct contact with GFRP. More specifically, this interaction is primarily due to van der Waals forces and a salt bridge formed between Arg_{11} of GFRP with Glu_{236} of GTPCH-1 (Bader et al., 2001; Maita et al., 2004). Asp_{42} of GFRP is also thought to form direct and water-mediated hydrogen bonds with Glu_{236} and Arg_{235} of GTPCH-1.

Figure 4.1 Amino acid sequence of Human GTPCH-1. A, Full-length human GTPCH-1 amino acid sequence with secondary α-helical (h1-h6) and β-strand (b1-b4) structures shown. Synthesized peptides are highlighted in yellow (Peptide 1), green (Peptide 2) and pink (Peptide 3). The amino acids involved in direct interaction with GFRP in the inhibitory complex are in bold, according to Maita et al (Maita et al., 2004). B, Schematic representations of full-length GTPCH-1, N-terminal domain with unknown structure (N42), N-terminal poly proline domain (N96), C-terminal core domain (ΔN42), and C-terminal 20 amino acid truncated domain (ΔC20).

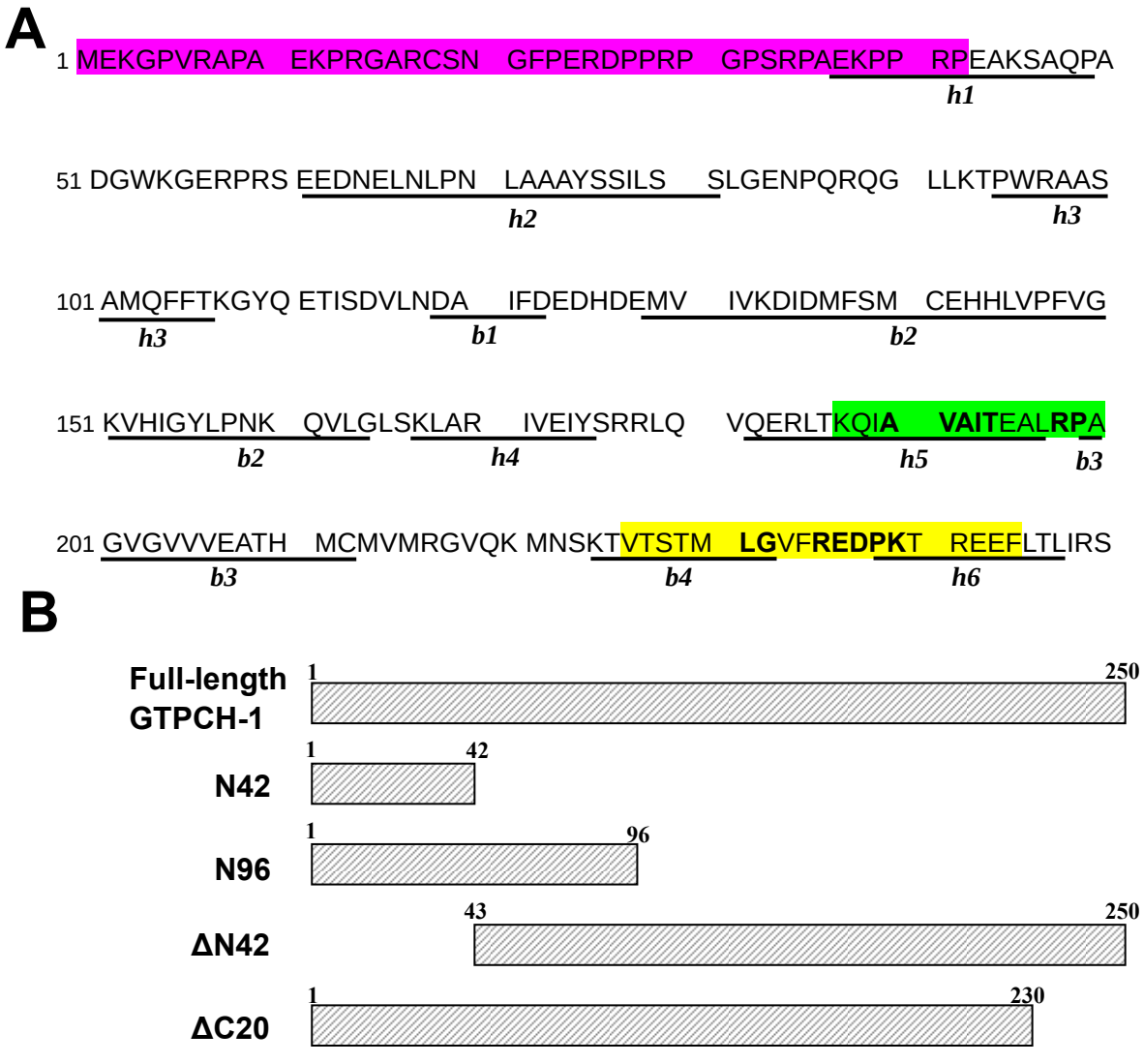

However, the N-terminal 56 amino acids of human GTPCH-1 remains structurally undefined, presumably due to the mobility of the N-terminal peptide (Maita et al., 2004). The 56 amino acids of human GTPCH-1 correspond to 47 amino acids in the N-terminus of rat GTPCH-1 and lack sequence homology to the N-terminal extension of *Drosophila* and *E.Coli* GTPCH-1. A yeast two-hybrid study showed that the 42 N-terminal peptide of human GTPCH-1 may also mediate interaction with GFRP (Swick and Kapatos, 2006). In this study, the absence of N-terminal amino acids 1–42 decreased the strength of the GTPCH-1/GFRP interaction by approximately 80%, indicating a significant role for extended h1 in the stabilization of the GTPCH-1/GFRP complex. Of note, we find that phosphorylation of human GTPCH-1 at S81 markedly increases its enzyme activity. It is therefore possible the N-terminal region of GTPCH-1 is involved in regulating its enzyme activity. This part of my dissertation was therefore performed to characterize which regions of GTPCH-1 are required and/or sufficient for interaction with GFRP and GFRP-mediated inhibition of GTPCH-1 activity. Thus, a peptide could be developed to inhibit GTPCH-1/GFRP interaction by competing with full length GTPCH-1 to bind to GFRP.

In order to discover small molecule compounds to disrupt GTPCH-1/GFRP interaction, in collaboration with Chemical Biology Discovery Center at Emory, I developed a homogenous time-resolved fluorescence resonance energy transfer (TR-FRET) assay to monitor this interaction. FRET is a process where a donor fluorophore in its excited state transfers resonance energy to a fluorophore in close

proximity (< 100Å). The FRET principle used in drug discovery typically involves energy transfer from a lanthanide chelate with long life time (e.g., > 100 ms) to a conventional fluorophore with short lifetime (e.g., < 100 ns) (Antonio et al., 2007). In the case of TR-FRET, by exciting the donor fluorophore with pulsed light and gating the emission with a 50 μs delay, background emission from the short lifetime acceptor can be eliminated (Gunther et al., 2009). The TR-FRET assay gives low background signals and can be run in a homogeneous and one step "mix-and-read" format, thus amenable to high throughput screening (HTS) automation.

In my TR-FRET assay system, His-tagged human GTPCH-1 is conjugated to a Europium chelate via a Europium-anti-His antibody as the FRET donor, and GST-tagged human GFRP is conjugated to an Allophycocyanin (APC) flurophore via an APC-anti-GST antibody as the FRET acceptor. Here, I present details of the development, optimization, and validation of a TR-FRET assay that monitors the interaction of GTPCH-1 and GFRP. The goal of this TR-FRET assay was to quantitatively measure GTPCH-1/GFRP interaction and to provide a method that can identify compounds that inhibit this interaction. This assay demonstrates an excellent signal-to-background ratio and a Z' factor compatible with an effective high throughput screening (HTS). We validated this assay in an HTS format using the Library of Pharmacologically Active Compound (LOPAC). Using a confirmatory protein-protein interaction assay and a cellular activity assay, we have identified compounds that disrupt GTPCH-1/GFRP interaction and increase endothelial cell biopterin levels. This HTS approach could be used to identify

small molecules that might be useful in the treatment of diseases in which BH_4 is deficient.

4.2 Materials and methods

4.2.1 Reagents

Europium-anti-His and Allophycocyanin (APC)-anti-GST antibody were purchased from Perkin Elmer (Waltham, MA). Library of Pharmacologically Active Compounds (LOPAC) was from Sigma-Aldrich (St.Louis, MO). The following peptides were synthesized and purified by Genscript (Piscataway, NJ): Peptide 1 (VTSTMLGVFREDPKTREEFC), Peptide 2 (KQIAVAITEALRPAC), and Peptide 3 (MEKPRGARCSNGFPERDPPRPGPSRPAEKPPRPC) (Figure 4.1). All other reagents were of highest purity and were obtained from Sigma-Aldrich.

4.2.2 DNA constructs

Human GTPCH-1 cDNA was obtained form GeneCopoeia (Cat.No.EX-X0381-M07) and was cloned into the pCMV-HA vector (Clontech) and the pET-30a(+) vector (EMDBiosciences, Madison, WI) to create pCMV-HA/GTPCH-1 and pET-30a/GTPCH-1 constructs, respectively. The human GFRP cDNA was synthesized by Genscript (Piscataway, NJ) and cloned into the pDsRed-Monomer-C1 vector (Clontech) and the pGEX-5X-3 vector (GE Healthcare) to create pDsRed/GFRP and pGEX-5X-3/GFRP constructs, respectively. Various segments of the GTPCH-1 gene were amplified from the full-length pCMV-HA/GTPCH-1 construct as a template by PCR (Figure 4.1). The primers for generation of each of these constructs are listed in Table 4.1. PCR products

Table 4.1 List of primers used to generate GTPCH-1 truncation constructs.

GTPCH-1 Constructs	Primers
N42	Forward: 5’- CCGGAATTCAATGGAGAAGGGCCCTGTGCGGGCACC-3’ Reverse: 5'- GACGTCGACTCAGGGCCGCGGGGGCTTCTCCGC -3'
N96	Forward: 5’- CCGGAATTCAATGGAGAAGGGCCCTGTGCGGGCA -3’ Reverse: 5'- GACGTCGACTCACCAGGGCGTCTTGAGCAGCCCTTG -3'
ΔN42	Forward: 5'- CCGGAATTCAGAGGCCAAGAGCGCGCAGCCC -3' Reverse:5'-GACGTCGACTCAGCTCCTAATGAGAGTCAGGAACTCTTCC-3'
ΔC20	Forward: 5’- CCGGAATTCAATGGAGAAGGGCCCTGTGCGGG -3’ Reverse: 5'-GACGTCGACTCACATTGTGCTGGTCACAGTTTTGCTGTTC-3'

were then purified and digested by restrictions enzymes EcoR I and Sal I (New England Biolabs) and inserted into the pCMV-FLAG-2 vector (Sigma-Aldrich). DNA sequencing was used to confirm construct sequences (Agencourt Biosciences, Beverly, MA).

4.2.3 Cell culture and transfection procedure

Human Aortic Endothelial Cells (HAEC) were purchased from Lonza (Walkersville, MD) and used between the 3rd and 6th passages. Plasmids were transfected in HAECs using PrimeFect II (Lonza).

4.2.4 Co-immunoprecipitation (Co-IP)

Cells were harvested in 1X RIPA lysis buffer (Millipore) supplemented with Complete Protease Inhibitor Cocktail Tablet (Roche). Supernatants (400 μg total protein) were pre-cleared with 20 μL of protein A/G Plus agarose beads (Santa Cruz Biotechnology) for 6 h at 4˚C and incubated overnight at 4˚C with 20 μL of protein A/G Plus agarose beads and 3 μL of anti-DsRed polycolonal antibody (Clontech), or an equal amount of non-immune rabbit IgG as a control. After four washes in phosphate-buffered saline buffer (PBS), the immunoprecipitated proteins were separated by SDS-PAGE, transferred to nitrocellulose membranes, and immunoblotted with anti-HA (Cell Signaling Technology), anti-FLAG (Sigma-Aldrich) or our custom made anti-GFRP antibodies.

4.2.5 Protein expression and purification of recombinant proteins

E. coli (strain BL21) was transformed with pET-30a/GTPCH-1 and pGEX-5X-3/GFRP constructs and cultured overnight in LB medium. The culture

was then diluted 1:100 with pre-warmed LB and incubated at 37°C with vigorous shaking. Recombinant His-GTPCH-1 and GST-GFRP were obtained by isopropyl-β-d-thiogalactopyranoside (IPTG, 0.5 mmol/L) induction for 4 h at 30°C. His-GTPCH-1 was purified by passing through a nickel column and GST-GFRP was purified by using the B-PER GST Fusion Protein Purification Kit (Thermo Scientific).

4.2.6 TR-FRET measurements

The assay buffer (FRET buffer) contained 20 mM Tris, pH 7.5, 0.01% Nonidet P40, and 50 mM NaCl. Black 384-well and 1536-well microplates (Corning Costar, Cambridge, MA) were used and FRET signals were recorded on an Envision Multilabel plate reader (Perkin Elmer). Europium excitation was at 337 nm, and emission from europium donor and APC acceptor was measured at 615 and 665 nm, respectively. All FRET signals were expressed as FRET ratios: FRET = F665 nm / F615 nm * 10^4. The FRET signal window was considered the difference between the maximal FRET value recorded for bound GTPCH-1/GFRP and the minimal FRET value (background), recorded in the absence of GFRP.

4.2.7 Assay development and optimization

The TR-FRET assay was first performed in black 384-well microplates with a total volume of approximately 30 μL per well. To determine its binding affinity to GFRP, His-GTPCH-1 was serially diluted into FRET buffer and containing GST-GFRP (80 nM), cofactors for GTPCH-1/GFRP interaction (10 μM BH_4, 100 μM GTP and 100 μM ascorbic acid), Europium-anti-His antibody (1 nM) and

APC-anti-GST antibody (50 nM). A 30-µL volume of this mixture was dispensed into each well, incubated at room temperature for up to 20 hours, and measured on the Envision Multilabel plate reader. The binding affinity of GST-GFRP to His-GTPCH-1 was determined by serial dilutions into FRET buffer, mixing with His-GTPCH-1 (80 nM), cofactors for GTPCH-1/GFRP interaction (10 µM BH_4, 100 µM GTP and 100 µM ascorbic acid), Europium-anti-His antibody (1 nM) and APC-anti-GST antibody (50 nM), and evaluating 30 µL of this mixture as described above.

To quantify the assay performance, the signal-to-background ratio (S/B) and the Z' factor were calculated based on the following equations: S/B = µb/µf where µb and µf are the FRET signals for bound (b) GTPCH-1/GFRP and free (f) GTPCH-1 or GFRP alone, respectively. The difference between mean signals for bound and free was represented by (µb-µf). The Z' factor was calculated using the following equation: $Z' = 1 - (3 \times SDb + 3 \times SDf)/(\mu b - \mu f)$, where SDb and SDf are the standard deviations for bound (b) and free (f) conditions (Ozers et al., 2005). The Z' factor reflects the quality of the assay and quantifies the suitability of a particular assay for use in a full-scale, high-throughput screen. A Z' factor between 0.5 and 1.0 is usually considered to be an excellent assay for HTS.

Assay stability was evaluated by monitoring interaction of GTPCH-1 and GFRP after incubation times from 10 minutes to 20 hours. The effect of DMSO on the maximal signal was evaluated by increasing solvent percentage up to 10% and measuring after 5 hour incubation at room temperature.

4.2.8 HTS format

The suitability of the TR-FRET assay for ultra HTS was determined by performing the assay in 1536-well microplates. To accommodate the 1536-well plate format all reaction volumes were scaled down. His-GTPCH-1 (80 nM), GST-GFRP (80 nM), Europium-anti-His antibody (1 nM) and APC-anti-GST antibody (50 nM) were diluted in FRET buffer and mixed together. The mixture reaction buffer (5 μl) was dispensed to 1536-well plates and FRET signals were measured using the Envision multilabel plate reader with laser excitation at 337 nM. The S/B ratios and Z' factors were calculated as described above.

In the ultra high throughput screening (uHTS) of compound libraries, the mixed assay reaction buffer was dispensed at 4.6 μl to 1536-well black assay plates. The library compounds were added as 0.1 μl of 1 mM DMSO stocks to reach a final compound concentration of 21.7 μM and DMSO of 2.2% (v/v) to each well in 4 replicates. Plates were incubated at room temperature for 2 hours, and the FRET signal was measured using the Envision Multilabel plate reader with an excitation at 337 nm and emissions at 615 nm and 665 nm.

4.2.9 GST pull-down assay

To detect association of GST-GFRP with His-GTPCH-1, the ProFound Pull-Down GST Protein:Protein Interaction Kit (Thermo Scientific) was employed. 0.7 μg of purified GST-GFRP recombinant protein was first bound to glutathione agarose beads and then incubated with 0.7 μg of purified His-GTPCH-1 recombinant protein in a buffer containing 10 μM BH_4, 100 μM GTP and 100 μM ascorbic acid.

Protein complexes were eluted from glutathione and then separated on a 12.5% gel by SDS–PAGE, followed by Western blot analysis using anti-His tag and anti-GFRP antibodies.

4.2.10 Data Analysis

Assay data were analyzed using CambridgeSoft. The percentage of control FRET was calculated with the following equations based on data from each plate: % of Control = (FRETcompound – FRETbackground) / (FRETcontrol – FRETbackground) * 100. The % of Inhibition was calculated as 100 - % of Control. In these equations, FRETcompound is the FRET ratio from a well with a test compound. FRETcontrol is an average FRET signal from wells without a test compound, which defines maximal FRET. FRETbackground is an average FRET ratio from wells lacking GST-GFRP, which defines minimal FRET. Compounds that caused % inhibition > 30 (or % Control < 70) were defined as positives. Nonlinear regression analysis using Prism 4.0 (Graphpad software) was employed to determine Kd values for the GTPCH-1/GFRP interaction in the TR-FRET assay.

IC_{50} value was defined as the concentration of inhibitor that generated a 50% reduction in assay signal. For the IC_{50} determinations, serial dilution of compounds were performed in 100% DMSO with a 2-fold dilution scheme resulting in 8 concentrations of compound starting at a high concentration of 50 μM in the final assay. These dilutions were spotted onto plates and the assay performed at 2% DMSO final concentration as described for the primary screen.

4.3 Results

4.3.1 Interaction of truncated GTPCH-1 proteins with GFRP by co-IP in HAECs

Crystal structures of GTPCH-1 and GFRP complexes in the presence of different small regulatory molecules, phenylalanine and BH_4, suggest that α-helix and β-strand at the C-terminal region of GTPCH-1 directly interact with GFRP (Maita et al., 2004; Maita et al., 2002). Of note, GFRP interacts with distinct residues in GTPCH-1, depending on which small regulatory molecule is present. Using yeast 2-hybrid, Swick et al. (Swick and Kapatos, 2006) showed that while not absolutely required for binding to GFRP, the GTPCH-1 N-terminal 42 amino acids are very much involved in this interaction. However, how the two proteins interact and what regions of GTPCH-1 are responsible for binding to GFRP in endothelial cells remain undefined. I therefore studied the interaction of truncated GTPCH-1 proteins with GFRP to characterize the regions of GTPCH-1 that are required to bind to GFRP in endothelial cells. If a short peptide of GTPCH-1 maintained the ability to bind to GFRP, this peptide could be used to disrupt the endogenous interaction of GTPCH-1 and GFRP. Expression of FLAG-tagged GTPCH-1 truncations was successfully obtained by transfection of HAECs with various GTPCH-1 constructs (Figure 4.2A). Co-IP of truncated GTPCH-1 and DsRed-GFRP demonstrated that none of the GTPCH-1 truncations maintained the ability to bind to GFRP (Figure 4.2C). Thus, deletion of the N-terminal 42 amino acids of GTPCH-1 eliminated its ability to bind to GFRP. The C-terminal 154 amino acids truncation of GTPCH-1 also eliminated its binding to GFRP. Taken together, these results suggest that both

Figure 4.2 Interaction of GFRP with GTPCH-1 truncations in HAECs by co-IP.

A, HAECs were transfected with various FLAG-tagged GTPCH-1 constructs to express GTPCH-1 truncations and the cell lysates were subject to Western blot using antibodies against FLAG-tag. B, HAECs co-transfected with HA-GTPCH-1 and DsRed-GFRP constructs were subjected to immunoprecipitation using anti-DsRed (IP:DsRed) antibody and Western blot using antibodies against HA-tag and GFRP. C, HAECs co-transfected with FLAG-tagged GTPCH-1 and DsRed-GFRP constructs were subjected to immunoprecipitation using anti-DsRed (IP:DsRed) antibody and Western blot using antibodies against FLAG-tag and GFRP.

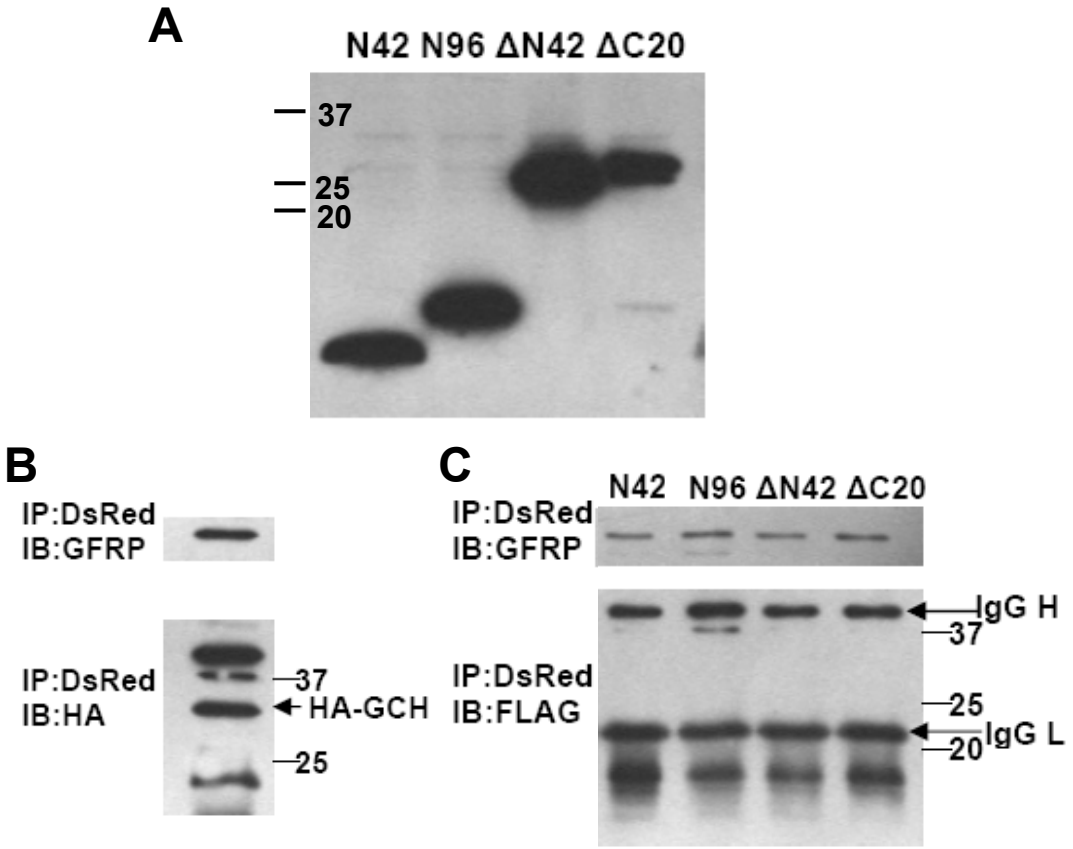

N- and C- terminal regions are required for GTPCH-1 binding to GFRP.

4.3.2 Effects of synthetic peptides in the interaction of GTPCH-1 and GFRP in HAECs

Since both N- and C-terminal regions of GTPCH-1 are required for binding to GFRP, it is likely that those regions are involved in direct contact with GFRP in the protein complex. It is therefore conceivable that peptides corresponding to these regions might interfere with the interaction of full-length GTPCH-1 with GFRP. We therefore synthesized two peptides corresponding to the reported C-terminal amino acid sequences of GTPCH-1 at the GFRP binding interface in both stimulatory and inhibitory complexes (Figure 4.1A). A third peptide was synthesized corresponding to N-terminal 1-42 amino acids of GTPCH-1 (Figure 4.1A). Notably, none of the three peptides individually or in combination had an effect on the interaction of full-length GTPCH-1 and GFRP as determined by GST pull-down assay using prokaryotically expressed and purified His-GTPCH-1 and GST-GFRP (Figure 4.3). In the pull-down assay, the molar amount of the peptides was in excess of that of GTPCH-1 or GFRP. These findings argue against a mechanism whereby GTPCH-1 interaction with GFRP is mediated simply by docking of the N- or C- terminal sequence to a site on GFRP surface. Accordingly, requirement of N- and C- terminal regions of GTPCH-1 in this interaction is likely to require a more complicated connection of these termini with other regions via peptide bonds or other forces.

4.3.3 Design of a TR-FRET assay to monitor GTPCH-1/GFRP interaction

Figure 4.3 GST Pull-down assay using GST-tagged GFRP to immunoprecipitate His-tagged GTPCH-1 in the presence of various synthetic peptides. Western blot below shows the amount of GFRP used as "bait", while the bound "prey" (His-GTPCH-1) is shown in the upper blot. Peptides were incubated with GTPCH-1 and GFRP for overnight at 4°C before the mixture was subject to GST pull-down assay.

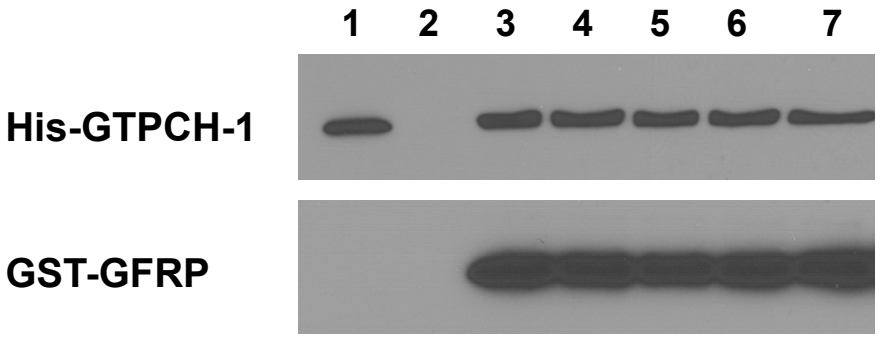

Lane 1: "Prey" (His-GTPCH-1) flow through
Lane 2: Negative control
Lane 3: Without peptides
Lane 4: With Peptide 1
Lane 5: With Peptide 2
Lane 6: With Peptide 3
Lane 7: With Peptide 1, 2 and 3

The above studies indicate that our designed peptides were incapable of disrupting GTPCH-1/GFRP binding. We then sought to identify small molecules that could disrupt binding of these proteins. Such a molecule might increase cellular BH_4 levels. I have previously demonstrated the interaction of GTPCH-1 and GFRP in vitro using purified proteins and in cultured cells by multiple independent methods, including GST pull-down, co-IP, spectral FRET imaging, and BRET assay. To quantitatively monitor the interaction of GTPCH-1 and GFRP for discovery of small molecule compounds that disrupt this interaction, I developed a homogenous TR-FRET assay for the measurement of GTPCH-1 binding to GFRP in vitro (Figure 4.4). Europium-tagged anti-His antibody and APC-tagged anti-GST antibody were used as the FRET pair in this assay. GTPCH-1 was expressed and purified as a His-tagged fusion protein and GFRP as a GST-tagged fusion protein. In the TR-FRET assay, the binding of GTPCH-1 to GFRP in the presence of necessary cofactors brings Europium and APC into close proximity so that energy transfer from an excited-state Europium to acceptor APC occurs. The ratio of the emission of APC at 665 nm and Europium at 615 nm reflects the extent of the interaction between GTPCH-1 and GFRP.

4.3.4 Development of the TR-FRET GTPCH-1/GFRP binding assay

To develop the TR-FRET assay that monitors the interaction of GTPCH-1 and GFRP, titrations of GTPCH-1 and GFRP proteins were carried out to find the protein concentrations that generate the highest signal-to-background (S/B) ratio. As shown in Figure 4.5A and 4.5B, increasing concentrations of either His-GTPCH-1 or

Figure 4.4 Design of a TR-FRET assay for monitoring the interaction of GTPCH-1 and GFRP. The assay measures the TR-FRET signal upon the binding of a His-tagged GTPCH-1 protein conjugated with a Europium-anti-His antibody and GST-GFRP conjugated with an APC-anti-GST antibody. Binding of GTPCH-1 and GFRP allows energy transfer from europium to APC and increases the fluorescence emission at 665 nm.

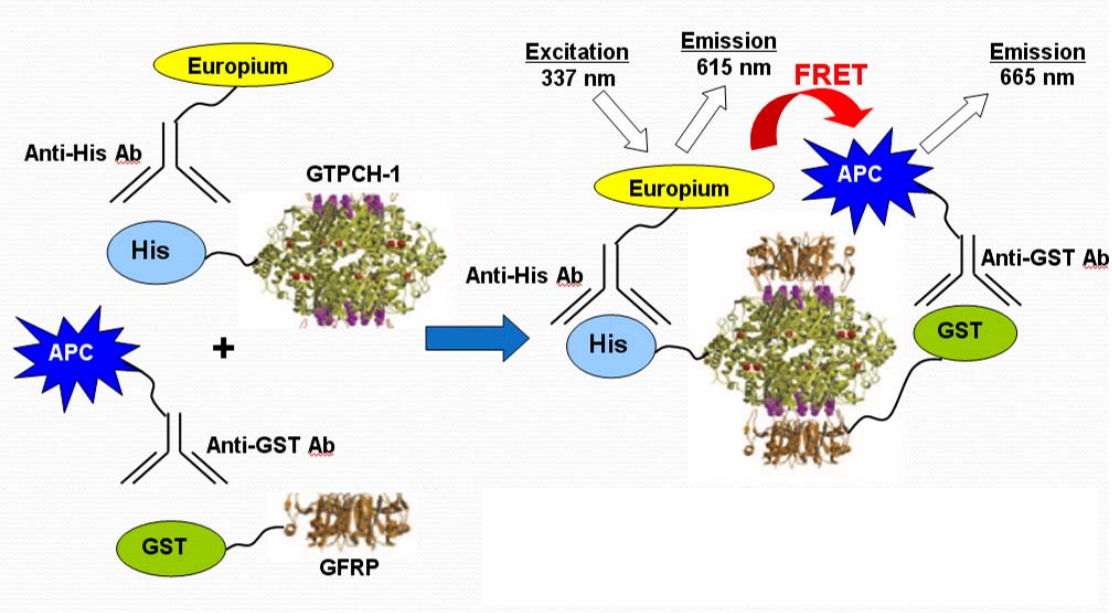

Figure 4.5 Optimization of the GTPCH-1/GFRP TR-FRET binding assay. A, His-GTPCH-1 titrated into solution of GST-GFRP, necessary cofactors for binding, Europium-anti-His, and APC-anti-GST and FRET signals recorded. B, GST-GFRP titrated into solution of His-GTPCH-1, Europium-anti-His, and APC-anti-GST with and without binding cofactors and FRET signals recorded. C, Z' factors and S/B ratios across the His-GTPCH-1 titration. D, Z' factors and S/B ratios across the GST-GFRP titration.

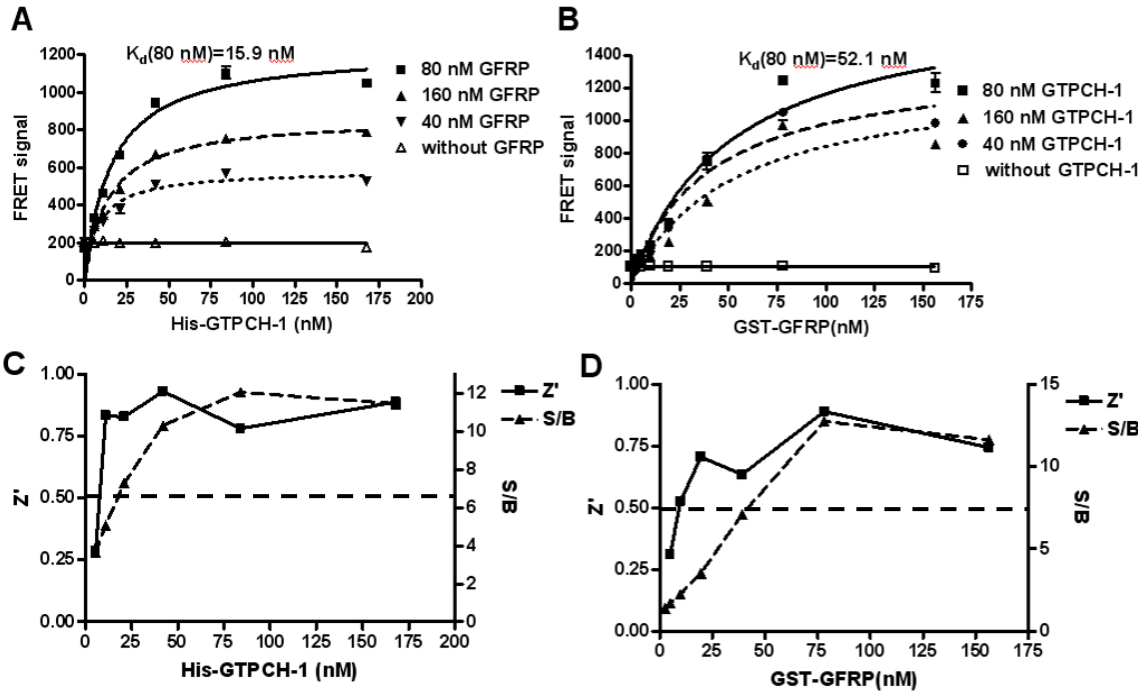

GST-GFRP resulted in a peak FRET value at approximately 80 nM for both proteins. The fact that equal molar amounts of GTPCH-1 and GFRP were required to produce the maximal FRET value is in accordance with the previous finding that the ratio of GTPCH-1 and GFRP in the GTPCH-1/GFRP complex is 1:1 (Maita et al., 2004). In keeping with this, the Kd values for binding of GTPCH-1 with GFRP and for GFRP with GTPCH-1 were similar (15.9 and 52.1 nM, respectively, Figure 4.5A and 4.5B). In both titrations, the quality of the assay was assessed by calculating S/B ratios and Z' factors over the concentration range. A maximal S/B ratio of 12 was obtained at 80 nM of His-GTPCH-1 and GST-GFRP and the Z' factor was approximately 0.8 at these concentrations (Figure 4.5C and 4.5D). The Z' factor of an assay reflects the variability of an assay and the suitability for HTS, and Z' factors between 0.5 and 1 reflect a reliable and robust assay (Ozers et al., 2005). The Z' factor of 0.9 for my assay indicated that it is very efficient.

The FRET signal increased progressively up to 6 hours after mixing GTPCH-1, GFRP and co-factors, and decreased slightly thereafter (Figure 4.6A). Thus, this assay provides sufficient stability for compound screening. HTS often employs compound libraries that are dissolved in DMSO. We therefore tested assay tolerance to DMSO at concentrations commonly used in screening. There was no appreciable decline in FRET signal with up to 10% DMSO in the 384-well plate format (Figure 4.6B). The S/B ratios and Z' factors remained constant at various DMSO concentrations (Figure 4.6C). The use of high-density microplates, most prominently 1536-well plates, allows miniaturizing screening volumes to realize

Figure 4.6 TR-FRET assay stability with time and in the presence of DMSO. A, TR-FRET signals of GST-GFRP titration assay at various time points. B, Effect of various concentrations of DMSO on the FRET signal using the 384-well and 1536-well plate formats. C, Z' factors and S/B ratios for assay with increasing DMSO concentrations using the 384-well and 1536-well plate formats.

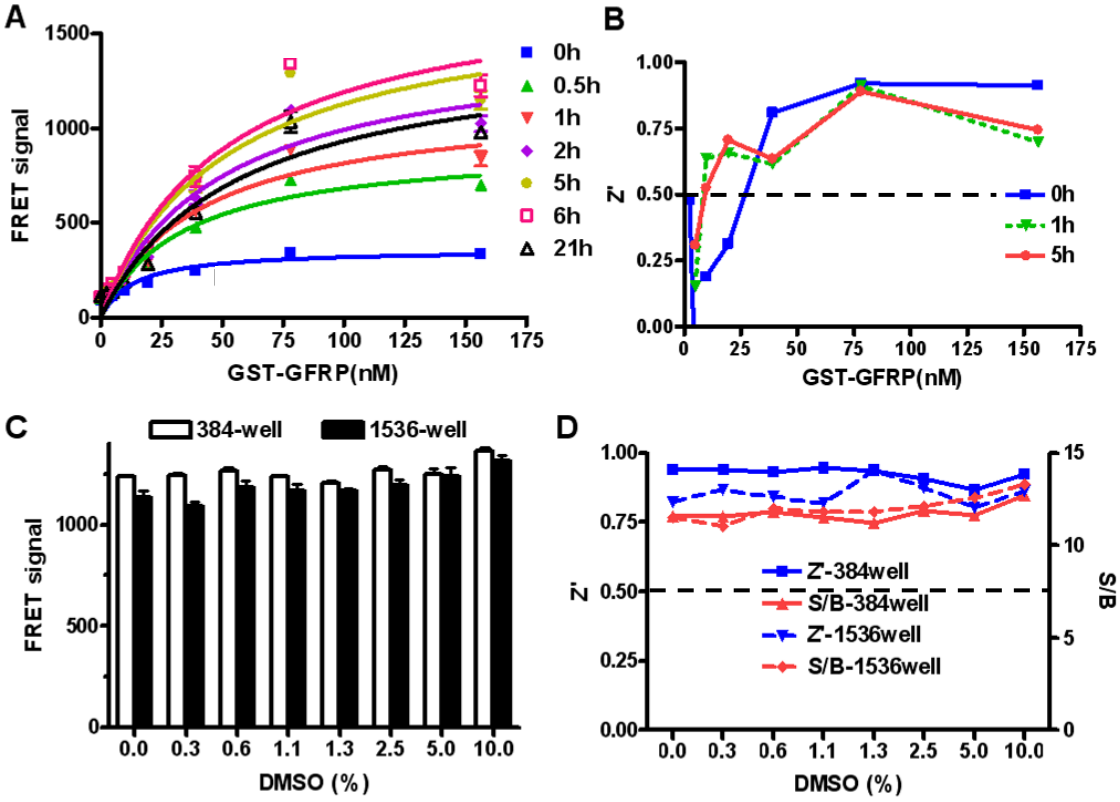

proportional savings in reagent costs. We therefore examined the assay performance in a 1536-well plate format. There were no appreciable changes in assay signal, S/B ratio, and Z' factor in response to increasing concentrations of DMSO in the 1536-well plate format (Figure 4.6B and 4.6C). This suggests that after optimization, the TR-FRET assay to monitor GTPCH-1/GFRP interaction is suitable for ultra HTS (uHTS) in a 1536-well plate format.

Taken together, these results provide a simple, reliable and robust assay for studying GTPCH-1/GFRP interaction and discovering small molecule compounds that disrupt this interaction.

4.3.5 Assay validation of uHTS for GTPCH-1/GFRP interaction inhibitors: Pilot screening of LOPAC library

The GTPCH-1/GFRP TR-FRET assay was validated for use in an HTS format by screening the Library of Pharmacologically Active Compounds (LOPAC), which is a collection of 1,280 pharmacologically active compounds frequently used for HTS assay validation (Benjamin et al., 2006; Rickardson et al., 2007). The condition of the screening was determined by optimization of the assay, with 80 nM His-GTPCH-1, 80 nM GST-GFRP, 1 nM Europium-anti-His, 50 nM APC-anti-GST, 10 μM BH_4, 100 μM GTP and 100 μM ascorbic acid to give the maximal FRET signal expected. Compounds were screened at a final concentration of 21.7 μM in the presence of 2% DMSO in 4 replicates in the 1536-well plate format. The average S/B ratio and Z' factor observed during LOPAC screening were consistent with our assay validation studies (Figure 4.7A and 4.7B). Compounds that

inhibited the binding of GTPCH-1 to GFRP by more than 30% were considered potential positives, and the screening results for the LOPAC library are shown in Figure 4.7C. Of the 1280 compounds, 15 were identified as potential positives, which resulted in a hit rate of 1.2%. Concentration-dependent responses of the positive compounds were further tested using the TR-FRET assay. Three representative dose response curves were shown in Figure 4.7D through 4.7F. These compounds were confirmed to inhibit GTPCH-1/GFRP interaction with IC_{50}s in the micromolar range. These findings suggest that this TR-FRET assay, developed to discover compounds that inhibit the binding of GTPCH-1 and GFRP, is suited for HTS and can be adapted for large scale compound screening.

4.3.6 Conformation of the hits from the LOPAC pilot screening

The 15 primary hits from the LOPAC pilot screening were then tested in GST pull-down assays in which His-tagged GTPCH-1 was exposed to GST-tagged GFRP bound to glutathione sepharose beads for pull down. Several of these compounds were confirmed to disrupt the interaction of GTPCH-1 and GFRP in the GST pull-down assay (Figure 4.8A through 4.8C), including cis-Diammineplatinum(II) dichloride, Carboplatin, and Protoporphyrin IX. Different concentrations of these compounds were also tested to determine their potencies in inhibiting GTPCH-1/GFRP interaction in vitro. Dose response curves and IC_{50} values of the compounds were obtained from the densitometry of the GST pull-down assay (Figure 4.8D through 4.8F). As apparent, these compounds identified from the TR-FRET assay were confirmed to disrupt the in vitro binding of GTPCH-1 and

Figure 4.7 Ultra-high-throughput Screening (uHTS) format assay validation. The TR-FRET assay that monitors the GTPCH-1/GFRP interaction was validated for uHTS using the LOPAC library in 4 replicates. S/B ratios (A) and Z' factors (B) were evaluated for 4 plates. C, The percentage of control is calculated as defined in the methods section and plotted against compound ID. D, The fluorescence intensity (FI) of the compound wells expressed as folds over vehicle control was plotted against the % inhibition. The potential positives are defined by the compound with % inhibition > 30 and FI over the control less than 2 and greater than 0.4.

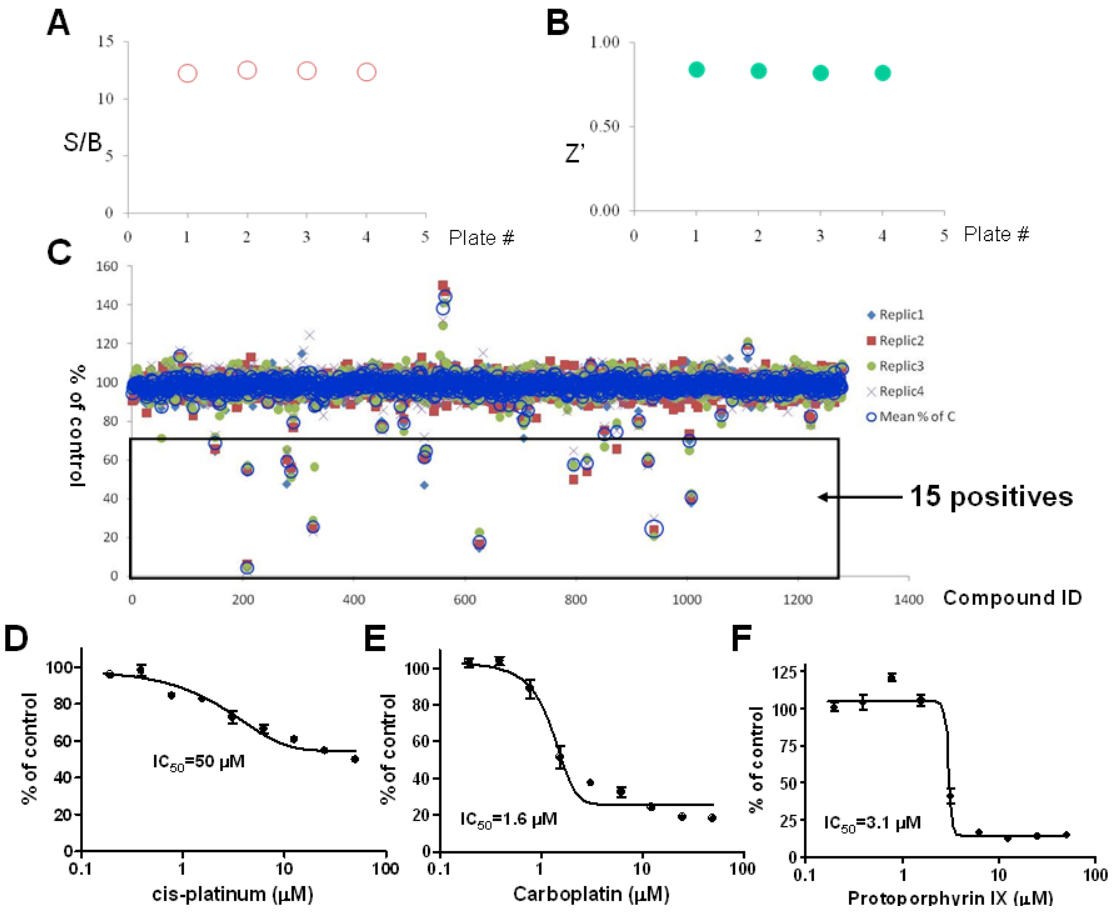

Figure 4.8 Confirmation of the compounds in the GST pull-down assay. GST-GFRP was bound to glutathione agarose beads and then His-tagged GTPCH-1 was added. These experiments were performed in the presence of various concentrations of compounds identified by initial HTS of the LOPAC library. Western blot above shows the amount of GFRP used as "bait", while the "trapped" GTPCH-1 is shown in the lower blot. The disappearance of a band in the upper panel indicates the disruption of the GTPCH/GFRP binding. The disappearance of a band in the upper panel indicates the disruption of the GTPCH/GFRP binding.

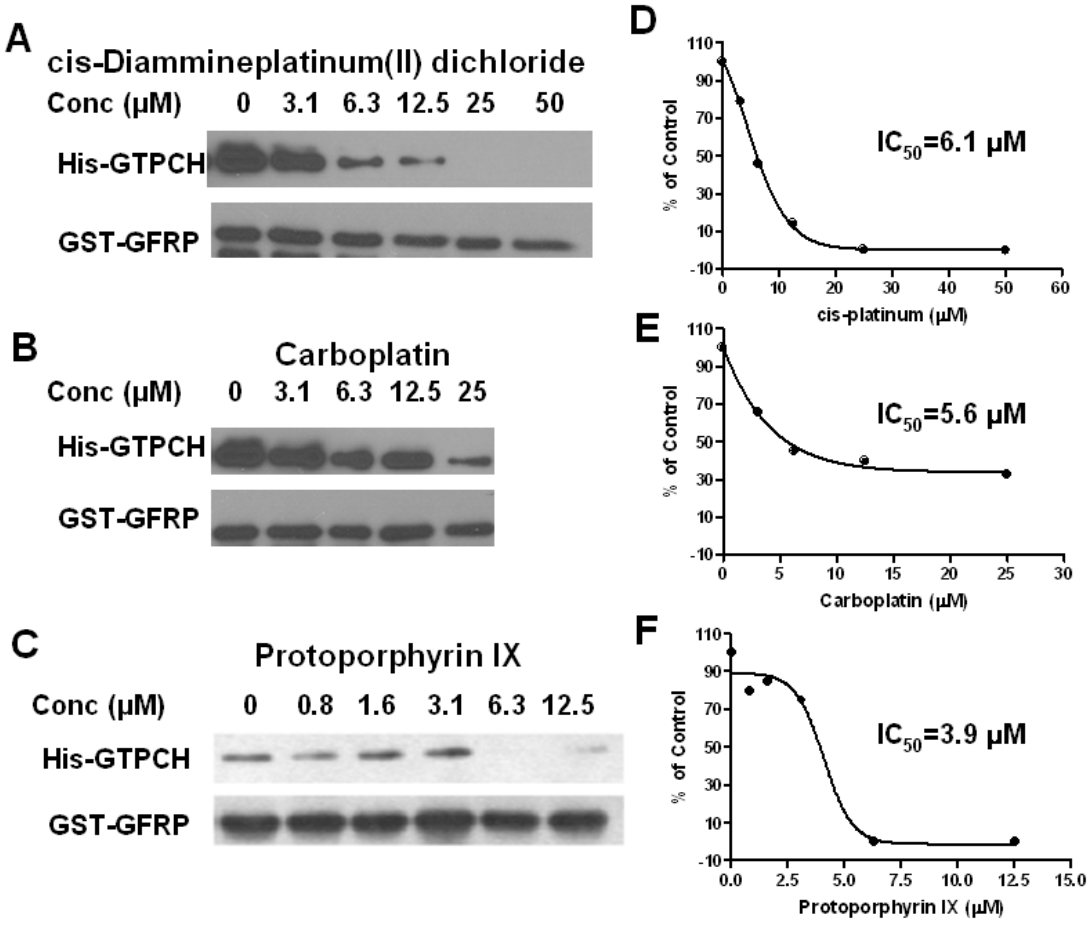

GFRP in an independent protein-protein interaction assay.

Given these results, I then performed additional studies in which these agents were added to cultured human aortic endothelial cells for 24 hours and subsequent changes in biopterin levels were measured using HPLC. I found that Carboplatin and Protoporphyrin IX increased biopterin levels in cultured endothelial cells at low micromoloar concentrations, with Carboplatin eliciting a 4-fold increase in biopterin levels at the concentration of 25 μM (Figure 4.9). Interestingly, higher concentrations of Carboplatin failed to elicit an increase on cellular biopterin levels. This is possibly due to low bioavailability of Carboplatin at higher concentrations. Further studies are needed to examine the mechanism of action of this drug. Thus, screening a small library of known compounds identified several compounds that disrupt the binding of GTPCH-1 and GFRP and significantly increase endothelial BH_4 levels at low micromolar concentrations.

4.4 Discussion

In this part of the dissertation, I sought to characterize the mechanisms underlying GTPCH-1 and GFRP binding and discover peptides or small molecule compounds to inhibit this protein-protein interaction. I first evaluated which regions of GTPCH-1 were required for binding to GFRP, as discovery of such peptides could lead to potential peptide inhibitors of this interaction and binding assays for future discovery of small molecule compounds. I found that both N- and C- terminal sequences of GTPCH-1 are required for interaction with GFRP in HAECs, because deletion of these regions prevented this interaction individually.

Figure 4.9 Effect of the disruption of GTPCH-1/GFRP binding on endothelial cell biopterin levels. HAECs were treated with compounds at the concentrations indicated for 24 hours and biopterin levels were measured using HPLC (n=6). Insets on the right show representative biopterin peaks for cells treated with DMSO, Carboplatin or Protoporhyrin XI at indicated concentrations. Values were compared using ANOVA and selected comparisons were made using a Bonferroni post hoc test.

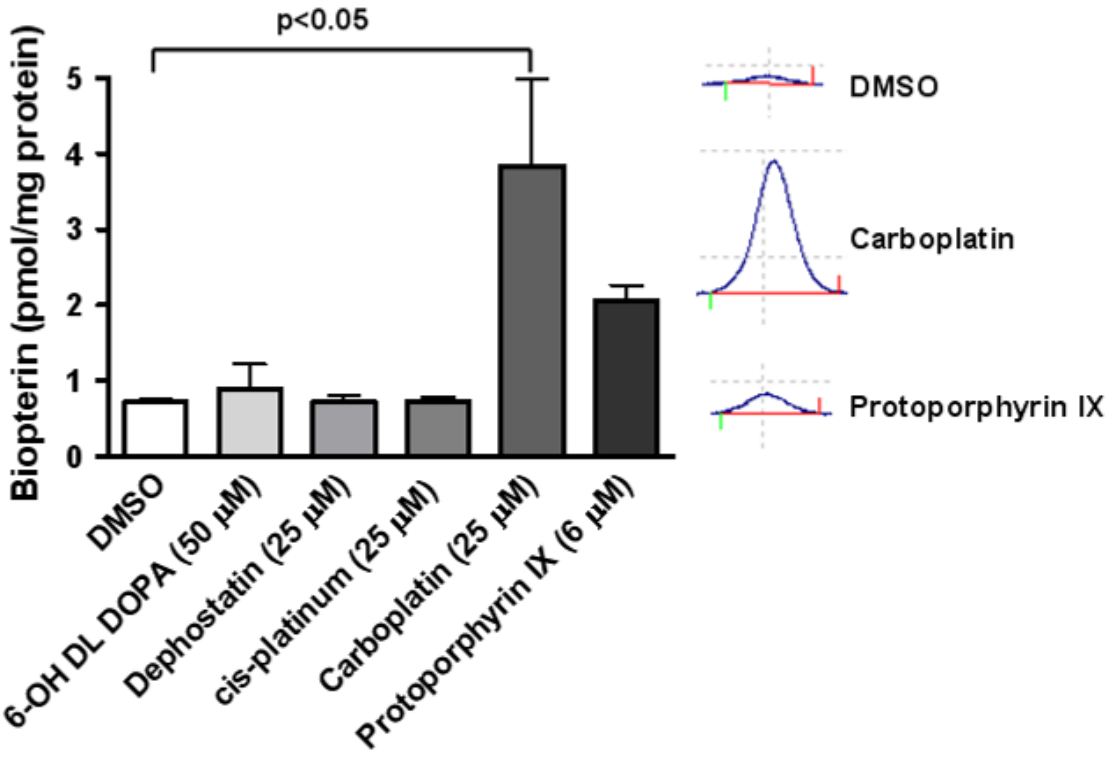

This is in accordance with the concept that Arg_{235} and Glu_{236} of GTPCH-1 in the C-terminal region form a direct chemical bond with GFRP, as determined from the crystal structure analysis (Maita et al., 2004), and that the complete N-terminal peptide is required for normal interaction in a yeast 2-hybrid assay (Swick and Kapatos, 2006). In keeping with this, I found that synthetic peptides corresponding to the N- and C- terminal regions of GTPCH-1 failed to interfere with the interaction of full-length GTPCH-1 and GFRP in vitro, suggesting that GFRP pentamer is likely to bind to a more complex structure of GTPCH-1 rather than a single peptide.

Previous biochemical and crystal structural studies have shown that only the GTPCH-1 decamer is capable of interaction with the GFRP pentamer (Yoneyama and Hatakeyama, 1998) (Maita et al., 2002). It is therefore conceivable that deletion of the N- or C- terminal regions could impair the self-assembly of GTPCH-1 into a decamer. Results from a yeast 2-hybrid study showed that full length GTPCH-1 and N-terminal 42 amino acid truncated GTPCH-1 can form functional decamers. In contrast, C-terminal deleted form of GTPCH-1 lost the structural integrity necessary to form the decamer (Swick and Kapatos, 2006). Taken together, these observations support the concept that the C-terminal region of GTPCH-1 is directly involved in decamer formation and interaction with GFRP, while the N-terminal region is not required for decamer formation, but is crucial to the GTPCH-1/GFRP interaction and may be involved in stabilizing this protein-protein complex. Interestingly, a very recent study by Higgins et al. (Higgins and Gross, 2010) reported that the N-terminal peptide of mammalian

GTPCH-1 is an autoinhibitory control element and contributes to binding to GFRP. In keeping with my finding, they found that compared to full-length GTPCH-1, the N-terminal 45 amino acid truncated form of GTPCH-1 was unable to interact with GFRP, as indicated by native-PAGE immunoblot studies and the response to GFRP in activity assays.

Findings demonstrated in Chapter 2 of this dissertation suggest a model where GFRP plays an inhibitory role in GTPCH-1 activity, BH_4 levels and NO production in human endothelial cells by binding to GTPCH-1 in the presence of BH_4. I found that siRNA inhibition of GFRP causes a striking increase in GTPCH-1 activity and BH_4 levels and prevents eNOS uncoupling in the setting of oscillatory shear. Therapeutic interventions to reduce levels of an intracellular protein seem rather difficult, but inhibition of protein–protein interaction has been considered feasible in drug discovery. We therefore sought to identify agents to disrupt the interaction of GTPCH-1 and GFRP, thereby achieving the effect of removing GFRP inhibition on GTPCH-1 to increase its activity. In keeping with the in vitro situation, in Chapter 3, I demonstrate lower levels of BH_4 and NOS uncoupling at regions of disturbed flow created by partial carotid ligation, which contribute to accelerated atherosclerosis at these sites. Currently, there is no specific treatment to reduce atherosclerosis at sites of disturbed flow. We propose that agents that disrupt binding of GTPCH-1 and GFRP would increase BH_4 levels at these sites and would reduce atherosclerosis.

According to previous studies reporting the involvement of N- and C- termini of

GTPCH-1 in its binding to GFRP, we synthesized three peptides mimicking these regions. Of note, none of these peptides had an effect on the interaction of full-length GTPCH-1 and GFRP. Similarly, in the study by Higgins et al. (Higgins and Gross, 2010), N-terminal 45 amino acid peptide of GTPCH-1 failed to modulate full-length GTPCH-1 activity or its interaction with GFRP. These findings suggest that GFRP may fail to bind to the N-terminal peptide of GTPCH-1 because the interaction requires a more complicated interaction of this peptide with other GTPCH-1 structures. An alternative explanation is that simple binding of the N-terminal peptide to GFRP is not sufficient to or perturb GFRP binding to full-length GTPCH-1.

I then designed, optimized and validated an assay to monitor the interaction of GTPCH-1 and GFRP. The goals in establishing a robust and simple to use assay for measuring GTPCH-1 and GFRP interactions were, first, to allow the quantification of this interaction in vitro and second, to optimize a homogeneous assay for identifying small molecule regulators of GTPCH-1 and GFRP interaction in an HTS format. This TR-FRET assay has a high Z' factor and S/B ratio, exhibits high stability, solvent tolerance, and good performance in small volumes, suggesting that it is particularly well suited for uHTS. This assay can be performed in a simple "mix-and-read" format and seems robust and reliable for discovery of small molecules that disrupt the GTPCH-1/GFRP interaction. I further confirmed utility of the assay by studying identified compounds in a GST pull-down assay and in cell culture. Thus, this newly developed TR-FRET assay might prove useful in

screening larger chemical libraries to identify compounds that could increase cellular BH_4 levels.

TR-FRET offers the ability to record both acceptor and donor signals. The derived acceptor/donor ratio minimizes the variations from pipetting errors and well-to-well differences. However, a compound with non-specific effects on only the donor or only the acceptor signal will influence the calculation of the ratio and lead to false positives or negatives. This potential artifact can be addressed by visualization and analysis of the donor and accepter signals separately (Imbert et al., 2007). For example, assuming that the compounds being tested have no influence on the donor signal, the europium fluorescence should be equal in all the wells of an assay plate.

This TR-FRET assay employs two antibodies that bind to investigated proteins as fluorescent donors and acceptors in the FRET pair. Using labeled antibodies instead of directly labeling the proteins with fluorophores makes the TR-FRET assay very flexible (Hu et al., 2008). It can be easily adapted to other protein interaction pairs. The fluorophores in the TR-FRET pair can also be replaced by just labeling antibody with a different fluorophore. However, the affinity of the fluorophore labeled antibodies with proteins may vary and become buffer dependent. Excessive or insufficient antibodies can both lead to artifacts from the assay. Thus, the concentrations of the antibodies need to be carefully determined during the assay optimization.

One limitation of this study is that there are no known GTPCH-1/GFRP

inhibitors available as positive controls to validate the TR-FRET assay and correlate their IC_{50} values obtained from the TR-FRET assay with those obtained from a secondary activity assay. Despite this, we could validate a fraction of the compounds identified from the TR-FRET assay in the GST pull-down assay. The fact that we could not validate all of the positive hits might be due to the higher sensitivity of the TR-FRET assay and the involvement of fluorescence energy transfer. It is also possible that some molecules might quench the TR-FRET fluorescence, without disrupting GTPCH-1/GFRP binding. Some compounds might additionally interfere with antibody binding to the target proteins, and thus would artificially disrupt the TR-FRET signal. Such compounds would be identified as false positives. These considerations emphasize the need for the secondary screening using an assay, such as the GST pull-down approach. Cellular uptake of compounds might also be limited, and therefore further screening using cultured cells is necessary.

Using these sequential screening approaches, we identified two compounds that can increase endothelial BH_4 levels at low micromolar concentrations. Carboplatin is an alkylating agent used for a variety of cancers, including ovarian and lung carcinoma (Go and Adjei, 1999). It has significant side effects, including severe myelosuppression. Protoporphyrin IX is a precursor to heme, myoglobin and other compounds such as catalase. Protoporphyrin IX has been used as a specific probe to activate heme oxygenase (Li and Stocker, 2009). Our studies indicate that it might have additional effects in increasing cellular BH_4 and activities of

BH_4-dependent enzymes, such as NOS. Due to their cytotoxicity profiles, carboplatin and Protoporphyrin IX will unlikely be employed to increase cellular BH_4. Our results, however, support the utility of this optimized uHTS approach to screening larger libraries to identify potent and specific compounds with promising chemical properties for effective modulation of cellular BH_4.

The mechanisms by which these compounds induce the dissociation of GTPCH-1 and GFRP remain unknown. A common mechanism for inhibiting protein-protein interaction is that small molecules bind at the interface of the interaction. Crystal structure analysis of GTPCH-1/GFRP complex suggests that that Arg_{235} and Glu_{236} of GTPCH-1 in the C-terminal region form a direct chemical bond with GFRP (Maita et al., 2004). A yeast 2-hybrid assay (Swick and Kapatos, 2006) and studies from our own laboratory (data not shown) have demonstrated that the complete N-terminal peptide of GTPCH-1 is required for interaction with GFRP. Compounds that interfere with binding between these regions could disrupt GTPCH-1/GFRP interaction. In addition, the compounds could also cause allosteric inhibition by inducing conformational changes of the proteins. Further investigation using methods that address the compound binding to the proteins, such as X-ray crystallography, would help define the exact mechanisms of the action of these compounds (Arkin et al., 2003). These identified compounds may serve as tools to facilitate the further study of the mechanism of GPTCH-1 and GFRP interaction.

BH_4 is an essential co-factor for NOS and a key regulator of NOS activity and

coupling. BH_4 deficiency has been found in experimental models of various cardiovascular diseases, such as hypertension (Landmesser et al., 2003), atherosclerosis (Takaya et al., 2007), and diabetes (Du et al., 2006). BH_4 also functions as a critical co-factor for aromatic amino acid hydroxylases, and thus regulates some neurological diseases. Oral BH_4 supplementation has been shown effective in ameliorating these disease conditions in animal models (Hattori et al., 2007; Landmesser et al., 2003), but the effect of BH_4 in humans is likely limited due to its poor bioavailability and cellular uptake (Katusic et al., 2009). Accordingly, Antoniades et al. reported that patients with coronary artery disease have paradoxically high biopterin levels in the plasma but low biopterin levels in the vessels (Antoniades et al., 2007). Thus, compounds identified by our screening approaches to increase intracellular BH_4 biosynthesis are highly desirable and could have therapeutic potential in treating diseases associated with intracellular BH_4 deficiency.

In summary, my in vitro characterization of the GTPCH-1 and GFRP interaction indicates that structural integrity of the GTPCH-1 decamer is required for its binding to GFRP. This property is likely to be related to the requirement that small molecule modulators bind at the interface of the two proteins. Because of the inhibitory effect of GFRP on GTPCH-1 activity through protein-protein interaction, we sought to discover peptides or small molecules to disrupt this interaction. We failed to develop any effective peptides to interfere with this interaction, probably because GFRP only binds to GTPCH-1 decamer and peptides that do not form the

decamer structure can not bind to GFRP. To discover small molecule compounds to disrupt this protein-protein interaction, we have successfully developed a one-step "mix-and-read" TR-FRET assay and validated the assay for monitoring GTPCH-1/GFRP interaction. This assay is highly sensitive and stable and has achieved a robust performance in 384-well and 1536-well formats with a signal-to-background ratio greater than 12 and a Z' factor greater than 0.75. We have employed this assay in uHTS and results from a pilot screening showed that positive hits from the primary screening can be confirmed in an independent protein binding assay and in cell culture. Screening of a larger libraries and additional structure activity work is needed to identify compounds that could be used therapeutically.

Chapter 5:

Discussion and future directions

5.1 What are other mechanisms of GTPCH-1 regulation?

The data presented in Chapters 2, 3 and 4 of this dissertation demonstrate that shear forces encountered by the endothelium regulate GTPCH-1 activity by modulating GTPCH-1 phosphorylation and the interaction of GTPCH-1 with GFRP. Of note, laminar and oscillatory shear exert opposite effects on GTPCH-1 phosphorylation and the interaction of GTPCH-1 with GFRP, thereby having different effects on GTPCH-1 activity. For the first time, I demonstrated that two post-translational modifications of GTPCH-1 interplay with each other. Unidirectional laminar shear promotes dissociation of GFRP from GTPCH-1, which leads to GTPCH-1 phosphorylation and reduced GTPCH-1 binding with GFRP. This leads to a feed-forward paradigm of GTPCH-1 activation. In contrast, oscillatory shear fails to disrupt the interaction of GTPCH-1 and GFRP, and therefore does not induce phosphorylation and activation of GTPCH-1. Thus, our findings explain the loss of GTPCH-1 activity and deficient BH_4 levels at areas of disturbed flow in vivo.

Although our findings have enhanced understanding of GTPCH-1 regulation, there are other regulatory mechanisms for modulating GTPCH-1 activity that are unclear. For example, a recent study indicates that GTPCH-1 might be regulated by phosphorylation at multiple sites, both positively and negatively (Du et al., 2009a). By mutating several potential phosphorylation sites of GTPCH-1, the authors characterized how they could potentially modulate GTPCH-1 activity, biosynthesis of BH_4 and BH_2, and enzyme localization. This study did not prove

that these sites are phosphorylated in the cell, and it is unclear whether they regulate in vivo levels of BH_4.

The subcellular localization of GTPCH-1 and its regulatory protein, GFRP, remain elusive. Shear stress causes dramatic changes in cell shape and in the endothelial cell cytoskeleton, and thus could alter the subcellular localization of GTPCH-1 and GFRP to modulate GTPCH-1 enzyme activity. My transfection studies showed that most of the overexpressed GTPCH-1 resides in the cytoplasm, whereas its binding partner, GFRP, is localized in both cytoplasm and the nucleus. Whether the different localizations of GTPCH-1 and GFRP modulate GTPCH-1 activity remains unknown. Although I did not find nuclear localization of transfected GTPCH-1 in HAECs, other studies have reported the presence of GTPCH-1 in the nucleus of COS-1 cells (Elzaouk et al., 2004), epidermal keratinocytes, and melanocytes (Chavan et al., 2006). A recent proteomic study of GTPCH-1 also revealed that 20% of the proteins that GTPCH-1 interacts with are nuclear proteins (Du et al., 2009b). While the NOS enzymes are not nuclear, some of the aromatic amino acid hydroxylases that utilize BH_4 as a co-factor are nuclear. It is conceivable that nuclear translocation of GTPCH-1 might affect its enzyme activity.

Recent studies have shown that GTPCH-1 might interact with multiple protein binding partners. Using mass spectrometry-based proteomics, Du et al. (Du et al., 2009b) identified 29 proteins that interact with GTPCH-1 in HEK 293 cells. These proteins come from multiple subcellular locations and are involved in a variety of

biological processes such as signal transduction, apoptosis, metabolism, transport and cell organization. Although the functionality of these interactions needs to be confirmed in specific cell types, this finding indicates that the role of GTPCH-1 in cell biology may be much greater than previously considered.

In Chapter 4, we found that the N-terminus of GTPCH-1 is required for binding to GFRP. In keeping with our finding, a very recent study revealed that the N-terminal 45 amino acids of rat GTPCH-1 importantly regulate GTPCH-1 (Higgins and Gross, 2010). Using deletion studies, they found that this N-terminal peptide contributes to the interaction with GFRP and exhibits autoinhibitory effects on GTPCH-1 activity, possibly due to GFRP-mediated inhibitory interaction that involve the N-terminal peptide of GTPCH-1.

Another type of post-translational modification of GTPCH-1 is ubiquitination in the presence of high concentrations of glucose. Xu et al. (Xu et al., 2007) reported that hyperglycemia and diabetes mellitus activate the ubiquitin-proteasome pathway, promoting GTPCH-1 degradation and ultimately BH_4 deficiency. The authors also demonstrated that the proteasome is activated by NAD(P)H oxidase–derived $O_2^{\cdot-}$ and $ONOO^{\cdot-}$ in the setting of hyperglycemia. This partially explains why diabetic animals and patients have reduced amounts of NO and increased levels of reactive oxygen species, a condition that leads to endothelial dysfunction and vascular disease.

In addition to post-translational modifications, some evidence suggests that GTPCH-1 expression is regulated at the mRNA level. In a glucocorticord-induced

rat model of hypertension, GTPCH-1 mRNA levels are reduced, and eNOS is uncoupled due to reduced BH_4 bioavailability (Mitchell et al., 2003). It is unclear, however, whether these abnormalities are a direct glucocorticoid effect or secondary to hypertension, and the relevance of these findings to human vascular disease remains uncertain.

5.2 What is the role of BH_4 deficiency and NOS uncoupling in atherosclerosis?

All major risk factors for atherosclerosis such as hyperlipidemia, diabetes, hypertension, and smoking are associated with endothelial dysfunction. Although the underlying mechanisms of endothelial dysfunction are multifactorial, major causes include a loss of bioavailable NO due to NO oxidation and decreases of NO synthesis. Decreased synthesis can be caused by NOS uncoupling, where the enzymatic reduction of molecular oxygen by NOS is no longer coupled to L-arginine oxidation, resulting in production of $O_2^{\cdot-}$ rather than NO. BH_4 deficiency seems to be a predominant cause for NOS uncoupling in pathophysiology.

NOS uncoupling has been demonstrated in animal models of atherosclerosis. In $ApoE^{-/-}$ mice, aortic $O_2^{\cdot-}$ production can be reduced by NOS inhibitor L-NAME (Alp et al., 2004), indicating that NOS is a source of $O_2^{\cdot-}$ in this disease model. Importantly, it is the stoichiometric relationships between BH_4 and NOS rather than the absolute BH_4 levels that are important for the functionality of NOS. Thus, even in the absence of vascular disease, eNOS overexpression in the endothelium without a concomitant increase in BH_4 can result in eNOS uncoupling, as seen in eNOS transgenic mice (Bendall et al., 2005). In eNOS-overexpressing $ApoE^{-/-}$ mice,

eNOS has also been found in an uncoupled state (Ozaki et al., 2002). My findings in Chapter 3 showed that disturbed flow can lead to BH_4 deficiency and cause NOS uncoupling. Disturbed flow likely reduces BH_4 by two major mechanisms. One is via reduced GTPCH-1 phosphorylation leading to decreased GTPCH-1 activity and diminished total biopterin production. Secondly, the increased ROS production caused by disturbed flow can oxidize BH_4 and reduce bioavailable BH_4.

As illustrated in my studies, inflammation is likely an important consequence of BH_4 deficiency and NOS uncoupling. Immunocompetent and antigen-presenting cells have been identified at areas of disturbed flow (Wick et al., 1999), suggesting that shear modulates inflammation. Increased ROS caused by disturbed flow promotes expression of adhesion molecules, chemokines, and other inflammatory genes by endothelial cells. Leukocyte adhesion molecules, such as VCAM-1 and ICAM-1, cause blood cell rolling along the vascular surface, adhere at the sites of activation, and translocate to the underlying sub-endothelial space, where they differentiate into macrophages. It is thought that antigens presented by macrophages and other antigen presenting cells trigger the activation of T cells in the artery. The activated T cells produce Th1 cytokines (e.g., TNF-α and INF-γ), which further activate macrophages and vascular cells, and exacerbate inflammation and atherosclerotic lesion development. Of note, increased oxidative stress caused by $O_2^{\cdot -}$ and $ONOO^{\bullet -}$ generated from partially uncoupled NOS at areas of disturbed flow can cause oxidative and nitrosative damage to lipids, DNA or proteins and generate various inflammatory molecules. We speculate that these oxidized lipoproteins,

oxidative adducts of DNA, reactive aldehyde attached proteins, or other modified molecules, may be processed as neoantigens and presented by antigen-presenting cells to active T cells and induce an adaptive immune response (Harrison et al., 2011). This proposed mechanism of atherosclerosis development initiated by inflammation is illustrated in Figure 5.1. Measures to increase endothelial BH_4 levels and to prevent NOS uncoupling could improve endothelial function and reduce endothelial monocyte adhesion. Prevention of NOS uncoupling could also reduce oxidative stress in the vessel wall and possibly decrease the formation of neoantigens, thereby suppressing T cell activation and the inflammatory response that exacerbate atherosclerosis.

Taken together, BH_4 deficiency and NOS uncoupling play crucial roles in the initiation and progression of atherosclerosis at areas of disturbed flow. It is therefore conceivable that strategies to prevent BH_4 deficiency and NOS uncoupling could become a rational therapy for atherosclerosis, especially for atherosclerosis at areas of flow disturbances in the arterial tree. Figure 5.2 depicts different NO-based therapeutic approaches for atherosclerosis.

5.3 Is BH_4 supplementation effective in long-term treatment of human diseases?

Treatment with BH_4 has been shown to reduce or reverse endothelial dysfunction in numerous animal studies, including my study presented in Chapter 3. In small animals, it is relatively easy to achieve high cellular concentrations of BH_4 over the short term by oral treatment with this pterin. Some small studies in humans have also shown a beneficial effect of short-term BH_4 treatment.

Figure 5.1 Proposed mechanism for the role of NOS uncoupling in atherosclerosis induced by disturbed flow. Oscillatory shear stress reduces endothelial BH_4 levels by decreasing BH_4 synthesis and increasing BH_4 oxidation. Deficiency of bioavailable BH_4 leads to NOS uncoupling and production of $O_2^{\bullet-}$. Reduced NO bioavailability and increased oxidative stress induce endothelial dysfunction, induce the gene expression of adhesion molecules, and trigger the initiation of an inflammatory cascade in the vessel wall. Blood monocytes are then recruited to the site of disturbed flow mediated by chemokines and differentiate into macrophages. Activated macrophages and dendritic cells present antigens to T cells and activate T cells, resulting in the secretion of cytokines that promote the progression of atherosclerotic lesion. Re-coupling of NOS by BH_4 supplementation reduces $O_2^{\bullet-}$ levels, increases NO production, inhibits inflammation and prevents endothelial dysfunction, thereby preventing atherosclerosis in the setting of disturbed flow.

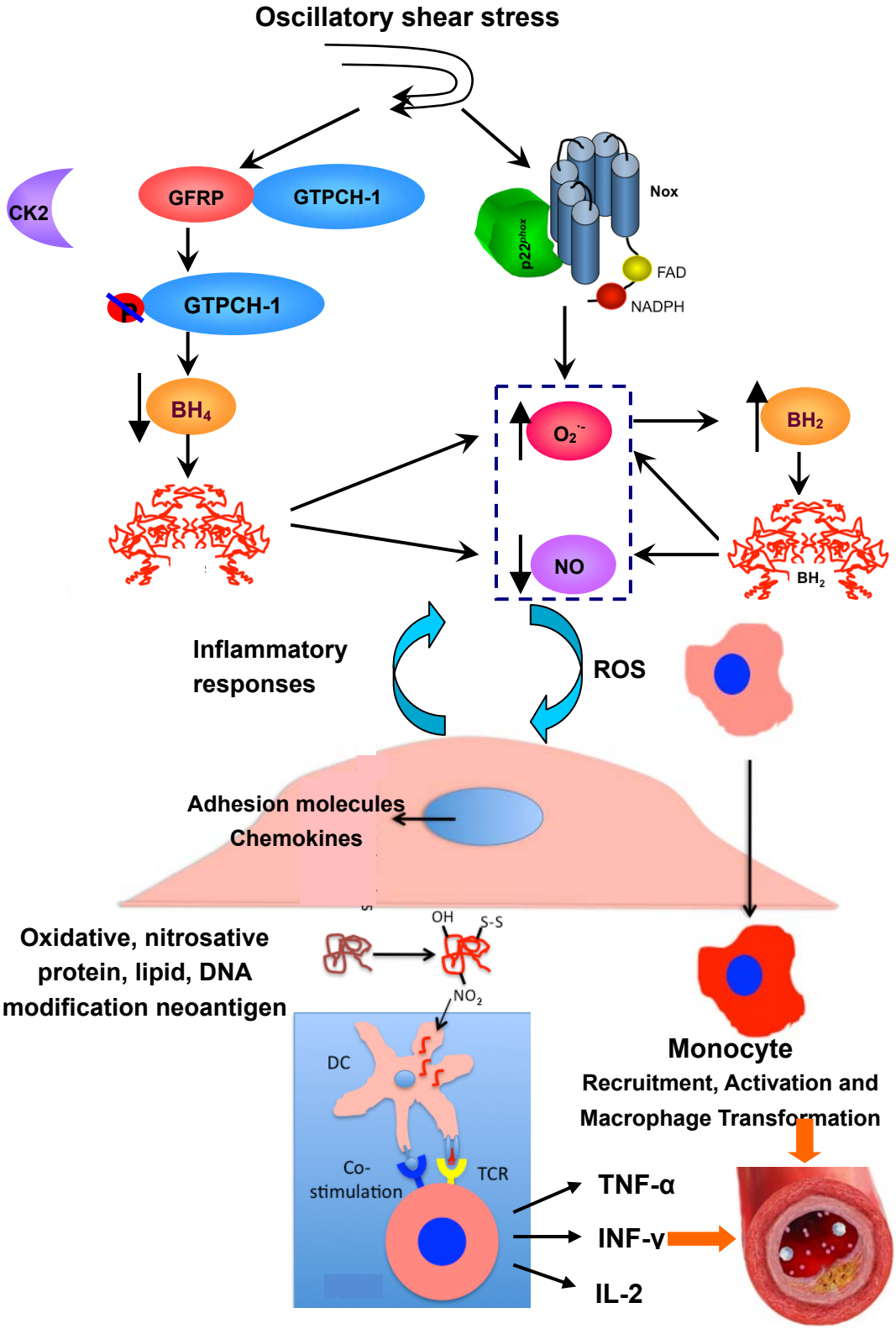
Oscillatory shear stress
CK2
GFRP
GTPCH-1
GTPCH-1
P
BH4
Nox
p22phox
FAD
NADPH
O2·-
NO
BH2
BH2
Inflammatory responses
ROS
Adhesion molecules
Chemokines
Oxidative, nitrosative protein, lipid, DNA modification neoantigen
OH
S-S
NO2
DC
Co-stimulation
TCR
TNF-α
INF-γ
IL-2
Monocyte
Recruitment, Activation and Macrophage Transformation

Figure 5.2 NO-based therapeutic approaches for atherosclerosis. Under pathological conditions such as hypercholesterolemia, hypertension or diabetes, NADPH oxidase-derived $O_2^{\bullet-}$ can react with NO and produce $ONOO^{\bullet-}$, which oxidizes BH_4 to BH_2. BH_4 deficiency leads to NOS uncoupling and $O_2^{\bullet-}$ production from NOS. Folic acid has been reported to improve NOS functionality by stabilizing BH_4 and stimulating the endogenous regeneration of q-BH_2 back to BH_4. In cells, sepiapterin can be converted to BH_2 by sepiapterin reductase (SR), and further by DHFR to form BH_4. Statins upregulate eNOS and concomitantly decrease NADPH oxidase expression. NADPH oxidase inhibitors, such as gp91ds-tat, apocynin, DPI, angiotensin-converting enzyme (ACE) inhibitors and Angiotensin II type 1 receptor blockers (ARBs) prevent BH_4 oxidation by decreasing the expression and/or activity of NADPH oxidases (Williams and Griendling, 2007). Potential GTPCH-1/GFRP inhibitors can enhance BH_4 synthesis by increasing GTPCH-1 activity. Scavengers for $ONOO^{\bullet-}$ (ebselen) and $O_2^{\bullet-}$ (tempol) decrease levels of reactive oxygen species and prevent BH_4 oxidation, thereby protecting against atherosclerosis.

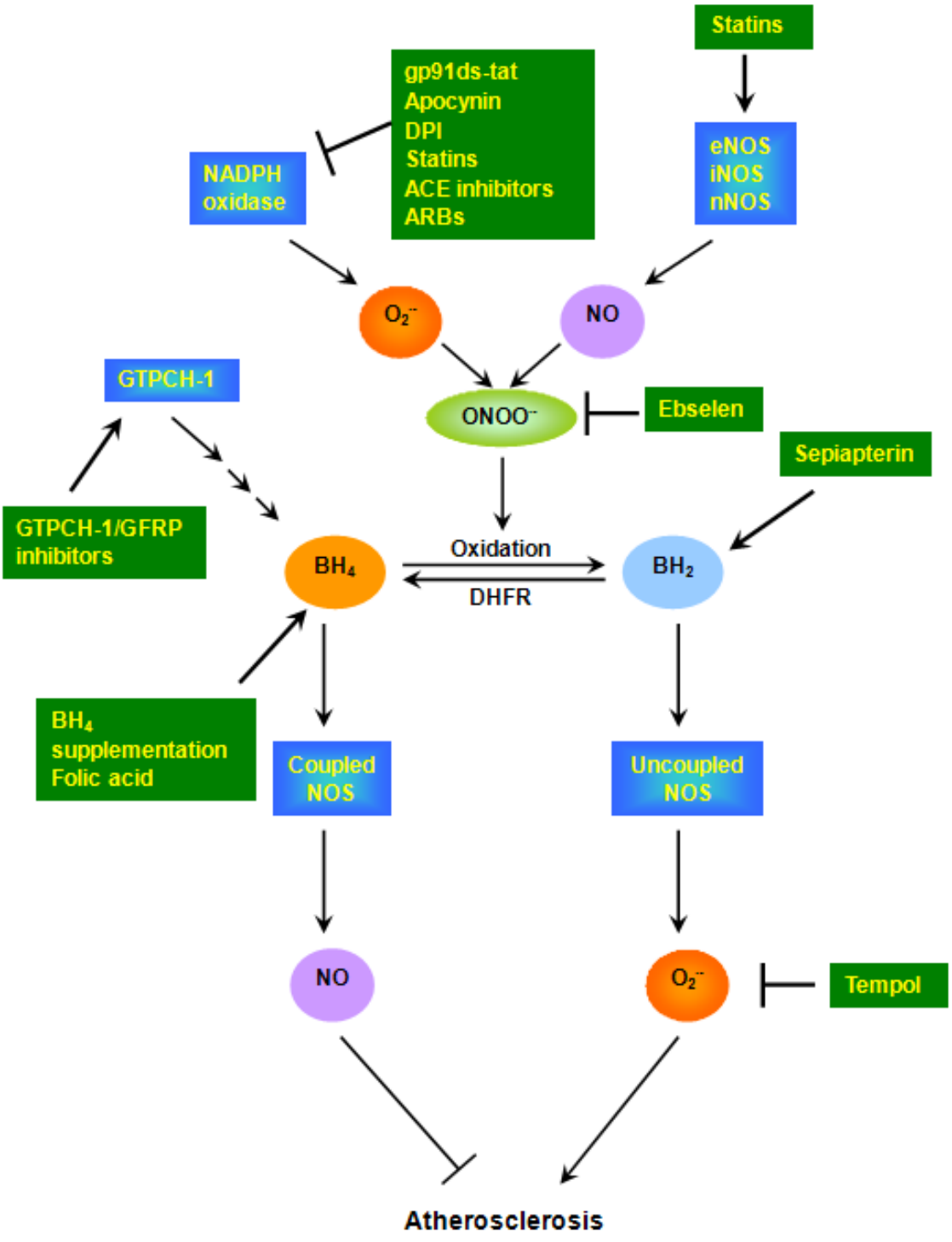
Statins
gp91ds-tat
Apocynin
DPI
Statins
ACE inhibitors
ARBs
NADPH oxidase
eNOS
iNOS
nNOS
$O_2^{\cdot-}$
NO
GTPCH-1
ONOO$^{\cdot-}$
Ebselen
Sepiapterin
GTPCH-1/GFRP inhibitors
BH_4
Oxidation
DHFR
BH_2
BH_4 supplementation
Folic acid
Coupled NOS
Uncoupled NOS
NO
$O_2^{\cdot-}$
Tempol
Atherosclerosis

Treatment of 22 hypercholesterolemic patients with oral BH_4 for 4 weeks improved oxidative stress and endothelial function (Cosentino et al., 2008). Another short-term study from our own group showed a beneficial effect of BH_4 on both blood pressure and endothelial function in patients with poorly controlled hypertension (Porkert et al., 2008).

In contrast to the above studies, a phase II clinical trial conducted by BioMarin Pharmaceutical Inc. failed to demonstrate an effect of BH_4 administration (5 mg/kg, twice daily for 2 months) on blood pressure relative to placebo in patients with poorly controlled hypertension. It is possible that the lack of efficacy observed with such administration of BH_4 is due to inefficient cellular uptake of BH_4 from the plasma to the endothelial cells. Indeed, whether elevation of BH_4 in plasma leads to increased intracellular concentration of BH_4 in the endothelium is questionable (Katusic et al., 2009). Of note, in patients with coronary artery atherosclerosis, although BH_4 levels in the vasculature are low, they are paradoxically high in the plasma (Antoniades et al., 2007). Hasegawa et al. (Hasegawa et al., 2005) found that BH_4 does not diffuse freely from circulating blood into the endothelium and might require oxidation to BH_2 in order to be imported into the endothelium. Extracellular BH_2 is more readily transported into cells and then is regenerated back to BH_4 by DHFR through the salvage pathway. In pathological states, endothelial DHFR activity often becomes limiting. For example, under conditions of oxidative stress, endothelial DHFR activity is decreased (Chalupsky and Cai, 2005). Thus, the study by Hasegawa et al. provided intriguing insights into the

pharmacokinetics and biodistribution of BH_4 and might explain the lack of efficacy of exogenously administered high-concentration of BH_4 for the treatment of vascular diseases. The bioavailability of BH_4 in endothelial cells does not solely depend on exogenous BH_4 supplementation, but also relies on intracellular DHFR activity to enable an increase in intracellular concentrations of BH_4 following oral supplementation with BH_4. Therefore, the intracellular concentration of BH_4 is determined by a complex network of mechanisms that influence metabolism, recycling and transport of BH_4. These factors could limit the therapeutic potential of oral BH_4.

5.4 Development of new therapeutic agents that disrupt GTPCH-1/GFRP interaction and increase intracellular BH_4

The above considerations indicate that alternative strategies to increase endogenous endothelial BH_4 might be necessary to exert salutary effects on endothelial function. Based on my finding that GFRP binding to GTPCH-1 inhibits GTPCH-1 phosphorylation and enzymatic activity, I started searching for peptides or small molecules that can disrupt the interaction of GTPCH-1 and GFRP. I envision that disrupting the GTPCH-1/GFRP interaction could increase GTPCH-1 activity and enhance cellular production of BH_4.

Inhibition of protein–protein interaction has been considered as a desirable target for assay development and drug discovery. For this purpose, a number of peptide inhibitors have been described for a variety of interacting protein pairs (Wells and McClendon, 2007). Peptides however have several drawbacks, such as a

lack of oral bioavailability, instability due to the cleavage of the peptide backbone, and inconvenient route of administration that often requires injections (Hamman et al., 2005). In this dissertation, I found that both N- and C- terminal regions of GTPCH-1 are required for its binding to GFRP. In keeping with this, peptides corresponding to GTPCH-1 N- or C- terminal sequences failed to disrupt the interaction of GTPCH-1 with GFRP. These findings suggest that the interaction of GTPCH-1 and GFRP likely involves a tertiary structure of GTPCH-1. It is conceivable that simple peptides might not mimic this complex structure and thus can not disrupt the binding.

Compared to peptides, small molecule inhibitors of protein–protein interactions have been considered more desirable, albeit more difficult to obtain. In order to screen for small molecules that disrupt the interaction of GTPCH-1 and GFRP, I developed and optimized a robust, sensitive and simple TR-FRET assay to monitor this protein-protein interaction. I employed this assay in HTS and results from a pilot screening of 1,280 compounds showed that positive hits can disrupt GTPCH-1/GFRP interaction in an independent binding assay and promise to increase endothelial cell BH_4 levels. This proof-of-principle study suggests that this approach can be applied in future screening for additional active compounds that increase GTPCH-1 activity. Further validation and Structure-Activity Relationship (SAR) studies of these inhibitors in cells and in vivo will likely give rise to lead compounds that can be optimized for potential drugs. These identified compounds might also serve as tools to facilitate the further study of the mechanism of

GTPCH-1 and GFRP interaction.

5.5 Future directions

Our findings have enriched the understanding of post-translational regulation of GTPCH-1 through phosphorylation and interaction with GFRP. We find that laminar and oscillatory shear induce opposite changes on GTPCH-1, thereby differentially regulating vascular redox state and homeostasis. Whether other physiological and pathological conditions have similar effects on GTPCH-1 and GFRP remains unclear. Of note, the role of GFRP in vivo has not been completely understood and our findings suggest that additional in vivo studies examining its expression and the binding of GFRP to GTPCH-1 are needed.

Additional studies need to be performed to elucidate the signaling mechanism by which laminar shear causes dissociation of GTPCH-1 and GFRP. It is unknown whether this dissociation is related to endothelial cell shape change that accompanies laminar shear. We speculate that this mechanism observed in the setting of laminar shear should differ in cells exposed to oscillatory shear stress. Changes in subcellular localizations of these two proteins in response to laminar and oscillatory shear could be examined using FRET imaging of GTPCH-1/GFRP interaction in live cells.

To further study the importance of GTPCH-1 phosphorylation in vivo, we are creating two knock-in (KI) animals, where the Serine 72 of GTPCH-1 in mouse is replace by aspartate (S72D) to mimic phosphorylation and by alaline (S72A) to block phosphorylation, respectively. We hypothesize that the S72D KI mouse will

be resistant to cardiovascular diseases, because their GTPCH-1 is constitutively activated and BH_4 levels will be elevated. In contrast, the S72A KI mouse is expected to be more prone to diseases because their GTPCH-1 can not be phosphorylated and activated.

The relative inefficiency of exogenous BH_4 supplementation in human studies suggests that efforts to increase intracellular BH_4 are desirable. Future studies of pterin transport would be helpful. These studies will facilitate the development of a delivery system that allows a more efficient increase in intracellular BH_4 levels.

Ultra high throughput screening of the Lead Gene-Novelty Library generated 10 compounds that inhibit GTPCH-1/GFRP interaction in an in vitro GST pull-down assay. These 10 compounds will be tested in cultured human aortic endothelial cells to examine their effects on basal BH_4 levels, GTPCH-1 phosphorylation and activity, and cellular NO production. Effective compounds will be further analyzed in chemical structures to conduct SAR studies. Additional high throughput screening using the TR-FRET approach is needed to identify additional compounds that have biological activity.

Beyond the role in cardiovascular biology, GTPCH-1 and BH_4 also regulate aromatic amino acid synthesis, neurotransmitters levels and the pain pathway. Whether GTPCH-1 is similarly regulated by phosphorylation and interaction with GFRP in neurologic tissues remains unclear. Consequently, there is an obvious interest in identifying the mechanisms by which GTPCH-1 activity is regulated in those tissues. We recently identified a previously unknown role of GTPCH-1 and

BH_4 in modulating T cell function upon activation. We found that T cell receptor ligation by anti-CD3 stimulation markedly increases GTPCH-1 expression, GTPCH-1 phosphorylation and T cell BH_4 levels. GTPCH-1 activation and the concomitant stimulation of NOS enzymes promote T cell NO production and modulate T cell polarization and cytokine production.

In summary, the results reported in this dissertation may help in our overall understanding of shear stress and BH_4 biology and have implications for multiple areas of cardiovascular health. Unraveling the mechanisms of GTPCH-1 regulation and its role in atherosclerosis may further our understanding of specific diseases such as atherosclerosis and aid in the development of potential new treatment of cardiovascular diseases.

Chapter 6:

References

Alderton WK, Cooper CE and Knowles RG (2001) Nitric oxide synthases: structure, function and inhibition. *Biochem J* **357**(Pt 3):593-615.

Ali ZA, Bursill CA, Douglas G, McNeill E, Papaspyridonos M, Tatham AL, Bendall JK, Akhtar AM, Alp NJ, Greaves DR and Channon KM (2008) CCR2-mediated antiinflammatory effects of endothelial tetrahydrobiopterin inhibit vascular injury-induced accelerated atherosclerosis. *Circulation* **118**(14 Suppl):S71-77.

Alp NJ, McAteer MA, Khoo J, Choudhury RP and Channon KM (2004) Increased endothelial tetrahydrobiopterin synthesis by targeted transgenic GTP-cyclohydrolase I overexpression reduces endothelial dysfunction and atherosclerosis in ApoE-knockout mice. *Arterioscler Thromb Vasc Biol* **24**(3):445-450.

Antoniades C, Shirodaria C, Crabtree M, Rinze R, Alp N, Cunnington C, Diesch J, Tousoulis D, Stefanadis C, Leeson P, Ratnatunga C, Pillai R and Channon KM (2007) Altered plasma versus vascular biopterins in human atherosclerosis reveal relationships between endothelial nitric oxide synthase coupling, endothelial function, and inflammation. *Circulation* **116**(24):2851-2859.

Antonio CN, Grazia PM, Marialessandra C, Francesco B and Roberto P (2007) Receptor-drug interaction: europium employment for studying the biochemical pathway of g-protein-coupled receptor activation. *Met Based Drugs* **2007**:12635.

Arkin MR, Randal M, DeLano WL, Hyde J, Luong TN, Oslob JD, Raphael DR, Taylor L, Wang J, McDowell RS, Wells JA and Braisted AC (2003) Binding of small molecules to an adaptive protein-protein interface. *Proc Natl Acad Sci U S A* **100**(4):1603-1608.

Bader G, Schiffmann S, Herrmann A, Fischer M, Gutlich M, Auerbach G, Ploom T, Bacher A, Huber R and Lemm T (2001) Crystal structure of rat GTP cyclohydrolase I feedback regulatory protein, GFRP. *J Mol Biol* **312**(5):1051-1057.

Baek KJ, Thiel BA, Lucas S and Stuehr DJ (1993) Macrophage nitric oxide synthase subunits. Purification, characterization, and role of prosthetic groups and substrate in regulating their association into a dimeric enzyme. *J Biol Chem* **268**(28):21120-21129.

Bendall JK, Alp NJ, Warrick N, Cai S, Adlam D, Rockett K, Yokoyama M, Kawashima S and Channon KM (2005) Stoichiometric relationships between endothelial tetrahydrobiopterin, endothelial NO synthase (eNOS) activity, and eNOS coupling in vivo: insights from transgenic mice with endothelial-targeted GTP cyclohydrolase 1 and eNOS overexpression. *Circ Res* **97**(9):864-871.

Benjamin ER, Pruthi F, Olanrewaju S, Ilyin VI, Crumley G, Kutlina E, Valenzano KJ and Woodward RM (2006) State-dependent compound inhibition of Nav1.2 sodium channels using the FLIPR Vm dye: on-target and off-target effects of diverse pharmacological agents. *J Biomol Screen* **11**(1):29-39.

Boulanger CM, Heymes C, Benessiano J, Geske RS, Levy BI and Vanhoutte PM (1998) Neuronal nitric oxide synthase is expressed in rat vascular smooth muscle cells: activation by angiotensin II in hypertension. *Circ Res* **83**(12):1271-1278.

Buchwalow IB, Podzuweit T, Bocker W, Samoilova VE, Thomas S, Wellner M, Baba HA, Robenek H, Schnekenburger J and Lerch MM (2002) Vascular smooth muscle and nitric oxide synthase. *FASEB J* **16**(6):500-508.

Bussolari SR, Dewey CF, Jr. and Gimbrone MA, Jr. (1982) Apparatus for subjecting living cells to fluid shear stress. *Rev Sci Instrum* **53**(12):1851-1854.

Chalupsky K and Cai H (2005) Endothelial dihydrofolate reductase: critical for nitric oxide bioavailability and role in angiotensin II uncoupling of endothelial nitric oxide synthase. *Proc Natl Acad Sci U S A* **102**(25):9056-9061.

Channon KM (2004) Tetrahydrobiopterin: regulator of endothelial nitric oxide synthase in vascular disease. *Trends Cardiovasc Med* **14**(8):323-327.

Chatzizisis YS, Coskun AU, Jonas M, Edelman ER, Feldman CL and Stone PH (2007) Role of endothelial shear stress in the natural history of coronary atherosclerosis and vascular remodeling: molecular, cellular, and vascular behavior. *J Am Coll Cardiol* **49**(25):2379-2393.

Chavan B, Gillbro JM, Rokos H and Schallreuter KU (2006) GTP cyclohydrolase feedback regulatory protein controls cofactor 6-tetrahydrobiopterin synthesis in the cytosol and in the nucleus of epidermal keratinocytes and melanocytes. *J Invest Dermatol* **126**(11):2481-2489.

Chen H, Puhl HL, 3rd, Koushik SV, Vogel SS and Ikeda SR (2006) Measurement of FRET efficiency and ratio of donor to acceptor concentration in living cells. *Biophys J* **91**(5):L39-41.

Cheng C, van Haperen R, de Waard M, van Damme LC, Tempel D, Hanemaaijer L, van Cappellen GW, Bos J, Slager CJ, Duncker DJ, van der Steen AF, de Crom R and Krams R (2005) Shear stress affects the intracellular distribution of eNOS: direct demonstration by a novel in vivo technique. *Blood* **106**(12):3691-3698.

Chien S (2008) Effects of disturbed flow on endothelial cells. *Ann Biomed Eng* **36**(4):554-562.

Corson MA, James NL, Latta SE, Nerem RM, Berk BC and Harrison DG (1996) Phosphorylation of endothelial nitric oxide synthase in response to fluid shear stress. *Circ Res* **79**(5):984-991.

Cosentino F, Hurlimann D, Delli Gatti C, Chenevard R, Blau N, Alp NJ, Channon KM, Eto M, Lerch P, Enseleit F, Ruschitzka F, Volpe M, Luscher TF and Noll G (2008) Chronic treatment with tetrahydrobiopterin reverses endothelial dysfunction and oxidative stress in hypercholesterolaemia. *Heart* **94**(4):487-492.

Crabtree MJ, Tatham AL, Hale AB, Alp NJ and Channon KM (2009) Critical role for tetrahydrobiopterin recycling by dihydrofolate reductase in regulation of endothelial nitric-oxide synthase coupling: relative importance of the de novo biopterin synthesis versus salvage pathways. *J Biol Chem*

284(41):28128-28136.

Davies PF (2002) Multiple signaling pathways in flow-mediated endothelial mechanotransduction: PYK-ing the right location. *Arterioscler Thromb Vasc Biol* **22**(11):1755-1757.

Davignon J and Ganz P (2004) Role of endothelial dysfunction in atherosclerosis. *Circulation* **109**(23 Suppl 1):III27-32.

Davis ME, Cai H, McCann L, Fukai T and Harrison DG (2003) Role of c-Src in regulation of endothelial nitric oxide synthase expression during exercise training. *Am J Physiol Heart Circ Physiol* **284**(4):H1449-1453.

De Keulenaer GW, Chappell DC, Ishizaka N, Nerem RM, Alexander RW and Griendling KK (1998) Oscillatory and steady laminar shear stress differentially affect human endothelial redox state: role of a superoxide-producing NADH oxidase. *Circ Res* **82**(10):1094-1101.

Du J, Wei N, Xu H, Ge Y, Vasquez-Vivar J, Guan T, Oldham KT, Pritchard KA, Jr. and Shi Y (2009a) Identification and functional characterization of phosphorylation sites on GTP cyclohydrolase I. *Arterioscler Thromb Vasc Biol* **29**(12):2161-2168.

Du J, Xu H, Wei N, Wakim B, Halligan B, Pritchard KA, Jr. and Shi Y (2009b) Identification of proteins interacting with GTP cyclohydrolase I. *Biochem Biophys Res Commun* **385**(2):143-147.

Du X, Edelstein D, Obici S, Higham N, Zou MH and Brownlee M (2006) Insulin resistance reduces arterial prostacyclin synthase and eNOS activities by

increasing endothelial fatty acid oxidation. *J Clin Invest* **116**(4):1071-1080.

Duch DS, Bowers SW, Woolf JH and Nichol CA (1984) Biopterin cofactor biosynthesis: GTP cyclohydrolase, neopterin and biopterin in tissues and body fluids of mammalian species. *Life Sci* **35**(18):1895-1901.

Elzaouk L, Laufs S, Heerklotz D, Leimbacher W, Blau N, Resibois A and Thony B (2004) Nuclear localization of tetrahydrobiopterin biosynthetic enzymes. *Biochim Biophys Acta* **1670**(1):56-68.

Fink B, Laude K, McCann L, Doughan A, Harrison DG and Dikalov S (2004) Detection of intracellular superoxide formation in endothelial cells and intact tissues using dihydroethidium and an HPLC-based assay. *Am J Physiol Cell Physiol* **287**(4):C895-902.

Fleming I and Busse R (1999) NO: the primary EDRF. *J Mol Cell Cardiol* **31**(1):5-14.

Garcia-Cardena G, Fan R, Shah V, Sorrentino R, Cirino G, Papapetropoulos A and Sessa WC (1998) Dynamic activation of endothelial nitric oxide synthase by Hsp90. *Nature* **392**(6678):821-824.

Gesierich A, Niroomand F and Tiefenbacher CP (2003) Role of human GTP cyclohydrolase I and its regulatory protein in tetrahydrobiopterin metabolism. *Basic Res Cardiol* **98**(2):69-75.

Ghosh DK and Stuehr DJ (1995) Macrophage NO synthase: characterization of isolated oxygenase and reductase domains reveals a head-to-head subunit interaction. *Biochemistry* **34**(3):801-807.

Glagov S, Zarins C, Giddens DP and Ku DN (1988) Hemodynamics and atherosclerosis. Insights and perspectives gained from studies of human arteries. *Arch Pathol Lab Med* **112**(10):1018-1031.

Go RS and Adjei AA (1999) Review of the comparative pharmacology and clinical activity of cisplatin and carboplatin. *J Clin Oncol* **17**(1):409-422.

Griffith OW and Stuehr DJ (1995) Nitric oxide synthases: properties and catalytic mechanism. *Annu Rev Physiol* **57**:707-736.

Gunnett CA, Lund DD, McDowell AK, Faraci FM and Heistad DD (2005) Mechanisms of inducible nitric oxide synthase-mediated vascular dysfunction. *Arterioscler Thromb Vasc Biol* **25**(8):1617-1622.

Gunther JR, Du Y, Rhoden E, Lewis I, Revennaugh B, Moore TW, Kim SH, Dingledine R, Fu H and Katzenellenbogen JA (2009) A set of time-resolved fluorescence resonance energy transfer assays for the discovery of inhibitors of estrogen receptor-coactivator binding. *J Biomol Screen* **14**(2):181-193.

Guzik TJ, West NE, Black E, McDonald D, Ratnatunga C, Pillai R and Channon KM (2000) Vascular superoxide production by NAD(P)H oxidase: association with endothelial dysfunction and clinical risk factors. *Circ Res* **86**(9):E85-90.

Hamman JH, Enslin GM and Kotze AF (2005) Oral delivery of peptide drugs: barriers and developments. *BioDrugs* **19**(3):165-177.

Hansson GK (2005) Inflammation, atherosclerosis, and coronary artery disease. *N Engl J Med* **352**(16):1685-1695.

Harada T, Kagamiyama H and Hatakeyama K (1993) Feedback regulation

mechanisms for the control of GTP cyclohydrolase I activity. *Science* **260**(5113):1507-1510.

Harrison DG (2005) The shear stress of keeping arteries clear. *Nat Med* **11**(4):375-376.

Harrison DG, Chen W, Dikalov S and Li L (2010) Regulation of endothelial cell tetrahydrobiopterin pathophysiological and therapeutic implications. *Adv Pharmacol* **60**:107-132.

Harrison DG, Guzik TJ, Lob HE, Madhur MS, Marvar PJ, Thabet SR, Vinh A and Weyand CM (2011) Inflammation, immunity, and hypertension. *Hypertension* **57**(2):132-140.

Hart CM, Kleinhenz DJ, Dikalov SI, Boulden BM and Dudley SC, Jr. (2005) The measurement of nitric oxide production by cultured endothelial cells. *Methods Enzymol* **396**:502-514.

Hasegawa H, Sawabe K, Nakanishi N and Wakasugi OK (2005) Delivery of exogenous tetrahydrobiopterin (BH4) to cells of target organs: role of salvage pathway and uptake of its precursor in effective elevation of tissue BH4. *Mol Genet Metab* **86 Suppl 1**:S2-10.

Hattori Y, Hattori S, Wang X, Satoh H, Nakanishi N and Kasai K (2007) Oral administration of tetrahydrobiopterin slows the progression of atherosclerosis in apolipoprotein E-knockout mice. *Arterioscler Thromb Vasc Biol* **27**(4):865-870.

Hattori Y, Nakanishi N, Akimoto K, Yoshida M and Kasai K (2003) HMG-CoA

reductase inhibitor increases GTP cyclohydrolase I mRNA and tetrahydrobiopterin in vascular endothelial cells. *Arterioscler Thromb Vasc Biol* **23**(2):176-182.

Higgins CE and Gross SS (2010) The N-terminal peptide of mammalian GTP cyclohydrolase I is an autoinhibitory control element and contributes to binding the allosteric regulatory protein GFRP. *J Biol Chem*.

Higman DJ, Strachan AM, Buttery L, Hicks RC, Springall DR, Greenhalgh RM and Powell JT (1996) Smoking impairs the activity of endothelial nitric oxide synthase in saphenous vein. *Arterioscler Thromb Vasc Biol* **16**(4):546-552.

Hink U, Li H, Mollnau H, Oelze M, Matheis E, Hartmann M, Skatchkov M, Thaiss F, Stahl RA, Warnholtz A, Meinertz T, Griendling K, Harrison DG, Forstermann U and Munzel T (2001) Mechanisms underlying endothelial dysfunction in diabetes mellitus. *Circ Res* **88**(2):E14-22.

Hong HJ, Hsiao G, Cheng TH and Yen MH (2001) Supplemention with tetrahydrobiopterin suppresses the development of hypertension in spontaneously hypertensive rats. *Hypertension* **38**(5):1044-1048.

Hu LA, Zhou T, Hamman BD and Liu Q (2008) A homogeneous G protein-coupled receptor ligand binding assay based on time-resolved fluorescence resonance energy transfer. *Assay Drug Dev Technol* **6**(4):543-550.

Imbert PE, Unterreiner V, Siebert D, Gubler H, Parker C and Gabriel D (2007) Recommendations for the reduction of compound artifacts in time-resolved fluorescence resonance energy transfer assays. *Assay Drug Dev Technol*

5(3):363-372.

Ishii M, Shimizu S, Nagai T, Shiota K, Kiuchi Y and Yamamoto T (2001) Stimulation of tetrahydrobiopterin synthesis induced by insulin: possible involvement of phosphatidylinositol 3-kinase. *Int J Biochem Cell Biol* **33**(1):65-73.

Jo H, Song H and Mowbray A (2006) Role of NADPH oxidases in disturbed flow- and BMP4- induced inflammation and atherosclerosis. *Antioxid Redox Signal* **8**(9-10):1609-1619.

Kalivendi S, Hatakeyama K, Whitsett J, Konorev E, Kalyanaraman B and Vasquez-Vivar J (2005) Changes in tetrahydrobiopterin levels in endothelial cells and adult cardiomyocytes induced by LPS and hydrogen peroxide--a role for GFRP? *Free Radic Biol Med* **38**(4):481-491.

Kase H, Hashikabe Y, Uchida K, Nakanishi N and Hattori Y (2005) Supplementation with tetrahydrobiopterin prevents the cardiovascular effects of angiotensin II-induced oxidative and nitrosative stress. *J Hypertens* **23**(7):1375-1382.

Katusic ZS, d'Uscio LV and Nath KA (2009) Vascular protection by tetrahydrobiopterin: progress and therapeutic prospects. *Trends Pharmacol Sci* **30**(1):48-54.

Katusic ZS, Stelter A and Milstien S (1998) Cytokines stimulate GTP cyclohydrolase I gene expression in cultured human umbilical vein endothelial cells. *Arterioscler Thromb Vasc Biol* **18**(1):27-32.

Kawashima S and Yokoyama M (2004) Dysfunction of endothelial nitric oxide

synthase and atherosclerosis. *Arterioscler Thromb Vasc Biol* **24**(6):998-1005.

Klatt P, Schmidt K, Lehner D, Glatter O, Bachinger HP and Mayer B (1995) Structural analysis of porcine brain nitric oxide synthase reveals a role for tetrahydrobiopterin and L-arginine in the formation of an SDS-resistant dimer. *EMBO J* **14**(15):3687-3695.

Kolinsky MA and Gross SS (2004) The mechanism of potent GTP cyclohydrolase I inhibition by 2,4-diamino-6-hydroxypyrimidine: requirement of the GTP cyclohydrolase I feedback regulatory protein. *J Biol Chem* **279**(39):40677-40682.

Koshimura K, Miwa S and Watanabe Y (1994) Dopamine-releasing action of 6R-L-erythro-tetrahydrobiopterin: analysis of its action site using sepiapterin. *J Neurochem* **63**(2):649-654.

Ku DN, Giddens DP, Phillips DJ and Strandness DE, Jr. (1985a) Hemodynamics of the normal human carotid bifurcation: in vitro and in vivo studies. *Ultrasound Med Biol* **11**(1):13-26.

Ku DN, Giddens DP, Zarins CK and Glagov S (1985b) Pulsatile flow and atherosclerosis in the human carotid bifurcation. Positive correlation between plaque location and low oscillating shear stress. *Arteriosclerosis* **5**(3):293-302.

Kuzkaya N, Weissmann N, Harrison DG and Dikalov S (2003) Interactions of peroxynitrite, tetrahydrobiopterin, ascorbic acid, and thiols: implications for uncoupling endothelial nitric-oxide synthase. *J Biol Chem*

278(25):22546-22554.

Landmesser U, Dikalov S, Price SR, McCann L, Fukai T, Holland SM, Mitch WE and Harrison DG (2003) Oxidation of tetrahydrobiopterin leads to uncoupling of endothelial cell nitric oxide synthase in hypertension. *J Clin Invest* **111**(8):1201-1209.

Lapize C, Pluss C, Werner ER, Huwiler A and Pfeilschifter J (1998) Protein kinase C phosphorylates and activates GTP cyclohydrolase I in rat renal mesangial cells. *Biochem Biophys Res Commun* **251**(3):802-805.

Laufs U, La Fata V, Plutzky J and Liao JK (1998) Upregulation of endothelial nitric oxide synthase by HMG CoA reductase inhibitors. *Circulation* **97**(12):1129-1135.

Laursen JB, Somers M, Kurz S, McCann L, Warnholtz A, Freeman BA, Tarpey M, Fukai T and Harrison DG (2001) Endothelial regulation of vasomotion in apoE-deficient mice: implications for interactions between peroxynitrite and tetrahydrobiopterin. *Circulation* **103**(9):1282-1288.

Li C and Stocker R (2009) Heme oxygenase and iron: from bacteria to humans. *Redox Rep* **14**(3):95-101.

Li H and Forstermann U (2000) Nitric oxide in the pathogenesis of vascular disease. *J Pathol* **190**(3):244-254.

Li L, Rezvan A, Salerno JC, Husain A, Kwon K, Jo H, Harrison DG and Chen W (2010) GTP cyclohydrolase I phosphorylation and interaction with GTP cyclohydrolase feedback regulatory protein provide novel regulation of

endothelial tetrahydrobiopterin and nitric oxide. *Circ Res* **106**(2):328-336.

Libby P, Ridker PM and Maseri A (2002) Inflammation and atherosclerosis. *Circulation* **105**(9):1135-1143.

Litchfield DW (2003) Protein kinase CK2: structure, regulation and role in cellular decisions of life and death. *Biochem J* **369**(Pt 1):1-15.

Lotz GP, Lin H, Harst A and Obermann WM (2003) Aha1 binds to the middle domain of Hsp90, contributes to client protein activation, and stimulates the ATPase activity of the molecular chaperone. *J Biol Chem* **278**(19):17228-17235.

Maita N, Hatakeyama K, Okada K and Hakoshima T (2004) Structural basis of biopterin-induced inhibition of GTP cyclohydrolase I by GFRP, its feedback regulatory protein. *J Biol Chem* **279**(49):51534-51540.

Maita N, Okada K, Hatakeyama K and Hakoshima T (2002) Crystal structure of the stimulatory complex of GTP cyclohydrolase I and its feedback regulatory protein GFRP. *Proc Natl Acad Sci U S A* **99**(3):1212-1217.

McNally JS, Davis ME, Giddens DP, Saha A, Hwang J, Dikalov S, Jo H and Harrison DG (2003) Role of xanthine oxidoreductase and NAD(P)H oxidase in endothelial superoxide production in response to oscillatory shear stress. *Am J Physiol Heart Circ Physiol* **285**(6):H2290-2297.

Milstien S, Jaffe H, Kowlessur D and Bonner TI (1996) Purification and cloning of the GTP cyclohydrolase I feedback regulatory protein, GFRP. *J Biol Chem* **271**(33):19743-19751.

Milstien S and Katusic Z (1999) Oxidation of tetrahydrobiopterin by peroxynitrite: implications for vascular endothelial function. *Biochem Biophys Res Commun* **263**(3):681-684.

Mitchell BM, Dorrance AM and Webb RC (2003) GTP cyclohydrolase 1 downregulation contributes to glucocorticoid hypertension in rats. *Hypertension* **41**(3 Pt 2):669-674.

Nam D, Ni CW, Rezvan A, Suo J, Budzyn K, Llanos A, Harrison D, Giddens D and Jo H (2009) Partial carotid ligation is a model of acutely induced disturbed flow, leading to rapid endothelial dysfunction and atherosclerosis. *Am J Physiol Heart Circ Physiol* **297**(4):H1535-1543.

Nandi M, Kelly P, Vallance P and Leiper J (2008) Over-expression of GTP-cyclohydrolase 1 feedback regulatory protein attenuates LPS and cytokine-stimulated nitric oxide production. *Vasc Med* **13**(1):29-36.

Nar H, Huber R, Auerbach G, Fischer M, Hosl C, Ritz H, Bracher A, Meining W, Eberhardt S and Bacher A (1995a) Active site topology and reaction mechanism of GTP cyclohydrolase I. *Proc Natl Acad Sci U S A* **92**(26):12120-12125.

Nar H, Huber R, Meining W, Schmid C, Weinkauf S and Bacher A (1995b) Atomic structure of GTP cyclohydrolase I. *Structure* **3**(5):459-466.

Nerem RM, Harrison DG, Taylor WR and Alexander RW (1993) Hemodynamics and vascular endothelial biology. *J Cardiovasc Pharmacol* **21 Suppl 1**:S6-10.

Nichol CA, Smith GK and Duch DS (1985) Biosynthesis and metabolism of

tetrahydrobiopterin and molybdopterin. *Annu Rev Biochem* **54**:729-764.

Ozaki M, Kawashima S, Yamashita T, Hirase T, Namiki M, Inoue N, Hirata K, Yasui H, Sakurai H, Yoshida Y, Masada M and Yokoyama M (2002) Overexpression of endothelial nitric oxide synthase accelerates atherosclerotic lesion formation in apoE-deficient mice. *J Clin Invest* **110**(3):331-340.

Ozers MS, Ervin KM, Steffen CL, Fronczak JA, Lebakken CS, Carnahan KA, Lowery RG and Burke TJ (2005) Analysis of ligand-dependent recruitment of coactivator peptides to estrogen receptor using fluorescence polarization. *Mol Endocrinol* **19**(1):25-34.

Palmer RM, Ashton DS and Moncada S (1988) Vascular endothelial cells synthesize nitric oxide from L-arginine. *Nature* **333**(6174):664-666.

Panaretou B, Siligardi G, Meyer P, Maloney A, Sullivan JK, Singh S, Millson SH, Clarke PA, Naaby-Hansen S, Stein R, Cramer R, Mollapour M, Workman P, Piper PW, Pearl LH and Prodromou C (2002) Activation of the ATPase activity of hsp90 by the stress-regulated cochaperone aha1. *Mol Cell* **10**(6):1307-1318.

Pastor CM, Williams D, Yoneyama T, Hatakeyama K, Singleton S, Naylor E and Billiar TR (1996) Competition for tetrahydrobiopterin between phenylalanine hydroxylase and nitric oxide synthase in rat liver. *J Biol Chem* **271**(40):24534-24538.

Patel KB, Stratford MR, Wardman P and Everett SA (2002) Oxidation of

tetrahydrobiopterin by biological radicals and scavenging of the trihydrobiopterin radical by ascorbate. *Free Radic Biol Med* **32**(3):203-211.

Peterson TE, d'Uscio LV, Cao S, Wang XL and Katusic ZS (2009) Guanosine triphosphate cyclohydrolase I expression and enzymatic activity are present in caveolae of endothelial cells. *Hypertension* **53**(2):189-195.

Pfleger KD, Seeber RM and Eidne KA (2006) Bioluminescence resonance energy transfer (BRET) for the real-time detection of protein-protein interactions. *Nat Protoc* **1**(1):337-345.

Pieper GM (1997) Acute amelioration of diabetic endothelial dysfunction with a derivative of the nitric oxide synthase cofactor, tetrahydrobiopterin. *J Cardiovasc Pharmacol* **29**(1):8-15.

Porkert M, Sher S, Reddy U, Cheema F, Niessner C, Kolm P, Jones DP, Hooper C, Taylor WR, Harrison D and Quyyumi AA (2008) Tetrahydrobiopterin: a novel antihypertensive therapy. *J Hum Hypertens* **22**(6):401-407.

Pou S, Pou WS, Bredt DS, Snyder SH and Rosen GM (1992) Generation of superoxide by purified brain nitric oxide synthase. *J Biol Chem* **267**(34):24173-24176.

Presta A, Siddhanta U, Wu C, Sennequier N, Huang L, Abu-Soud HM, Erzurum S and Stuehr DJ (1998) Comparative functioning of dihydro- and tetrahydropterins in supporting electron transfer, catalysis, and subunit dimerization in inducible nitric oxide synthase. *Biochemistry* **37**(1):298-310.

Rickardson L, Wickstrom M, Larsson R and Lovborg H (2007) Image-based

screening for the identification of novel proteasome inhibitors. *J Biomol Screen* **12**(2):203-210.

Ross R (1999) Atherosclerosis--an inflammatory disease. *N Engl J Med* **340**(2):115-126.

Schmidt TS, McNeill E, Douglas G, Crabtree MJ, Hale AB, Khoo J, O'Neill CA, Cheng A, Channon KM and Alp NJ (2010) Tetrahydrobiopterin supplementation reduces atherosclerosis and vascular inflammation in apolipoprotein E-knockout mice. *Clin Sci (Lond)* **119**(3):131-142.

Schrader LI, Kinzenbaw DA, Johnson AW, Faraci FM and Didion SP (2007) IL-6 deficiency protects against angiotensin II induced endothelial dysfunction and hypertrophy. *Arterioscler Thromb Vasc Biol* **27**(12):2576-2581.

Shiman R, Jones SH and Gray DW (1990) Mechanism of phenylalanine regulation of phenylalanine hydroxylase. *J Biol Chem* **265**(20):11633-11642.

Stec DE, Vera T, McLemore GR, Jr., Kelsen S, Rimoldi JM, Gadepalli RS and Ryan MJ (2008) Heme oxygenase-1 induction does not improve vascular relaxation in angiotensin II hypertensive mice. *Am J Hypertens* **21**(2):189-193.

Stroes E, Kastelein J, Cosentino F, Erkelens W, Wever R, Koomans H, Luscher T and Rabelink T (1997) Tetrahydrobiopterin restores endothelial function in hypercholesterolemia. *J Clin Invest* **99**(1):41-46.

Sugiyama T, Levy BD and Michel T (2009) Tetrahydrobiopterin recycling, a key determinant of endothelial nitric-oxide synthase-dependent signaling

pathways in cultured vascular endothelial cells. *J Biol Chem* **284**(19):12691-12700.

Suo J, Ferrara DE, Sorescu D, Guldberg RE, Taylor WR and Giddens DP (2007) Hemodynamic shear stresses in mouse aortas: implications for atherogenesis. *Arterioscler Thromb Vasc Biol* **27**(2):346-351.

Swick L and Kapatos G (2006) A yeast 2-hybrid analysis of human GTP cyclohydrolase I protein interactions. *J Neurochem* **97**(5):1447-1455.

Tada K, Yoshida T, Mochizuki K, Konno T and Nakagawa H (1970) Two siblings of hyperphenylalaninemia: suggestion to a genetic variant of phenylketonuria. *Tohoku J Exp Med* **100**(3):249-253.

Takaya T, Hirata K, Yamashita T, Shinohara M, Sasaki N, Inoue N, Yada T, Goto M, Fukatsu A, Hayashi T, Alp NJ, Channon KM, Yokoyama M and Kawashima S (2007) A specific role for eNOS-derived reactive oxygen species in atherosclerosis progression. *Arterioscler Thromb Vasc Biol* **27**(7):1632-1637.

Tanaka K, Kaufman S and Milstien S (1989) Tetrahydrobiopterin, the cofactor for aromatic amino acid hydroxylases, is synthesized by and regulates proliferation of erythroid cells. *Proc Natl Acad Sci U S A* **86**(15):5864-5867.

Tatham AL, Crabtree MJ, Warrick N, Cai S, Alp NJ and Channon KM (2009) GTP cyclohydrolase I expression, protein, and activity determine intracellular tetrahydrobiopterin levels, independent of GTP cyclohydrolase feedback regulatory protein expression. *J Biol Chem* **284**(20):13660-13668.

Taylor CA, Hughes TJ and Zarins CK (1998) Finite element modeling of

three-dimensional pulsatile flow in the abdominal aorta: relevance to atherosclerosis. *Ann Biomed Eng* **26**(6):975-987.

Thaler C, Koushik SV, Blank PS and Vogel SS (2005) Quantitative multiphoton spectral imaging and its use for measuring resonance energy transfer. *Biophys J* **89**(4):2736-2749.

Traub O and Berk BC (1998) Laminar shear stress: mechanisms by which endothelial cells transduce an atheroprotective force. *Arterioscler Thromb Vasc Biol* **18**(5):677-685.

Tsuji T, Suzuki J, Shimamoto R, Yamazaki T, Nakajima T, Nagai R, Komatsu S, Ohtomo K, Toyo-Oka T and Omata M (2002) Vector analysis of the wall shear rate at the human aortoiliac bifurcation using cine MR velocity mapping. *AJR Am J Roentgenol* **178**(4):995-999.

Tzima E (2006) Role of small GTPases in endothelial cytoskeletal dynamics and the shear stress response. *Circ Res* **98**(2):176-185.

Upmacis RK, Crabtree MJ, Deeb RS, Shen H, Lane PB, Benguigui LE, Maeda N, Hajjar DP and Gross SS (2007) Profound biopterin oxidation and protein tyrosine nitration in tissues of ApoE-null mice on an atherogenic diet: contribution of inducible nitric oxide synthase. *Am J Physiol Heart Circ Physiol* **293**(5):H2878-2887.

VanderLaan PA, Reardon CA and Getz GS (2004) Site specificity of atherosclerosis: site-selective responses to atherosclerotic modulators. *Arterioscler Thromb Vasc Biol* **24**(1):12-22.

Vasquez-Vivar J (2009) Tetrahydrobiopterin, superoxide, and vascular dysfunction. *Free Radic Biol Med* **47**(8):1108-1119.

Vasquez-Vivar J, Kalyanaraman B and Martasek P (2003) The role of tetrahydrobiopterin in superoxide generation from eNOS: enzymology and physiological implications. *Free Radic Res* **37**(2):121-127.

Vasquez-Vivar J, Kalyanaraman B, Martasek P, Hogg N, Masters BS, Karoui H, Tordo P and Pritchard KA, Jr. (1998) Superoxide generation by endothelial nitric oxide synthase: the influence of cofactors. *Proc Natl Acad Sci U S A* **95**(16):9220-9225.

Vasquez-Vivar J, Martasek P, Whitsett J, Joseph J and Kalyanaraman B (2002) The ratio between tetrahydrobiopterin and oxidized tetrahydrobiopterin analogues controls superoxide release from endothelial nitric oxide synthase: an EPR spin trapping study. *Biochem J* **362**(Pt 3):733-739.

Wang D, Westerheide SD, Hanson JL and Baldwin AS, Jr. (2000) Tumor necrosis factor alpha-induced phosphorylation of RelA/p65 on Ser529 is controlled by casein kinase II. *J Biol Chem* **275**(42):32592-32597.

Wang Y, Nagase S and Koyama A (2004) Stimulatory effect of IGF-I and VEGF on eNOS message, protein expression, eNOS phosphorylation and nitric oxide production in rat glomeruli, and the involvement of PI3-K signaling pathway. *Nitric Oxide* **10**(1):25-35.

Wei CC, Crane BR and Stuehr DJ (2003) Tetrahydrobiopterin radical enzymology. *Chem Rev* **103**(6):2365-2383.

Wells JA and McClendon CL (2007) Reaching for high-hanging fruit in drug discovery at protein-protein interfaces. *Nature* **450**(7172):1001-1009.

Werner ER, Bahrami S, Heller R and Werner-Felmayer G (2002) Bacterial lipopolysaccharide down-regulates expression of GTP cyclohydrolase I feedback regulatory protein. *J Biol Chem* **277**(12):10129-10133.

Wick G, Perschinka H and Xu Q (1999) Autoimmunity and atherosclerosis. *Am Heart J* **138**(5 Pt 2):S444-449.

Widder JD, Chen W, Li L, Dikalov S, Thony B, Hatakeyama K and Harrison DG (2007) Regulation of tetrahydrobiopterin biosynthesis by shear stress. *Circ Res* **101**(8):830-838.

Wilcox JN, Subramanian RR, Sundell CL, Tracey WR, Pollock JS, Harrison DG and Marsden PA (1997) Expression of multiple isoforms of nitric oxide synthase in normal and atherosclerotic vessels. *Arterioscler Thromb Vasc Biol* **17**(11):2479-2488.

Williams HC and Griendling KK (2007) NADPH oxidase inhibitors: new antihypertensive agents? *J Cardiovasc Pharmacol* **50**(1):9-16.

Wojciak-Stothard B and Ridley AJ (2003) Shear stress-induced endothelial cell polarization is mediated by Rho and Rac but not Cdc42 or PI 3-kinases. *J Cell Biol* **161**(2):429-439.

Xu J, Wu Y, Song P, Zhang M, Wang S and Zou MH (2007) Proteasome-dependent degradation of guanosine 5'-triphosphate cyclohydrolase I causes tetrahydrobiopterin deficiency in diabetes mellitus. *Circulation*

116(8):944-953.

Yoneyama T, Brewer JM and Hatakeyama K (1997) GTP cyclohydrolase I feedback regulatory protein is a pentamer of identical subunits. Purification, cDNA cloning, and bacterial expression. *J Biol Chem* **272**(15):9690-9696.

Yoneyama T and Hatakeyama K (1998) Decameric GTP cyclohydrolase I forms complexes with two pentameric GTP cyclohydrolase I feedback regulatory proteins in the presence of phenylalanine or of a combination of tetrahydrobiopterin and GTP. *J Biol Chem* **273**(32):20102-20108.

Zimmermann T (2005) Spectral imaging and linear unmixing in light microscopy. *Adv Biochem Eng Biotechnol* **95**:245-265.

Zou MH, Shi C and Cohen RA (2002) Oxidation of the zinc-thiolate complex and uncoupling of endothelial nitric oxide synthase by peroxynitrite. *J Clin Invest* **109**(6):817-826.